UNIVERSIDADE FEDERAL FLUMINENSE

BRUNO JOSÉ DEMBOGURSKI

Adaptive Hierarchical Mesh Detail Mapping and Deformation

NITERÓI

2014

UNIVERSIDADE FEDERAL FLUMINENSE

BRUNO JOSÉ DEMBOGURSKI

Adaptive Hierarchical Mesh Detail Mapping and Deformation

Thesis presented to the Computing Graduate Program of the Universidade Federal Fluminense in partial fulfillment of the requirements for the degree of Doctor of Science. Area: Computer Graphics

Advisor:
ANSELMO ANTUNES MONTENEGRO

NITERÓI

2014

BRUNO JOSÉ DEMBOGURSKI

ADAPTIVE HIERARCHICAL MESH DETAIL MAPPING AND DEFORMATION

Thesis presented to the Computing Graduate Program of the Universidade Federal Fluminense in partial fulfillment of the requirements for the degree of Doctor of Science. Area: Computer Graphics

Approved in July of 2014.

Prof. Anselmo Antunes Montenegro - Advisor, UFF

Prof. Esteban Walter Gonzalez Clua, UFF

Prof. Leandro Augusto Frata Fernandes, UFF

Prof. Waldemar Celes Filho, PUC-Rio

Prof. André de Almeida Maximo, GE GRC

Niterói

2014

"I would rather discover a single fact, than to debate the great issues at length, without discovering anything."

Galileo Galilei

To my family for their love and support.

Acknowledgment

First of all, I would like to thank God for giving me the opportunity, strength and perseverance to complete this work.

I would like to thank everyone who contributed to the completion of this thesis.

My adviser, Anselmo Antunes Montenegro, for all the patience, support and countless hours of dedication to help me finish this work.

Professors of the IC-UFF (Institute of Computing) for the valuable classes that helped me better understand my field of expertise.

I thank my family: my mother Maria and my brother Renan, for the unconditional support that help me through the difficult times.

I thank my fiance Vivian, for standing by my side and cheer for me through all this time.

I thank my friends, Carlos Henrique (Carlão!), Edelberto and Gustavo for all we went through while sharing an apartment since the beginning of this work.

I thank all my friends, José Luiz, Tadeu, Rafael Barra, Frederico Kniest (Fanboy!), Felipe Gomes (Cabral!) for all the nights talking, laughing and having fun online. Also, Fernando Magalhães and Raphael Khoury for all the fun we had working together and for all the words of motivation.

I thank CAPES (Coordenação de Aperfeiçoamento de Pessoal de Nível Superior) for the financial support during this doctorate.

Resumo

Neste trabalho apresentamos um novo método para a adição de detalhes, gerados por funções de ruído, a superfícies de genus arbitrário, utilizando uma representação baseada em malhas de resolução variável, as quais generalizam malhas multiresolução. A entrada de dados é uma superfície originalmente representada por uma malha poligonal densa e um conjunto de parâmetros que guia a deformação e inserção de detalhes nos diferentes níveis de resolução e localização espacial. A estrutura de multiresolução é construída por um processo de simplificação que gera concomitantemente uma parametrização hierarquizada da malha. O nível mais grosseiro da representação define o domínio base, o qual armazena a geometria original através de um processo de parametrização local. Aplicamos modificações locais a esse domínio base de acordo com funções pré-definidas (i.e ruído de Perlin, ruído de Gabor ou uma deformação local específica) e a propagamos para a malha original. O processo de decimação e parametrização local, utilizados na construção da representação, são feitos simultaneamente utilizando-se operações estelares. Nossa principal contribuição é um método que explora todo o poder de estruturas hierárquicas adaptativas para gerar detalhes com maior grau de controle. Além disso, o método proposto preserva as características da malha original com maior intensidade via um processo de decimação sensível a feições. As mesmas feições detectadas são utilizadas juntamente com informações sobre a geometria discreta para guiar a geração e mapeamento do ruído.

Palavras-chave: Mapeamento de Detalhes em Malhas, Malhas Hierárquicas, Decimação Sensível à Feições, Parametrização de Malhas, Processamento de Malhas, Deformação de Malhas, Geração Procedural, Ruído Procedural.

Abstract

In this work, we present a new method for adding details generated by noise functions to arbitrary genus surfaces using a representation based on variable resolution meshes, which generalizes multiresolution meshes. The input data is a surface originally represented by a dense polygonal mesh and a set of parameters that guide the deformation and detail generation both in different levels of resolution and spatial location. The hierarchical adaptive structure is constructed by an iterative simplification process that concomitantly generates a hierarchical parametrization of the mesh. The coarsest level of the representation defines the base domain which stores the original geometry via a local parameterization process. We apply local modifications to this base domain according to predefined functions (i.e. Perlin noise, Gabor Noise or a specific localized deformation) and propagate it to the original mesh. The decimation process and the local parameterization are done simultaneously using stellar operations. Our main contribution is a method that explores the power of adaptive hierarchical structures to generate detail with a greater degree of control. Also, the proposed method preserves the characteristics of the original mesh with more intensity through a process of decimation, which is sensitive to features. The same detected features are used along with discrete geometry properties to guide the generation and mapping of the noise.

Keywords: Detail Mapping on Meshes, Hierarchical Meshes, Feature-sensitive Decimation, Mesh Processing, Mesh Deformation, Procedural Generation, Procedural Noise

List of Figures

List of Tables

Acronyms and Abbreviations

DAG : Discrete Acyclic Graph;
LOD : Level of Detail;
NVC : Neighboring Vertex Coincidence;
PRN : Pseudo-Random Number;
ROI : Region of Interest;

Contents

Chapter 1

Introduction

In Geometric Modeling and Computer Graphics, polygonal meshes are the most common representation for shapes and objects [1]. The recent evolution of laser scanning techniques and geometry processing algorithms has made the research related to dense meshes, with high complexity, a topic of great interest in the graphics and modeling community. This can be partially explained by the challenges posed by issues regarding storage, transmission and rendering. Such models are highly oversampled and the sheer amount of data in their representations can easily overwhelm most applications.

An important issue is mesh geometry fine editing, which can be burdensome considering the high amount of vertices that must be moved in order to make an impactful change [2]. Modifying such meshes in order to generate sharp details, such as a terrain specific erosion/topography, local bone wearing or any other common representation we find in nature, is a demanding task. This is even more difficult when dealing with arbitrary genus surfaces, where mapping these details, considering the majority of the available methods, is tightly related to the need of solving global parametrization problems. Another aspect arises when the mesh is rather plain lacking appalling details that must be added for a greater impactful effect. This is one of the main aspects we are concerned here.

1.1 Investigated problem

In few words, we can say that in this work we investigate the problem of adding details, specifically, procedurally generated details, onto meshes with arbitrary genuses with considerable level of control on the insertion process.

1.2 Objective

Our main objective is to tackle issues concerning detail manipulation on meshes by proposing a method that enables greater control when adding details both in space and scale of the mesh representation. We also require that the process of detail addition and manipulation can be applied to meshes with arbitrary topology regardless of its genuses.

1.3 Hypothesis

Our hypothesis is that tools from geometric modeling and geometry processing, as well as hierarchical representation and parameterization, are the essential components to achieve the desired results concerning both easiness of manipulation and control in the process of detail addition. We believe that an adaptive hierarchical representation is the way to cope with the complexity of dense meshes and parameterization is what leads us to deal with the problem in a simpler way by mapping the surface represented by the mesh onto a set of local Euclidean bidimensional spaces described by a triangulated coarse mesh.

1.4 Overview of the methodology

The proposed methodology is based on building a pipeline of geometry modeling and processing techniques applied to an appropriate representation and parameterization of the considered mesh. Such pipeline relies heavily on hierarchical mesh representation, feature sensitive decimation, parametrization, procedural noise generation and subdivision schemes. All these tools were carefully chosen, adapted, modified and assembled to produce a new method for dealing with the problem of detail editing on meshes with complex topology. We show the feasibility of our approach by adding different kinds of detail to different meshes that may vary in geometry and topology. Examples of localized detail addition in space and scale are presented in the results chapter. We also show results illustrating feature guided detail addition. A brief analysis of the impact of sensitive feature decimation to the base domain generation and its impact on the parameterization is also described in the same chapter.

There are many advantages of using variable resolution approaches for representing meshes. These include:

- possibility of adaptive mesh simplification;

- progressive display;
- level of detail control;
- more importantly, multiresolution editing.

The latter is one of the most important, as details usually appear in different scales and require the matching of the detail scale with the level of detail of the geometry being processed.

Adaptive hierarchical data structures can be used to construct a generalization of a multiresolution mesh obtained by subdivision. The mesh representation used in this work is based on [3], which presents a mesh simplification method that generates a variable resolution hierarchical structure called *4-K* mesh. This method is based on simple local operators for mesh modification, which are applied in parallel to an independent set of four-face clusters. We also construct a smooth parametrization of the original mesh over the base domain, where the parametrization is defined by a composition of a sequence of mappings built during the simplification process. This approach was first introduced by [4] and our method is based on it (a detailed description can be found in section 4.4.1). Although our method is based on [3] and [4] we can cite some characteristics that distinguish our approach from them. We build the 4-k mesh using a feature sensitive decimation process which enables us to build base meshes closer to the original one. By using 4-k meshes, our parameterization, in spite of being similar to [3], relies heavily on stellar operation which makes the process simpler than in [4].

This work relies on procedural noise generation approaches and subdivision schemes combined with the previous described techniques in order to produce rich details and also enable some sort of control over the pseudo-random appearance of the applied noise. The two main noise functions discussed here are the Perlin noise [5] and the Gabor noise [6]. The subdivision technique used here inspired by Loop's [7] scheme, which provides a nice manipulation tool when dealing with the problem of inserting band limited noise which is not compatible with the resolution or desired level of detail of the mesh. It is also a powerful tool for local manipulation as will be presented in Chapter 5. We must emphasize that we do not use Loop's approach here, but a mesh refinement and smoothing scheme based on it. A full demonstration of our approach and methodology can be seen in Figure 1.1.

The process described in Figure 1.1 starts with an input dense mesh with approximately 40k vertices. A decimation process then is performed, creating an adaptive hier-

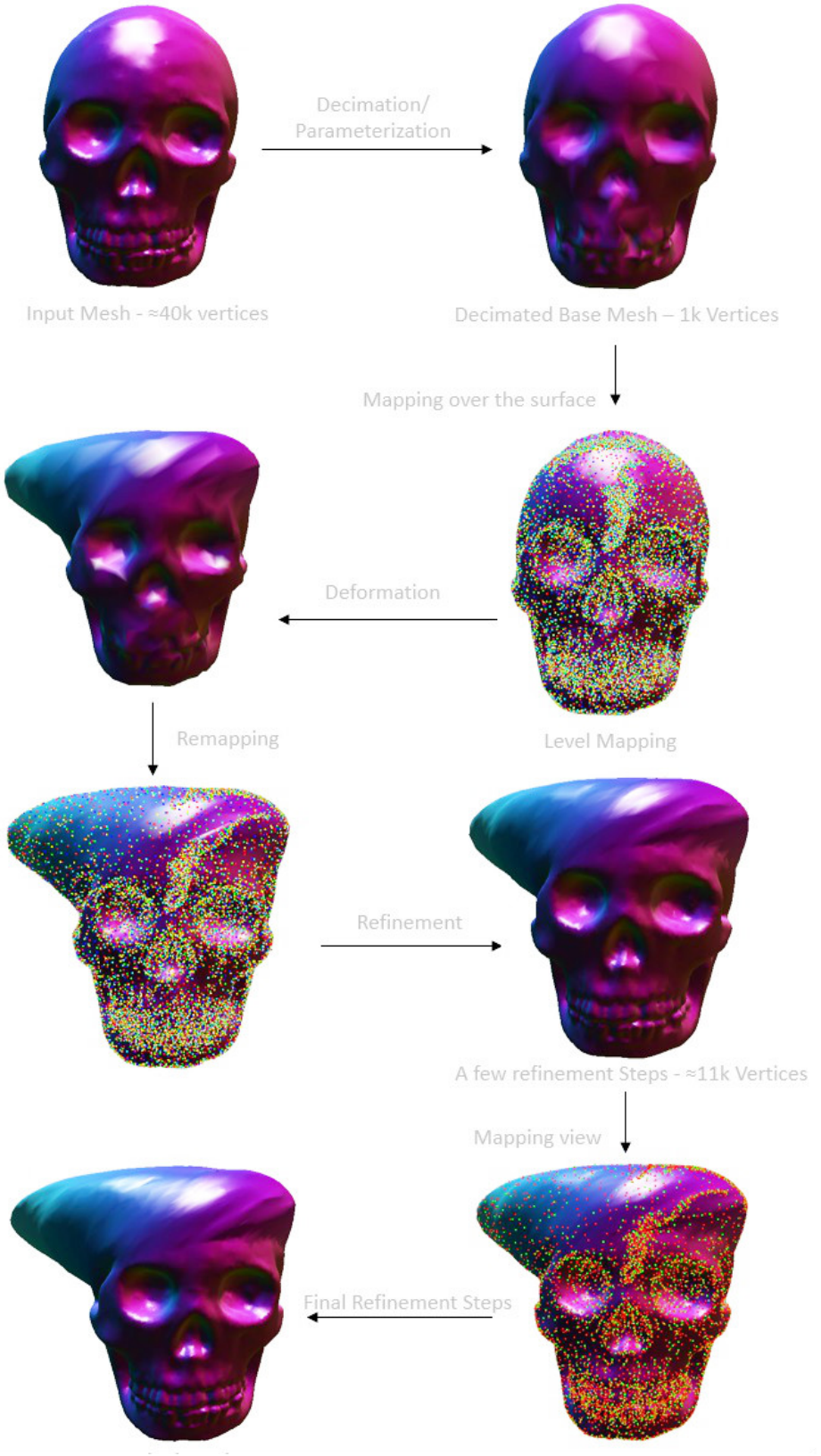

Figure 1.1: Steps representing our approach and methodology, where an input mesh is simplified, deformed and refined. Model obtained from [8].

archical structure through successive parametrizations, reducing the number of vertices by a factor of 40. The mapping of the parameterized points can also be seen in Figure 1.1 (fourth and fifth skulls). At a given resolution level (this level is user defined), a deformation is performed and a correction of the parametrization is applied (fifth skull). Then, the refinement process is initiated. One can notice that skulls six (11k vertices) and seven (40k vertices) are really similar, indicating that the input mesh is oversampled. All the steps and procedures mentioned previously will be explained in the following chapters of this thesis.

1.5 Contributions

The main contributions of this work are:

- a new method based on a combination of variable resolution mesh representations, procedural noise generation and subdivision schemes for adding details to meshes with arbitrary genuses with control over the noise scales and mesh local resolution. The insertion is done in a controlled way by matching the details in the different scales of the procedurally generated signal (a noise) with the meshes' levels of resolution.
- a novel way to build 4-k meshes without relying on storing local combinatorial operations. We simply store the original vertices in the base domain and refine it by inserting the vertices in the decimation order. To achieve this, we apply a vertex degree fix algorithm, which approximates the original geometry.
- an improvement in the 4-k base domain generation by using feature guided decimation.
- a new way to map details onto meshes using features and geometric properties of the mesh to guide the detail generation.

1.6 Thesis Organization

This work is organized as follows: the Chapter 2 presents a review of the related works, which are the basis for the development of this thesis; Chapter 3 presents a background overview, including summary of the fundamentals and main findings in the literature, which will serve as base to the models and methods that are presented in the next chapter;

Chapter 4 describes our work and its details, covering all contributions made; Chapter 5 shows the results obtained through our experiments; Finally, Chapter 6, traces future works for this research; After all chapters, we list the references cited throughout the text.

Chapter 2

Related Work

We classify the works related to the one presented here into three main categories: surface representation, procedural model or detail generation and mesh deformation.

In the surface representation category, the hierarchical structures that were considered more important for this work are reviewed, focusing on techniques that provide variable resolution representations, including the ones used as the basis for the design of algorithms proposed in this thesis.

In the procedural detail generation category, algorithms related to the procedural noise generation are analyzed. Many works are important, but we focus here in the two most commonly used: Perlin noise and the Gabor noise.

Finally, an overview of the mesh deformation approaches are presented. These include methods based on procedural approaches and the most relevant alternatives.

2.1 Surface Representation

Polygonal meshes are the main and *de facto* form of surface representation used in Computer Graphics. They can represent meshes of arbitrary topology, and resolve fine details when a sufficient amount of polygons is used. For an extremely dense mesh, interactive manipulation is a challenge. This is due to the considerable number of operations required to modify thousands or millions of vertex, edge and/or face information. In such situations, mesh simplification algorithms can provide a possible answer [9].

One of the first works dealing with hierarchical triangulations was presented by Floriani and Puppo [10], which consists of a subdivision scheme of the plane domain into nested triangulations and where the hierarchical structure is described by a tree. They

also discuss details regarding hierarchical triangulations, and provide a multiresolution surface model. Later, Puppo et al. [11] presented a generalization of the multiresolution class, extending the concepts presented in [12]. This generalization introduced the idea of variable resolution structures, where an application could extract a representation of minimum size for an arbitrary LOD (level of detail) in linear time.

In this work specifically, we make use of a variable resolution structure called hierarchical 4-k mesh, which is a powerful representation for non-uniform level of detail. This structure is based on the *Variable Resolution 4-k Meshes* introduced by Velho and Gomes [13] and is a specialization of the general variable resolution structure. To obtain such structure a hierarchical mesh simplification process is done [3].

This representation is ideal to our work, which focus on manipulating variable resolution meshes through procedural methods. This is a direct result of the characteristics of this structure, which can code all possible mesh hierarchies that can be generated from a sequence of local modifications. As presented by [11], the effectiveness of a variable resolution structure can be analyzed by three criteria: expressive power, depth and growth rate. 4-k meshes posses all these desirable properties. In Section 4.4, a detailed description of this structure is presented and for a more in-depth description we suggest reading [13].

On each step of the simplification process, a local parametrization process is performed, where the removed vertex is mapped to a lower resolution level face. In essence, this hierarchical parametrization is similar to the work presented by Lee in [4], but, as will be shown in Section 4.4.1, it has key differences when compared to our method. Lee introduced an algorithm to compute smooth parameterizations of dense 2-manifold meshes with arbitrary topology, which is used for adaptive hierarchical remeshing of these arbitrary meshes into subdivision meshes.

In [1] Maximo et al. presents an adaptive multiresolution mesh representation exploring the computational differences of the CPU and the GPU. This work considers a dense input mesh and simplify it to a base domain, similar to the work presented in [4], but here using an atlas structure. It also uses stellar operators in order to perform both, the simplification and the refinement processes. It's main objective is to show the adaptive control of the mesh resolution in CPU-GPU coupled applications. While our work is similar to Maximo's in the way the mesh representation is constructed, we can point out one key difference. Here we used a 4-k adaptation scheme instead of 4-8 used by Maximo and this choice is explained for two reasons: first we were not concerned with GPU processing; second, the use of feature decimation has led us to use 4-k meshes because of the distri-

bution of the valency of the vertices of the meshes we obtained, which made complicated the use of 4-8 meshes. Besides, in this thesis we focus in the use of 4-k structures in the problem of detail insertion. Maximo's work is also able to deal with such problem, but his approach is a more general one and not focused specifically in the aspect of detail generation. As they represent a mesh as a multiresolution atlas structure that can be used as a multiresolution grid parameterization of the mesh, general geometric processing techniques can be applied. The use of the techniques proposed here is a possibility, but this requires further investigation, in particular, how to consider feature decimation in the construction of their mesh representation. Due to the characteristics of our main objective, which is detail insertion, and not the extraction of all possible representations in the adaptive hierarchical representation, we do not store local modification operations as in the classical 4-8 and 4-k mesh. On the one hand, we only store the sequence of decimated vertices in order to navigate and manipulate the structure. On the other hand, this has obliged us to devise a new way to correct the refined mesh as we reinsert the vertices, which is our vertex valency fix algorithm. By doing this we made a trade off between local modification storage as a graph and procedural correction of the vertex fix. More about this issue will be discussed in the description of our method in Chapter 4.

2.2 Procedural Generation

Procedural methods have a great appeal and this can be explained by its characteristics. As presented by Ebert, in [14], the most important one is abstraction. In a procedural approach, every detail is abstracted into a function or an algorithm. This allows us to gain parametric control, making the manipulation of specific details an easier task, making procedural generation a powerful tool in texturing and modeling.

A variety of different effects can be produced by procedural techniques. Among them, the most basic one, is the generation of primitives with random (or pseudo-random) parameters. A plane with a randomly generated heightmap is an example of this technique and can be seen in Figure 2.1. Also, considering pseudo-random functions, it is possible to generate noise in order to create textures and natural looking formations [5]. The process of creating organic structures, such as a tree, a snow flake or a mountain silhouette can be achieved through fractal algorithms or even L-Systems. In their book, Ebert et al. [14], outline the most important features of procedural techniques: abstraction , parametric control and flexibility.

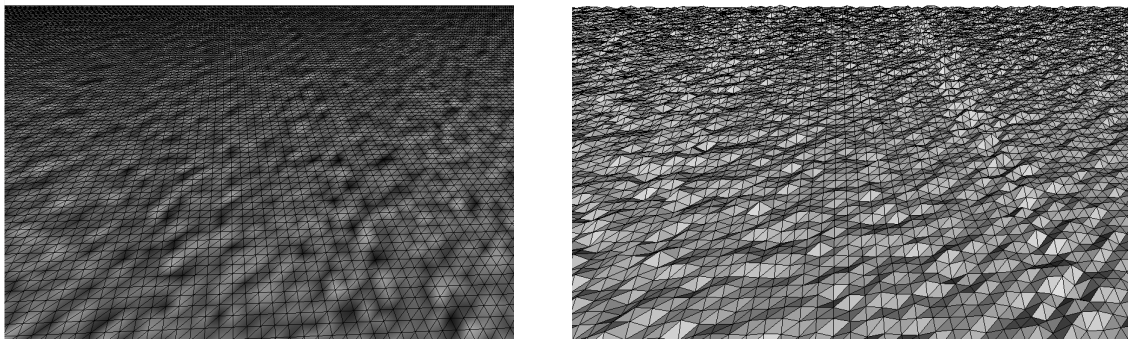

(a) (b)

Figure 2.1: (a) Pseudo-random heightmap generated over a plane. (b) Resulting deformation when applying the heightmap to modify the plane geometry.

In a procedural approach, any complex data is usually *abstracted* into a function or algorithm. This differs from non-procedural techniques, where all the data is explicitly specified and all complex detail of a scene is previously stored. This enables an on-the-fly evaluation of this function or algorithm to create the desired effect, also enabling the creation of inherent multiresolution models and textures that we can evaluate to the required resolution [14].

The *parametric control* is related to how the parameters represent information. These are defined and adjusted to match certain objectives or behavior of the procedural function or algorithm, an example is a variable that defines how rough or flat a terrain will be. This control allows the user to create as many as needed parameters amplifying its choices and possibilities for modeling or generating detail.

The *flexibility* of a procedural model is related to the possibility of designing an effect or structure without being bound to the real-world physics related to it. The process (algorithm or function) can capture the essence of the object being modeled and then, if necessary, insert the desired level of fidelity regarding the laws of physics.

These characteristics draw the attention of different industries, such as games and movies. These are always battling to meet the expectations of the public with great concern regarding the expenses to be invested for this purpose. In order to solve this issue, the most common methodology used to take care of consumer demand has always been to essentially expand the amount of artists to create more itemized, detailed and realistic content. Nonetheless, increasing the artistic pipeline does not necessarily imply in scaling the production [15].

A potential solution for the content creation problem is the application of procedu-

ral techniques. These techniques have been used for over 25 years in the field of computer graphics [14] for a wide range of applications: adding noise to existing textures and/or meshes [5], duplicate the appearance of natural materials such as marble and wood through 3D textures [16], creating and modeling life-like models of various tree and plant species [17] and generating detailed cellular textures such as skin or bark [18]. Entire procedural worlds are now possible and this is demonstrated in the MojoWorld [19] application, where assets including realistic natural features such as terrain, lakes, trees and shrubs are all generated using procedural techniques. Also, recent procedural applications have been expanded further, in order to simulate special effects including particle systems, water, and even the natural physical movements of assets [20]. Complex scenes containing many different models would normally take months to manually construct; now vast sections of these scenes can be created using specific procedural generation packages [21] that can generate detailed and varied models in minutes. Procedural generation is a time saving method of rapidly and efficiently generating content that can help to alleviate and potentially solve the problems of escalating content creation costs [22]. There are several works that deal with the procedural generation of terrains, which is one of the most discussed application of procedural techniques [23].

Existing procedural solutions primarily apply procedural techniques to the generation of natural phenomena, but many of the same techniques have obvious applications in the generation of man-made artificial phenomena.

An example are cityscapes, which presents many challenges to modeling. They are rich in visual and functional complexity, and are a result of development and evolution over hundreds of years under the influence of countless factors. Some of the major influential factors affecting cities include population, transport, environment, elevation, vegetation, geology and cultural influence. It is a formidable challenge for researchers and developers to create a realistic model of such a large and complex system [22].

In this scope, noise generation has always been of great importance to this end as it is one of the means to introduce randomized non-correlated features to the geometry or distribution of objects in scene. Specifically, Perlin noise [5] was one of the most used and explored one. Perlin in [24], deals with the important issue of controlling the appearance of the noise. This is done through spectral control and in [24] this is achieved by a weighted sum of band-limited octaves of noise. Although, this may not be the best solution, it is only a means of controlling the power spectrum of the noise. Later, Perlin [25] improved his noise by fixing discontinuities of the second order interpolation and optimizing the

gradient computation.

We consider noise control a key element to this work, and a noise generation approach that provides more of such control is presented by Lagae et al. [6]. He introduced a procedural noise using sparse Gabor convolution which provides accurate spectral control using Gabor kernels. Also, this approach has two qualities: it does not have the regularity and discontinuity problems of Perlin's noise function and at the same time enables anisotropic noise generation. Later, Lagae et al. in [26] presented a filtered version of the Gabor noise, where a slicing approach is introduced in order to preserve continuity across sharp edges. He also deals with the issue of keeping the anisotropic feature in a sliced solid noise. More recently, in [27], a generalization of the Gabor noise is introduced by Galerne, where a bandwidth-quantized Gabor noise with arbitrary power spectra is presented. This enables a robust parameter estimation and efficient procedural evaluation.

2.3 Mesh Deformation

Mesh deformation is a challenging topic, since the techniques involved must encapsulate complex mathematical formulations into an intuitive user interface and, more importantly, must be developed to achieve efficiency and robustness, allowing real-time interactions and manipulations.

Shape editing has been an extremely active field ever since the early beginnings of computer graphics and accordingly a variety of approaches exist ranging from classical splines to multiresolution techniques and space deformations. We will give only a brief overview of the principal approaches here and refer for a more general review of shape editing to [28] and [29].

Tensor product splines are nowadays the prevailing representation for surfaces in computer aided design. In many applications, surfaces are created from scratch in this representation. Spline basis functions have a number of desirable properties, e.g. local support and positive partition of unity that give linear coefficients - the control points - an intuitive interpretation and thus simplify subsequent editing. Conversion of large unstructured point clouds or triangle meshes as acquired by scanning devices or photometric stereo into a spline based representation is, however, difficult and still an active topic of research. Large or complex surfaces usually require tensor product spline patches with several hundreds of degrees of freedom. Except for changes to small details, the editing of such surfaces thus involves modifications of many control points and is therefore often

tedious and troublesome.

To overcome restrictions of tensor product spline surfaces, a second class of approaches [30, 31, 32] is based on what is called transformation propagation. The user initializes the editing process by selecting a subset of the surface as **region-of-interest** (ROI) R. Within this region, he then selects two further subsets: a fixed subset F and a handle subset H. The points in the handle subset H are then transformed interactively by some user specified transformation (usually translation, rotation and scaling). The deformable model interactively computes positions for the remaining surface points in the region-of-interest. This general editing metaphor introduced by [30] and [33] is also used in shape editing based on deformation potentials that will be discussed below. In transformation propagation approaches, the handle transformation is propagated through the regions of interest until it reaches the fixed subset F. Each point within R is transformed with an interpolation of the handle transformation and the original fixed transformation at F according to some function of its distance to these regions. As demonstrated in [29] transformation propagation does not necessarily lead to intuitive deformations.

Multiresolution deformation techniques decompose the original surface into a low-pass filtered coarse approximation and high-frequency details. The actual parameters of the filter can be configured by the user to select the level-of-detail of interest. Modifications are then applied to the coarse version of the surface e.g. by transformation propagation or any arbitrary editing technique. Finally, the stored high-frequency details are added on top of the edited version of the coarse approximation. Approaches differ, first of all, in the way high frequency detail is represented and fused with the edited coarse mesh.

In all surface-based deformation techniques the quality of deformations is inherently linked to mesh quality. Problems in the triangulation like cracks or degenerate triangles inevitably lead to deformation artifacts. Furthermore, the speed of such methods decreases with the mesh resolution so that very high mesh resolutions result in non-interactive frame rates. Space deformation methods avoid these problems by deforming the space surrounding the object. The embedded surface is deformed by applying this space deformation to every point. Space deformations can for example be defined by tensor product splines, radial basis functions or specially designed cages around the surface in question. The complexity of the deformation then only depends on the complexity of the control structure, e.g. the number of control points or cage cells. As the actual surface mesh is not involved in the computations, space deformation approaches handle meshing problems gracefully and can equally be applied to point sets. On the downside,

special care must be taken to ensure sufficient resolution and correct topology of control structures.

Finally, another class of approaches minimizes surface-based deformation potentials for shape editing. For user interaction the same general editing metaphor is used as with transformation propagation based editing. In contrast to transformation propagation, the unconstrained surface within the region-of-interest is updated by minimizing a potential functional on the surface. Possible choices of the potential functional include linear approximations of the elastic energy discussed in Section 3.2.1. Apart from these, mesh editing methods based on differential representations, as they have become very popular in the last years, also naturally lead to deformation potentials and can therefore be subsumed into this class of approaches.

In our scope, an important work is presented by Velho in [34] where he introduce a framework that integrates procedural shape synthesis on a modeling system. This is done using multiresolution analysis through surface subdivision based on Catmull-Clark [35]. This is a key difference in relation to our work, in which a variable resolution structure is used, where we guarantee feature preservation in the base domain. This last characteristic has some advantages, enabling, for instance, the creation of level of detail structures with better quality. Regarding feature guided mesh editing, Biermman [36] describe a method to introduce sharp features and trim regions on a surface. Similarly to Velho's work, he uses a multiresolution representation also using Catmull-Clark subdivision scheme.

The subdivision surfaces mentioned before, are defined by progressive refinement rules applied to an initial polygonal mesh (in some cases a base domain). For example, Catmull-Clark subdivision inserts new vertices at the center of each edge and face, and then displaces the vertices based on simple linear weights. Considering a initial quad-mesh, this process converges to a bi-cubic B-spline surface defined by this mesh [37]. However, this scheme lacks the adaptive feature of a variable resolution representation.

In this chapter we presented the most important references that relates to our problem and solution, including relevant surface representation methods, procedural detail generation algorithms and mesh deformation approaches. In the next Chapter, all the necessary background information, needed for a better understanding of the rest of this thesis, will be presented. Including object representations, parametrization and procedural noise functions.

Chapter 3

Background

This chapter presents the basic information needed to the comprehension of this thesis. The main objective is to expose the technical and theoretical background, establishing the basis for the methodology that will be described to solve the problem.

Here, we will focus on the following topics: representation of geometric data using meshes and the types of geometric and topological operators used by the majority of the problems of geometry processing; construction of topological data structures in variable resolution; simplification strategies, parameterization methods and procedural noise functions, considered in the methodology we propose.

3.1 Object Representations

In geometry processing, identifying the most prominent set of operators by which the computation is dominated is paramount to every problem. This leads to the definition of the most appropriate data structure used to support the efficient implementation of these operators. In this work, all objects can be approximated by polyhedral surfaces [38], which can be understood as geometric realizations of 2D meshes, which are usually used to describe the topology of a subdivision of two-dimensional domains.

3.1.1 Polyhedral Meshes

According to algebraic topology, a mesh M can be defined as a pair (K, V), where K is a simplicial complex that represents the connectivity of vertex, edges and faces, determining the topological type of the mesh. Thus, V is a set of vertex positions $\{v_1, ..., v_n\}$, $v_i \in \mathbb{R}^3$, which defines the mesh geometry.

A simplicial complex K is a vertex set $\{1, ..., n\}$, composed by a finite number of simplexes, which are non-empty subsets of these vertices. $0 - simplexes$ $\{i\} \in K$ are vertices, $1 - simplexes$ $\{i, j\} \in K$ are edges and $2 - simplexes$ $\{i, j, k\} \in K$ are faces (triangles). In general, $n - simplexes$ are polytopes with n+1 vertices.

One of the main mesh types used in geometry and graphics processing is the triangle mesh. Triangles have several properties that justify the previous statement. One of the most important, among such properties, is the ability to define coordinate systems in the mesh structure using barycentric coordinates. This allows the construction of parametrizations for surfaces with disk topology, solving both the problem of representation and reconstruction.

3.1.2 Geometric Operators Operators on Meshes

Since polygonal meshes are piecewise linear surfaces, the approximation of differential properties of the underlying surface can be obtained from the mesh data. This is due to the fact that meshes can be interpreted as piecewise linear approximations of smooth surfaces. The following definitions present the most basic operators and are based on Botsch's et al. [39].

3.1.2.1 Normal Vectors

Calculating normal vectors to either faces or vertices, is critical for most methods of geometry processing. For triangles described by vertices (x_i, x_j, x_k), the normalized normal vector can be obtained by equation 3.1.

$$n(T) = \frac{(x_j - x_i) \times (x_k - x_i)}{\|(x_j - x_i) \times (x_k - x_i)\|} \tag{3.1}$$

The normal vector at a vertex v can be calculated by a weighted average of the normals for each incident face $n(T)$ in a neighborhood N_1 of v, with weights given by $\alpha(T)$.

$$n(v) = \frac{\sum_{T \in N_1(v)} \alpha_T n(T)}{\left\| \sum_{T \in N_1(v)} \alpha_T n(T) \right\|} \tag{3.2}$$

Botsch et al. [39] discuss several possibilities for weights. Here we follow them closely:

- Uniform ($\alpha(T) = 1$) : it is efficient, but produces counter-intuitive results, since it does not consider edge lengths, triangle area or angle at the vertex. In other words,

it does not consider the geometry of the mesh.

- Based on the triangle area ($\alpha(T) = A_T$): also efficient, but can also lead to counter-intuitive results(Figure 3.1).
- Based on the incident angle of the triangle ($\alpha(T) = \theta_T$): corresponds to mean values computed in small geodesic disks; generally produces the best results.

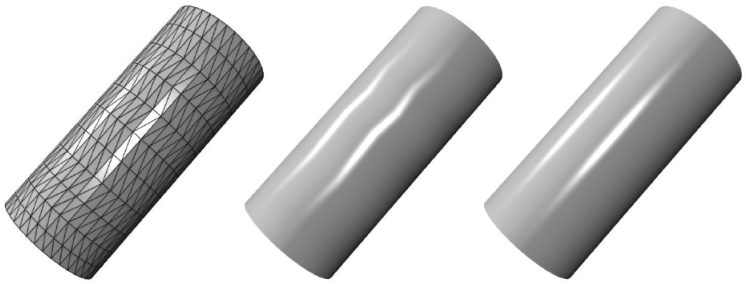

Figure 3.1: Different methods are used to compute per-vertex normals. Using constant and area weights yields the result in the center, while the results using angle weights can be seen on the right. Figure obtained from the book Polygon Mesh Processing [39].

3.1.2.2 Gradients

The discrete gradient of a piecewise linear function f_i defined at each vertex v_i, can be computed from Equation 3.3. In Equation 3.3, $f_i = f(v_i) = f(x_i) = f(u_i)$ and $u = (u, v)$ is an ordered pair in the conformal parameter space.

$$\nabla f(u) = (f_j - f_i)\frac{(x_i - x_k)^{\perp}}{2A_T} + (f_k - f_i)\frac{(x_j - x_k)^{\perp}}{2A_T} \tag{3.3}$$

3.1.2.3 Discrete Mean Curvature

The Laplace-Beltrami operator presented by Taubin [40] (see Equation 3.4), when applied to the coordinate x_i of a vertex v_i, yields a discrete approximation of the mean curvature.

$$\nabla f(v_i) = \frac{1}{2A_i} \sum_{v_j \in N_1(v_i)} (\cot \alpha_{i,j} + \cot \beta_{i,j})(f_j - f_i) \tag{3.4}$$

Therefore, it is possible to set the absolute mean curvature as:

$$H(v_i) = \frac{1}{2} \|\Delta x + i\| \tag{3.5}$$

For the Gaussian curvature, it is possible to use the following expression, based on the Gauss-Bonet theorem, where θ_j is the angle of the incident triangles of v_i:

$$K(v_i) = \frac{1}{A_i} \left(2\pi - \sum_{v_j \in N_1(v_i)} \theta_j \right) \tag{3.6}$$

Given the formulas for the discrete mean and Gaussian curvatures, it is possible to compute the principal curvatures k_1 and k_2 from the formula:

$$k_{1,2} = H(v_i) \pm \sqrt{H(v_i)^2 - K(v_i)} \tag{3.7}$$

To end this section, we can mention the following works that present, in greater depth, the various discrete operators and their properties and characteristics, such as convergence and robustness: [41, 42, 43, 44], and [45].

3.1.3 Topological Data-structures

The representation of an object by a polygonal mesh is the problem of describing a continuous model by a finite set of primitives. This process must guarantee that topological and geometrical characteristics of the original object are maintained. There is also, when dealing with the computational side of this problem, the implementation issues related to data structure definitions, in order to store such information.

The main issue to be dealt with is the definition of operations supposed to be performed on the models, which can be implemented as algorithms associated with such data structures. In the literature, there are many works that deal with this matter, as seen in Chapter 2, where each method seeks to meet a set of properties that vary according to the application or problem which it is intended to deal with. Nevertheless, there exists key requirements that every structure for mesh representation must be conformed with: minimize redundancy; efficient use of storage space; ability to respond to spatial and topological queries efficiently; ability to describe levels of detail and hierarchy relationships.

Velho et al. in [38], makes a parallel between a structure for mesh representation and a geometric database, due to the need to efficiently respond to geometrical and topological queries. This is of major importance when designing such data structure, where queries like boundary of a face or a vertex star must be answered in optimal time.

Indeed, these are the most common operations that can be applied to a mesh structure, but there are other ones that must be considered, for example, refinement and smoothing operations on surfaces, which are the result of subdivision processes ([7, 46, 47, 48, 49]); application of discrete differential operators, application of topological operators; and operations to manipulate levels of detail (local changes) ([10]).

In the literature, one can find many different topological data structures, usually proposed to solve a specific problem or problems that incorporate a variety of properties expanding precursor data structures. Although initially topological data structures have been created in order to represent subdivisions and objects with the topology of the sphere, these have evolved to deal with more complex problems.

Considering the most influential works related to the construction of such structures, we can name the Winged-Edge Baumgart [50] and Mäntylä's Half-Edge [51]. Also, others that should be cited in the text, are: the Corner Table [52], a compact and efficient structure to describe triangulations based on indexes and integer arithmetic operations; the Lage's [53] CHE and Gurung's [54] sQuad.

3.1.4 Representation of Meshes at Multiple Levels of Detail

In this thesis, the necessity of representing objects at different levels of detail is paramount. Also, it is important to have the ability to manipulate objects considering a greater level of detail in some areas than in others. This is also a concern in the geometry processing area, leading to an investigation of data structure algorithms that can support such functionality.

Due to the characteristics of the concept of level of detail, one can create a relation with the notion of hierarchy. Thus, according to Velho and Gomes in [13], hierarchical data structures are a natural option to give computational support to representations with multiple levels of detail. Still according to them, hierarchical data structures are the materialization of abstraction mechanisms used to deal with complexity and relationships between entities at different levels, where these relations depend on the application and the context of the problem.

Velho and Gomes define a mesh hierarchy as a sequence of meshes $H = M^j, j = 1..., n-1$, such that the size of a mesh M^j monotonically increases with the index j. It is important to mention that, the mesh hierarchy must capture and maintain the dependency relationships between faces of two consecutive levels j and $j+1$, whose support overlap. These are constructed through operations denominated *local movements*, which can both refine and simplify an initial mesh. Examples of operators that can perform local movements are *stellar operators*. The type of the local modification operator defines the properties of the hierarchy, which can be adaptive or non-adaptive.

3.1.4.1 Non-Adaptive Hierarchical Structures

A non-adaptive hierarchical structure defines a single mesh hierarchy [13]. Multiresolution and Progressive Meshes are typical examples of non-adaptive hierarchical data structures. On the one hand, multiresolution meshes are characterized by the fact that operations are applied in parallel on a whole set of independent regions covering the whole mesh, changing the resolution globally. On the other hand, progressive meshes apply these modifications sequentially to each specific region separately.

A tree data structure is used to capture the structure and relationships of a multiresolution mesh, which is usually built via multiresolution refinement(Figure 3.2).

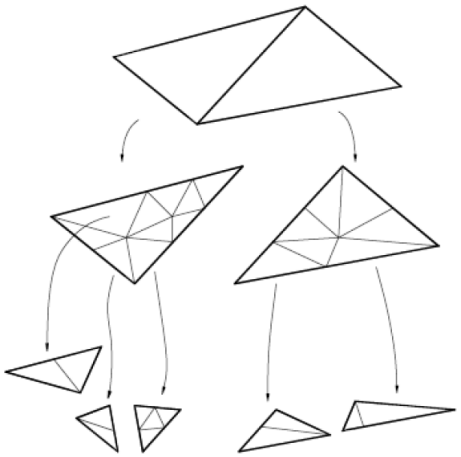

Figure 3.2: Tree representation of an enclosing hierarchy. Figure obtained from [10].

Differently, on progressive meshes, the corresponding data structure is a list data structure which is usually constructed via simplification.

3.1.4.2 Adaptive Hierarchical Structure

Adaptive hierarchical structures construct a family of mesh hierarchies. An example of this structure is a *variable resolution mesh* and the data structure for representing it is a DAG (Discrete Acyclic Graph). Such structures can be created either by refining or simplification processes, also known as decimation. In such data structures, local modification operations are applied to independent region sets, but they do not necessarily cover the entire mesh, with the constraint that the edges defining the boundary of the region must not be changed, generating the concept of *minimally compatible local changes*.

In the sequel, three hierarchical structures for meshes are presented, two adaptive ones and one non-adaptive structure.

Hierarchical Triangulation

Floriani and Puppo [10] introduced the idea of hierarchical triangulations, which is an example of multiresolution hierarchical structure. The proposed definition for this triangulation is a triple $TH = (Tr, E, l)$ representing a tree, where Tr are the nodes corresponding to a sequence of triangulations, E is a set of labeled arcs that connect the different triangulations according to the hierarchical relationships and l is a labeling function. Figure 3.2 shows exactly this type of structure.

Formally defined as:

- $Tr = \{\tau_0, \tau_1, ..., \tau_h\}, \forall_j = 0, ..., h$, $\tau_j = \{V_j, E_j, T_j\}$ with $T_j > 1$ and $\forall_j > 0$ there is only one triangle $t_j \in T_i$, for some $i < j$, $t_j = D(T_j)$ where $D(T_j)$ is the domain of the triangulation τ_j, defined by the union of the triangles in T_j.
- $E = (\tau_i, \tau_j), \tau_i, \tau_j \in T_r, \exists t_j \in T_i,\ t_j = D(T_j)$ where E is a set of labeled arcs connecting two triangulations τ_i and τ_j where τ_j is the refinement of a triangle in T_i.
- $l : E \rightarrow \cup_{\{i=0,...,h\}} T_i, l(\tau_i, \tau_j) = t_j$ if $t_j \in T_i$ and $t_j = D(T_j)$. Every triangle in $l(E)$ is a *macrotriangle*, while triangles that do not belong to $l(E)$ are considered *simple triangles*.

The data structure used to code a hierarchical triangulation is based on the Edelsbrunner's graph of incidence [55]. Thus, let $GI = \{GI_0, GI_1, ..., GI_h\}$ be a collection of

incidence graphs. Hence, a hierarchical graph of incidence is a triple $GIH = \{GI, E_g, l_g\}$ where:

- $E_g = \{(GI_j, GI_i) | (\tau_i, \tau_j) \in E\}$
- $l_g : E_g \rightarrow \cup_{\{i=0,...,h\}} NT_i, l_g(GI_j, GI_i) = \eta_T^{-1}(l(\tau_i, \tau_j))$

To search for the neighbors, the structure proposed by Floriani stores a set of arcs linking neighbors in the structure, which are called strings. The construction of the hierarchical graph of incidence is presented in details in [55].

4-k Meshes

A variable resolution 4-k mesh, proposed by Gomes and Velho, is a hierarchical structure that contains at each level approximately half of its vertices of valence four and other vertices of arbitrary valence k.

Variable resolution triangulations are based on the concept of **minimally compatible local changes**. The descriptions presented here are based on Gomes and Velho's work [13].

> **Definition 1 (Minimally Compatible Local Changes).** "A minimally compatible local change $W(K^i)$, applied to a submesh $M^i \subset M$ of a mesh $M = (V, E, F)$, is a substitution of M^i by $W(M^i)$, which satisfies the following properties:
>
> Edges of the border of M^i are not altered.
>
> Interior edges of M^i are replaced by new edges."

The submeshes K^i and $W(M^i)$ are the pre-image and image of the local modification operator W.

> **Definition 2 (Compatible mesh sequence).** "A mesh sequence $\{M^0, M^1, M^2, ..., M^n\}$, generated by applying a sequence of operators $\{W_1, W_2, ..., W_n\}$, starting with a initial mesh M^0, generates a compatible mesh sequence. The sequence generated by this approach is given by $\{M^0, W_1(M^1), ..., W_n(M^n)\}$ where $M^j = W_{j-1}(W_{j-2}(...W_1(M^1)))$, $j > 0$".

A fundamental difference between a mesh structure with variable resolution and a multiresolution structure is that, given a intermediate mesh M^m and two compatible operations W_i and W_j, it is possible to generate two new distinct meshes $M^{m+1} = W_i(M^i)$ or $M^{m+1} = W_j(M^j), M^i, M^j \subset M^m$.

The purpose of a variable resolution structure is being able to code all possible mesh hierarchies through a valid sequence of minimally compatible local changes.

> **Definition 3 (Variable resolution mesh).** "A mesh $M = (M^0, W, \leq)$ is defined by a initial mesh M^0, a set of operators $W = \{W_0, W_1, ..., W_n\}$ and a relation of partial order $\leq$, defined over the operators satisfying dependency and non redundancy properties. Dependency implies that, if $f \in F_i$, on the pre-image M^i of $W_i(M_i)$ and also belongs to $W_j(M^j)$ then W_i precedes W_j. The non-redundancy implies the fact that, if $f \in F_i$ of $W_i(M_i)$, then $f \notin F_j$ of $W_j(M_j)$ for all $i \neq j$".

The 4-k structure was proposed by Gomes and Velho through the specialization of the model described by Puppo for triangulations based on a 4-8 mesh, which itself is based on Laves tilings[4.8^2]. As will be presented in the next section, on regular 4-8 meshes, vertices always have valency 4 or 8, on semi-regular 4-8 meshes it is possible to find isolated extraordinary vertices, and on quasi-regular 4-8 meshes there are extraordinary vertices that are not necessarily isolated.

The 4-8 meshes are refinable and it is possible to build a multiresolution structure based on subdivision operators, which can be quaternary or interleaved binaries, the latter being the most widely used. The multiresolution representation for 4-8 meshes is done through a quaternary or binary tree structure, depending on the operator type.

On the other hand, 4-k meshes are hierarchical structures, with variable resolution, in which approximately half of the vertices have valency 4 and the other half has valency k. The local modification operators are restrained to clusters of two triangles forming a convex structure and can be of two types: edge split and edge swap(flip) (see Figure 3.3).

In the implementation of the 4-k mesh, a combination of elements of edge and face types are used. The edge split operator is a refinement operator, which makes the edge that separates two faces to be subdivided, making two faces give rise to four new faces. Therefore, the data structure for edges must maintain a pointer to the two faces thereto adjacent, and each face must maintain two pointers to their faces' children, which in turn points to the parent faces. The edge swap operator does not subdivide edges, then one of the pointers of the face structure is kept as null.

(a) (b)

Figure 3.3: Stellar operators:(a) Face split and face weld. (b) Edge split and edge weld.

An example of variable resolution mesh structure is the 4-k structure. The 4-k meshes have good expressiveness power, derived in part of some properties it shares with 4-8 meshes. Besides that, it is possible to easily implement, in the structure, variable resolution query operations and adaptive mesh extraction.

4-8 Tessellations and Meshes

A 4-8 tessellation is a refinable tiling. It exploits the self-similarity subdivision characteristic of a $[4.8^2]$. Therefore, it is possible to construct a multiresolution 4-8 tessellation using refinement. In this structure we can name some advantages:

- The $[4.8^2]$ Laves tiling is a triangulated quadrangulation, thus it combines the advantage of both triangular and quadrilateral meshes;
- They can generate adaptive tessellations in variable resolution, due to the support of both uniform and non-uniform refinement;
- Both available construction methods are intuitive and easy to implement.

There are two alternative construction methods: quaternary subdivision and interleaved binary subdivision.

The quaternary subdivision refinement algorithm for a given 4-8 mesh $M = (V, E, F)$ is shown in Algorithm 1 and is represented in Figure 3.4(a):

Algorithm 1. Quaternary Subdivision

1. Split all edges $e \in E$ at their midpoints m;

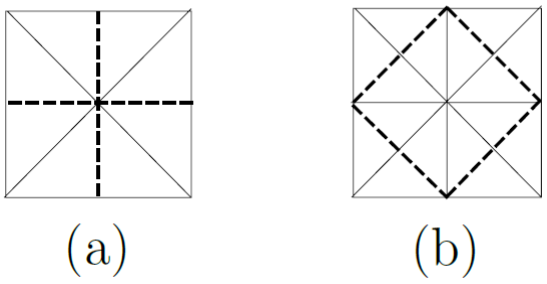

Figure 3.4: (a) Binary subdivision. (b) Quaternary subdivision. Image based on an image presented in [48]

2. Subdivide all faces $f \in F$ into four new faces, linking the degree four vertex, $v \in V_4$, to the midpoint m of the opposite edge.
3. Link m to the midpoints of the two other edges.

The interleaved binary subdivision is as follows and can be seen in Figure 3.4(b):

Algorithm 2. Interleaved Binary Subdivision

Repeat two times:

1. Split all edges $e = (v_i, v_j) \in E$ that are formed by two vertices of valence 8, $v_i, v_j \in V_8$;
2. Subdivide all faces $f \in F$ into two sub-faces, by linking the degree 4 vertex, $v \in V_4$, to the midpoint m of the opposing edge.

A multiresolution 4-8 mesh can be represented through a tree structure of triangles. Depending on the type of refinement used, this tree is a binary or quaternary one.

We have three types of 4-8 meshes: Regular 4-8 meshes, Semi-Regular 4-8 meshes and Quasi-Regular 4-8 meshes. A **Regular 4-8 mesh** is homogeneous simplicial complex that has the same connectivity of a $[4.8^2]$ tiling [13], meaning that all vertices in this representation has valence 4 or 8 and are all regular vertices. Another important characteristic is that all valence 4 vertices have only valence 8 neighbors(1-neighborhood), and all valence 8 vertices have neighbors consisting of vertices with alternating valences 4 and 8. A **Semi-Regular 4-8 mesh** is a tessellation that has isolated extraordinary vertices, whose valence is different than 4 or 8. Usually these meshes are created from a coarse irregular mesh by applying a semi-regular 4-8 refinement method that introduces only

regular vertices [56]. Finally, a **Quasi-Regular 4-8 mesh** is a tessellation where, differently from the previously mentioned representation, irregular vertices are not guaranteed to be isolated.

3.1.5 Simplification

A mesh simplification describes a class of algorithms that has the aim of transforming a mesh into another with fewer faces, edges and vertices [57]. There are two ways of defining this problem: a first approach that aims to generate a mesh of fixed size and a second one that seeks the best geometric approximation. Solving the simplification problem is also the starting point of the solution of other problems, like the construction of hierarchies, which is part of the proposal of this work.

The optimal solution of the simplification problem is not always possible, since it is NP-Hard, thus interactive heuristic methods were developed in order to achieve a defined criterion. This is done by applying a simplification operator onto the mesh.

In the literature, there are several approaches regarding the mesh simplification. Initially, as mentioned in [39], the complexity reduction can be done as a one-step operation or by an interactive process. These approaches are defined, by Paul Heckbert in [58] as: vertex clustering algorithms, incremental decimation algorithms, resampling algorithms and mesh approximation algorithms.

Also, an important observation is that all simplicial complexes can be transformed into a simpler one, through a simple sequence of *edge swap* and *edge collapse* operators, allowing the definition of simplification operators that preserve the mesh topology, a major concept to this work.

3.1.6 Simplification based on the quadric error metric

In order to provide a powerful, yet simple approach for a mesh simplification, Garland and Heckbert introduced an algorithm based on the vertex pair contraction [58]. This is one of the most common methods and is defined by selecting two vertices v_1 and v_2, and performing a contraction operation, where both vertices are moved to a new position v. Then, all incident edges connected to v_1 and v_2 are removed. Any face that becomes degenerated is removed, guaranteeing the model consistency.

The success of the pair contraction operation directly depends on the choice of which

vertex pairs should be contracted at each simplification step. Garland and Heckbert introduced a quadric error metric, that is associated to each pair, this gives an efficient way to estimate the geometric error between the original and simplified surfaces [3]. Specifically, for each vertex v_i, a symmetric matrix Q, of order 4×4, that encodes a quadric surface, and the error measured in v_i is given by the quadric form $\Delta v_i = v_i^T Q v_i$. Thus, to determine which pair to be chosen, we define the cost of the contraction operation of two vertices $(v_1, v_2) \rightarrow v$ by the form $\Delta v = v^T(Q_1 + Q_2)v$, where Q_1 and Q_2 are the quadrics associated to v_1 and v_2 respectively.

This algorithm has useful properties, given the local nature of its modification operator. It is possible, for example, to generate a sequence of models $(M_n, M_{n-1}, ..., M_g)$, based on a certain level of simplification, that can build a progressive mesh structure. This idea is really similar to Hoppe's algorithm defined in [9].

The simplification algorithm can be resumed in the following pseudo-code:

Algorithm 1. Simplification based on the quadric error metric

1. Determine all Q_i matrices for all initial vertices v_i;
2. Select all valid pairs {typically all vertices connected by an edge};
3. Determine the optimal v_{ij} positioning of each contraction pair v_i, v_j, considering the contraction cost of each pair is given by $v_{ij}^T(Q_i, Q_j)v_{ij}$;
4. Insert all pairs into a *heap* structure, where the key will be defined by the contraction cost;
5. Iteratively remove each pair (v_i, v_j) associated with the lower *heap* cost and update all costs of pairs related to v_1.

3.1.7 Simplification based on four-face clusters

As it will be seen in Chapter 4, in this work we use a simplification algorithm denominated four-face clusters mesh simplification [3].

This algorithm focus on removing vertices that has a valence equal to four. In its first step, all vertices of the mesh are associated with a removal cost. The definition of this metric is based on the configuration of the simplification operator, which is a combination of edge swaps and degree 4 vertex removal (the vertex removal can be achieved through a stellar *edge-weld* operation as Figure 3.6 shows). Thus, the error $E(v)$, which is the

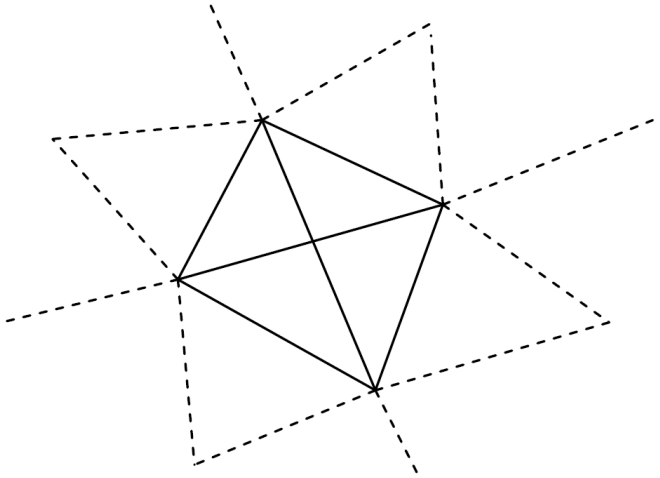

Figure 3.5: Four face cluster.

result of the removal of the vertex v, is computed as the sum of costs of performing the mentioned operations, as described in Equation 3.8:

$$E(v) = \alpha C(v) + \beta S(v), \tag{3.8}$$

where $C(v)$ is the cost of removing the vertex v and $S(v)$ is the cost of edge swaps necessary to make v a vertex of valence four [3]. This is equivalent to the vertex pair contraction cost used by Garland and Heckbert [58], meaning that, both, $C(v)$ and $S(v)$ are measured following Garland and Heckbert quadric error.

Algorithm 2. Simplification using four-face clusters

1. Order all vertices based on a quality criteria;
2. Select an independent set of four-face clusters that covers most of the mesh;
3. Simplify the four-face clusters using *edge swaps* and removal of vertices with degree equal to four.

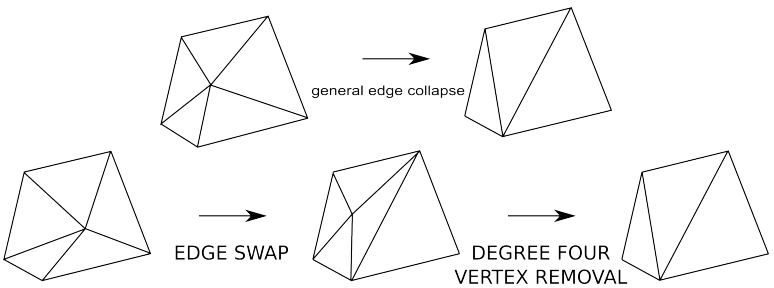

Figure 3.6: Edge contraction operation using edge swaps and edge weld.

This algorithm performs the sequence of operations in parallel, thus, to cover most of the mesh, Velho and Gomes in [3] introduced a cluster marking strategy, that creates an independent set of face clusters. To achieve this, vertices are fist stored in a priority queue ordered by the error $E(v)$. While the queue is not empty, the first vertex (associated with the lowest error) is removed, and if it is not marked, a sequence of edge swaps is applied to make the degree of v equal to four. The vertices on the star of the cluster surrounding v are marked to allow the construction of an independent set. Finally, the third step of the algorithm, all vertices in the center of the independent sets are removed in parallel, generating one level of simplification.

3.2 Parametrization

As presented by Botsch et al. in [39], the notion of parametrization attaches a geometric coordinate system to an object, which facilitates the conversion from one mesh representation to another. There are several applications of a mesh parametrization, such as: texture mapping, re-meshing algorithms and conversion from one mesh representation to an alternative one.

Parametrization is of major importance to this work, due to the possibility of transforming complex 3D modeling problems into a 2D space where, usually, they are easier to solve. Defining it more formally as presented in [39]: "a parametrization of a 3D surface is a function putting this surface in one-to-one correspondence with a 2D domain."

Parameterization methods belong to two main classes: local parametrizations which build the parameterization considering only the local aspects of the surface and the global parameterization that works on it as a whole. The description of all these methods is beyond the purpose of this thesis and here we only present two examples of such methods, the Floater's barycentric parameterization [59] and the Duchamp's parametrization based on conformal mapping [60].

3.2.1 Triangle Mesh Parametrization

Triangle surfaces can be defined by a mesh M and a set of positions $p_1, ..., p_n$. The mesh M is defined by the triplet (V, E, T), where V is a set of vertices, E is a set of edges and T is a set of triangular faces. These are naturally parameterized using piecewise linear functions, whose pieces, in this case, are related to the triangles of the surface. This associates to each point p an ordered pair u, v in the parameter space. At a given point

(u, v), in the parameter space, the parametrization is given by:

$$x(u, v) = \alpha p_i + \beta p_j + \gamma p_k \tag{3.9}$$

where p_i, p_j and p_k are the the vertices of the triangle $t \in T$, that contains the point (u, v), and α, β and γ are barycentric coordinates in relation to t. Also, in order to guarantee a valid parametrization, the image of the surface in the parameter space must have no self-intersections.

3.2.2 Barycentric Parametrization

The barycentric map is one of the most used methods in the literature for constructing a parametrization of a triangulated surface [39]. It was proposed by Floater [59] and is based on Tutte's theorem [61], from Graph Theory. The theorem states the following:

> **Theorem** [61]. "Given a triangulated surface homeomorphic to a disk, if the (u, v) coordinates at the boundary vertices lie on a convex polygon, and if the coordinates of the internal vertices are a convex combination of their neighbors, then the (u, v) coordinates form a valid parameterization (without self-intersections)."

The second condition of this theorem, as presented in [39], is expressed mathematically by:

$$\forall i \in \{1, ..., N_{int}\} : -a_{i,j} \begin{pmatrix} u_i \\ v_i \end{pmatrix} = \sum_{j \neq i} a_{i,j} \begin{pmatrix} u_j \\ v_i \end{pmatrix} \tag{3.10}$$

where the vertices are ordered such that $\{1, ..., N_{int}\}$ correspond to the indexes of the inner and vertices $\{N_{int} + 1, ..., N\}$ are the indexes of the vertices of the border. Furthermore, the coefficients $a_{i,j}$ are defined according to the following rule:

$a_{i,j} > 0$, if v_i and v_j are connected by an edge,

$a_{i,i} = -\sum_{j \neq i} a_{i,j}$

$a_{i,j} = 0$, otherwise.

Thus, the solution of the parameterization problem can be obtained by solving the following system, whose solution sets the coordinates in the parameter space of the interior

vertices, once determined the coordinates of the vertices of the edge.

$$\forall i \in \{1, ..., N_{int}\} : \begin{cases} \sum_{j=1}^{N_{int}} a_{i,j} u_j = \overline{u_i} = - \sum_{j=N_{int}+1}^{N} a_{i,j} u_j \\ \sum_{j=1}^{N_{int}} a_{i,j} v_j = \overline{v_i} = - \sum_{j=N_{int}+1}^{N} a_{i,j} v_j \end{cases} \tag{3.11}$$

3.2.3 Parametrization Based on Conformal Mapping

The idea of parametrization is related to the problem of defining and computing a good map between two surfaces. A straight forward approach is to find a map that minimizes angular distortions, leading to the preservation of local surface geometry. Hence, a natural choice are conformal maps. These are tightly related to complex analysis. It relies on the conformality condition, which defines a criterion with enough rigidity to offer good extrapolation capabilities that can compute natural boundaries [39].

In Lee et al. [4], a conformal mapping z^a is defined, which minimizes the distortion metric to map the neighborhood of a vertex to the plane. The advantages of a conformal mapping are that it always exists from any surface with a disk topology to a 2D planar domain, which is one-to-one, onto, and angle preserving.

According to Lee et al. [4], a conformal mapping is defined as follows: Let $\{i\}$ be a vertex to be removed. Cyclically enumerate the n vertices that belong to the 1-ring $N\{i\} = \{j_k | 1 \leq k \leq n\}$ so that $\{j_{k-1}, i, j_k\}$ be a triangle of the original triangulation and such that $j_0 = j_n$. A linear piecewise approximation of z^a is given by μ_i, which is defined for $\{i\}$ and its neighbors in $N\{i\}$ according to the following expression:

$$\begin{aligned} \mu_i(p_i) &= 0 \\ \mu_i(p_{j_k}) &= r_k^{\alpha} e^{i\theta_k \alpha} \end{aligned} \tag{3.12}$$

where:

$$
\begin{aligned}
r_k &= \|p_i - p_{j_k}\| \\
\theta_k &= \sum_{l=1}^{k} \angle(p_{j_{l-1}}, p_i, p_{j_i}) \\
a &= 2\pi/\theta_n
\end{aligned}
\tag{3.13}
$$

When the vertex is an edge vertex, the mapping is a semi-disk and, therefore, $a = \pi/\theta_n$, assuming that $j_1 = j_n$ and $\theta_1 = 0$.

3.3 Procedural Noise Functions

Procedural noise functions are widely used in Computer Graphics due to its ability to add rich visual detail to synthetic images, what has always been one of the major challenges of this research area. Furthermore, procedural noise functions have many desirable qualities, such as: fast evaluation of complex patterns in real-time; it has a very low memory cost, which is ideal for compactly generating complex visual detail; parametrization, meaning that a large variety of patterns can be created with a suitable set of parameters; independent evaluation, where every point can be processed independently and in parallel, making this property of great importance when working in a massively parallel environment, like modern GPU's systems [62].

According to Lagae et al. in [62], a procedural noise function is a "*procedural technique for simulating and evaluating noise*". Thus, a definition of noise is needed, which is also presented by the same work: "*A noise is a stationary and normal random process. Control of the power spectrum is provided, either directly, or through the summation of a number of independent scaled instances of (typically band-limited) noise.*"

This noise description is based on the various definitions from random process and Fourier analysis described in [63, 64]. Also, the main purpose of this definition is to summarize the properties of most existing noise functions and not define how these were designed.

The next sections follow the same classification presented in [62].

3.3.1 Lattice Gradient Noises

A noise generated by the interpolation of values and/or gradients, which are specified at the point of an integer lattice is called lattice gradient noise. Considering this definition, the first noise that comes to mind is the Perlin noise, which is one of the first and most successful procedural noises.

3.3.1.1 Perlin Noise

Considering an integer cubic lattice in Figure 3.7, Perlin noise determines the noise of a point p computing eight pseudo-random gradients, one for each of the nearest vertices and then proceeds with an interpolation, defined by a spline function. The interpolant must guarantee a continuous noise derivative, so Perlin chose a quintic polynomial, an hermite curve function of the form:

$$f(x) = 6x^5 - 15x^4 + 10x^3. \tag{3.14}$$

This function has both first and second derivatives of 0.0 at 0.0 and 1.0, ensuring C^2 continuity.

In order to create a pseudo-random selection of the gradient vectors, lattice points are hashed by successive application of a pseudo-random permutation to the coordinates and the result is used to choose a gradient from an array. The set of gradients consists of the 12 vectors defined by the directions from the center of a cube to its edges [25]. In three dimensions, there are eight surrounding grid points. A trilinear interpolation is required to combine their respective influences (linear interpolation in each of three dimensions).

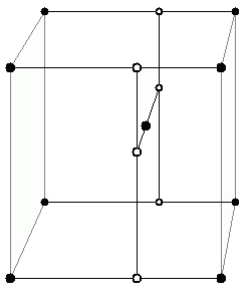

Figure 3.7: Three dimensional example of eight surrounding grid points [16].

Thus, the noise of a point p is given by the function

$$N(p) = \sum_{i=-\infty}^{+\infty} a_i * f_N(f^i * p), \tag{3.15}$$

where the stochastic function f_N is a procedural noise as described earlier, a is the amplitude and f is the principal frequency which is related by a factor of two. An example of the appearance of this noise can be seen in Figure 3.8.

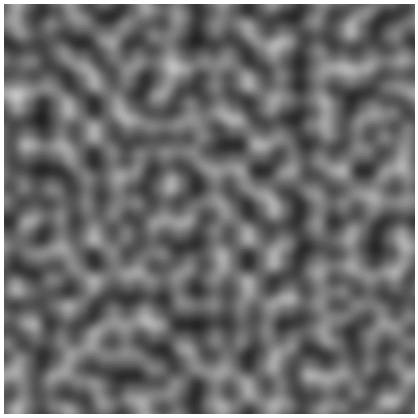

Figure 3.8: Example obtained performing a 2D Perlin noise.

In Figure 3.9, we can see the definition of amplitude and frequency. For example, given a sinusoidal wave (Figure 3.9 (a)), the amplitude is defined as the wave height and the frequency as $1/wavelength$. Considering now a noise function, the amplitude can be defined as the difference between the maximum and the minimum this function could achieve. In this case, the wavelength is the distance from one point to another and the frequency relation remains the same.

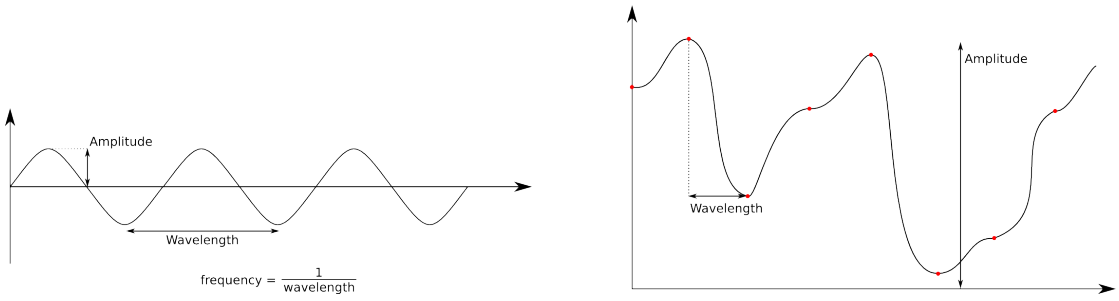

(a) (b)

Figure 3.9: (a) Amplitude and frequency definition on a sin wave. (b) A noise function example. Figure recreated from [65]

3.3.1.2 Other Lattice Gradient Noises

There are several other noise functions based on lattices. For instance, in [66] a lattice convolution noise is presented, which uses a non-integer lattice, represented by a more densely and evenly packed grid, based on sphere packing. In [67] simplex noise is introduced, which is based on a simplex grid. Perlin and Neyret [68] presented flow noise, that deals with time-varying flow textures. We can also name, curl noise [69] and better gradient noise [70]. A more in-depth description of the many different lattice noises can be found in [62].

3.3.2 Sparse Convolution Approaches

Sparse convolution noises use other methods to generate noise that are not based on a regular lattice of pseudo-random number (PRN). Specifically, noise is generated as the sum of randomly positioned and weighted kernels.

3.3.2.1 Sparse Convolution Noise

This method of generating noise involves taking random samples from a set of PRNs and filtering. Control over the power spectrum is provided in the filter parameters. The term sparse here is related to the random sampling of the PRNs, which is considered a sparse form of white noise. One draw back to this method over a lattice convolution noise is that the search space is increased for each call of the algorithm, which is computationally expensive.

Aiming for a better control over the noise power spectrum, Lewis [71] introduced the sparse convolution noise, where a three dimensional noise is synthesized by the convolution $(*)$ of a three dimensional kernel h with a Poisson noise process γ. Lewis presents an extensive mathematical framework regarding this in [71]. We strongly recommend it in order to better understand the following sections. The following noise equation is presented in his work:

$$f(p) = h * \gamma(p) \tag{3.16}$$

This Poisson process consist of impulses of uncorrelated intensity a_k distributed at uncorrelated locations p_k in space, which Lewis calls sparse white noise [71]:

$$\gamma(p) = \sum a_k \delta_{(p-p_k)}, \tag{3.17}$$

where p_k is the location of the kth impulse and $\delta_{(p-p_k)} = (x - x_k, y - y_k, z - z_k)$.

For the function h, Lewis proposed a smooth cosine kernel presented in Equation 3.18, but, according to [72], this function has the problem of generating a second derivative at $d = 1$ that is different from zero: $h_1''(1) = \pi^2/2$. This can be problematic in specific applications, such as hypertexturing generation, which needs to enforce C^2 continuity in order to create smooth surfaces. Regardless, the synthesis proposed by Lewis has a low computational cost without requiring sampling. Also, the noise quality can be manipulated by varying the Poisson process [71].

$$h_1(d) = (1 + cos(\pi * d))/2, \ \ (|d| \leq 1). \tag{3.18}$$

Lewis procedurally evaluates sparse convolution noise by introducing a grid, and generating the positions and weights of the kernels in each cell on the fly. The grid reduces the evaluation of the noise to the grid cells close to the point of evaluation.

The convolution integral can then be simplified to a basic summation over the impulses, this is due the impulsive nature of the noise, leading to the following equation:

$$f(p) = \sum a_k h(p - p_k). \tag{3.19}$$

3.3.2.2 Spot Noise

Spot noise is unique in that it shares properties of both sparse convolution noise and explicit noise. It is particularly useful for mapping textures to parametric surfaces as well as generating textures over curved surfaces [73].

3.3.2.3 Gabor Noise

This method follows the similar idea of convolution, but is unique in its choice of kernel. One of the drawbacks to sparse convolution noise is that more often than not a poor kernel is generated that reveals structure in the noise; violating the ideal noise requirements. Gabor noise solves this problem by using a kernel that is a combination of a Gaussian curve and a sinusoidal curve, both in two-dimensions.

Considering these characteristics, Lagae [6], proposed an anisotropic noise with accurate spectral control, which is able to provide a setup-free surface texturing. This noise is achieved by a sparse Gabor convolution which is an extension of the previously presented

sparse convolution noise. A band-pass Gabor noise presented in [6] is defined as:

$$N(p) = \sum_i w_i g(K_i, a_i, F_{0,i}, \omega_{0,i}; p - p_i), \tag{3.20}$$

where w_i are the random weights, K represents the amplitude, a_i is the bandwidth, F_0 and ω_0 are the frequency and the orientation of the cosine in the kernel as presented in Equation 3.21 and represented in Figure 3.10. g is the Gabor kernel proposed in [6]. It is possible to visualize that we have the same options to manipulate the Gabor noise as done with the Perlin noise. Also, the random positions p_i are distributed according to a Poisson process with mean λ. In this context g is defined as

$$g(p) = Ke^{-\pi a^2 |p|^2} cos\left[2\pi F_0 \left(p_x \cos\omega_0 + p_y \sin\omega_0\right)\right], \tag{3.21}$$

Basically, the kernel is a multiplication of a circular Gaussian and a cosine. The anisotropic feature of the Gabor Noise is paramount to the generation of detail aligned or guided by the features of a mesh as it will be shown later in this thesis.

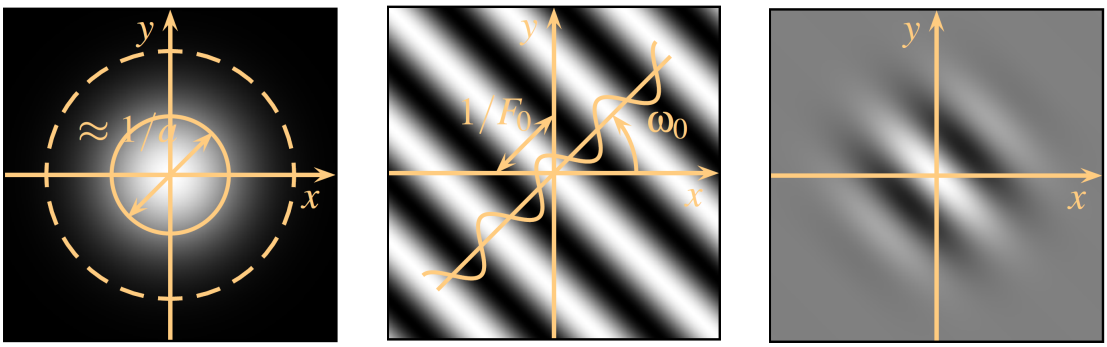

(a) (b) (c)

Figure 3.10: (a) Gaussian. (b) Cosine. (c) Gabor Kernel. Figures obtained from [6]

In this chapter an extensive review of techniques covering representation of geometric data, topological operators, topological data structures for variable resolution, simplification strategies, parametrization methods and procedural noise functions was presented. In the following chapter our method will be presented, which utilizes most of the techniques described herein.

Chapter 4

Adaptive Hierarchical Mesh Detail Mapping and Deformation

In this chapter we describe our method for mapping procedurally generated details onto arbitrary meshes. We start by posing a formulation for the problem we will solve in section 4.1. Later, in section 4.2, we describe the methodology used to solve the problem and, in section 4.3, we outline an overview of the method. In sections 4.4, 4.5 and 4.6, we describe each of the main steps of the method: section 4.4 describes the construction of the hierarchical parameterized mesh representation, section 4.5 describes the detail mapping approach using the data structure and finally, section 4.6 explains the adaptive refinement step used tho reconstruct the mesh after detail and deformation are applied to the input mesh.

4.1 Problem definition

Given a surface S represented by a mesh $M = (V, E, F)$ compute a new mesh $M'(V', E', F')$ by adding a detail function $f : V \rightarrow R^3$, defined on vertices $v \in V$, such that the details in different scales of f are added in a controllable way in different levels of detail of the geometry that describes M. An example of our method can be seen in Figure 4.1, where given an input mesh our method performs a local deformation.

4.2 Metodology

One of the most typical ways to solve the problem of adding details to a mesh in different scales is by using multiresolution analysis. Wavelets analysis [74] is one of the best choices

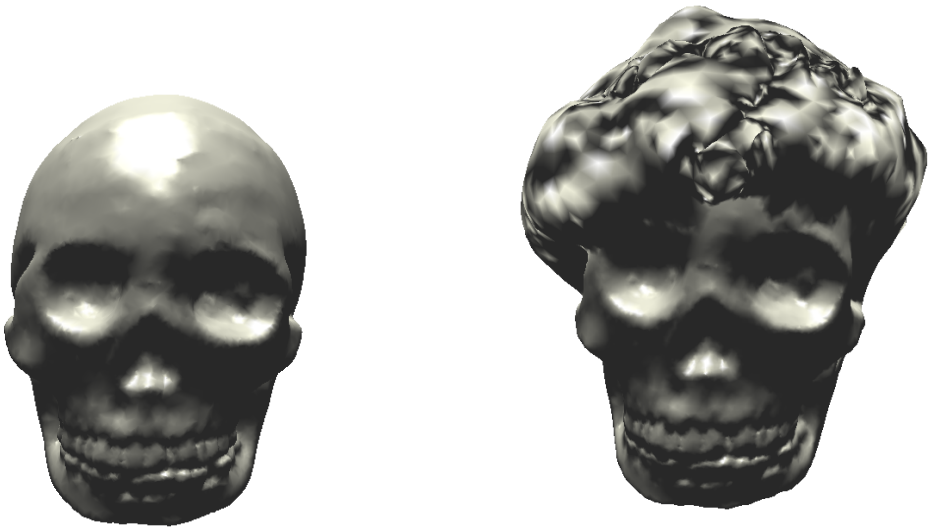

(a) (b)

Figure 4.1: (a) An input skull mesh, with approximately 30k vertices. (b) Resulting appearance after deforming its upper part with our method. Here, the head is deformed using a basic Perlin noise function in conjunction with a smoothing step to create the hair. Model obtained from [8].

because it represents functions both in scale and space, enabling a controlled way of adding the desired details.

A multiresolution analysis of a mesh is usually constructed by refinable scaling functions in order to obtain a set of nested linear spaces[74]. This also requires defining analysis and synthesis filtering operators that satisfy a set of properties required by multiresolution analysis.

The refinable scaling functions for meshes are typically defined in the context of subdivision surfaces. Computing a base domain which describes the coarsest level can be done by using several different decimation strategies. On the other hand, the step of reconstructing the original mesh M from the base domain M^0, using subdivision, requires storing the details at each level, that is the difference between the reconstruction from level M^l, using refinement, to level M^{l-1}, where l represents the current resolution level. The work in [75] follows this strategy. One of the drawbacks with this approach, is that it produces a representation of the mesh in the coarsest level obtained by low pass filtering, which may discard part of its features. In our proposal, we have an original mesh M whose features we want to preserve in the coarser level as much as possible. Preserving the most important features at the coarsest level would enable us to interactively edit the mesh, modifying the geometry of a base mesh, with a better overall description of the shape, achieving a more localized effect. The use of multiresolution analysis also does not

yield a natural way to apply adaptive strategies for detail creation. Although it is possible to insert detail in space and scale in a localized way using multiresolution analysis, one has to deal with how the mesh tessellation adapts in the neighborhood of the inserted features. This does not seem to be a trivial issue to solve in the usual representations for multiresolution analysis. For example, the work in [75], which describes a multiresolution approach for algorithmic shape modeling based on subdivision surfaces, uses the DK data structure [76]. The DK data structure, although capable of codifying hierarchical triangulations, is not so powerful and easy to manipulate as adaptive 4-k meshes (or simply a4-k meshes).

Hence, for all the reasons presented above, we opted to use a simpler strategy in which we do not compute a multiresolution analysis of the mesh based on coefficients of basis functions as, for example, using Wavelets tools. Instead, we represent the mesh via a variable resolution hierarchical data structure which describes a family of representations of the mesh in different local levels of detail. Each vertex v belongs to a level of detail given by an integer number l. The application of the detail uses l to modulate the intensity of the deformation caused by the detail defined by f. As the detail function f may be defined also in terms of its own scale and amplitude parameters, we may also combine then to achieve multiple effects.

As it will become evident in the sequel, our work is more focused in the controlled mapping of procedural detail generation onto meshes and does not have the general character of the work presented in [1]. In this context, our aims and emphasis are closer to those of [75] which has used a different approach. The details of our methodology to solve the stated problem are presented in the next subsections.

4.3 Proposed Method

Now we present an overview of our method which can be described diagrammatically in Figure 4.2. Initially, considering the mesh geometry, we must ensure that the input mesh is a triquad, in order to perform the the four-face cluster simplification process. If the mesh is not a triquad, we run an algorithm that make the necessary geometry changes.

The decimation/parameterization step is the one in which we build the mesh representation as a 4-k mesh. Here, the mesh is simplified according to specific user defined parameters, building the hierarchy through successive parameterizations of the removed vertices and previously removed ones. These parameters are: the minimum number of

vertices and the maximum error allowed(see Section 4.4.1). Also, the simplification can be done via levels, where the user can simplify the mesh defining the same error mentioned before and then proceed by making any amount of simplification steps until the desired coarse level is achieved. For achieving our proposals, we extended the four-faced cluster method so that it is also feature sensitive and also developed a simpler way to perform the construction of the hierarchy without relying on the storage of the local movement operators explicitly codified in a DAG structure. In both cases stellar operations are used. More details are described in section 4.5.

The adaptive refinement stage is the one in which the structure is navigated through its many levels, from the base domain towards the finest resolution level, and vertices are inserted performing the reconstruction of the mesh via the parameterization. At each refinement step, one mesh level is reconstructed. During each refinement step, detail generation can be introduced making the approach very flexible.

One aspect to be noticed is that the detail generation step can be accessed at any time after the mesh representation is built. This is due to the fact that at any given step a deformation or modification can be applied(see Section 4.5). Accordingly, this also gives the user the ability to modify both the original and the final mesh.

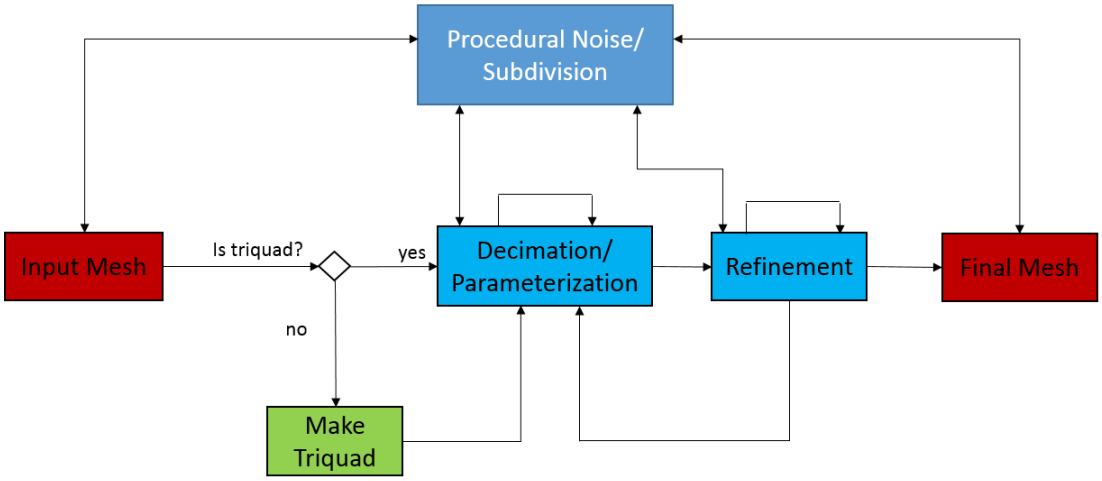

Figure 4.2: Flowchart showing all steps performed in our method. In red we have the initial and final states, in green a step that is performed once and in blue steps that are repeatable.

4.4 Variable Resolution Hierarchical Mesh

Our mesh representation is based on the variable resolution a4-k structure introduced by Velho in [13]. This is a powerful structure for the representation of objects at multiple levels of detail. The hierarchical structure of the variable resolution a4-k mesh is built from a restricted set of local modifications defined on a cluster of two triangle faces [13]. This modifications are made through stellar operators and cause minimum changes in a local neighborhood.

These operators are of great importance to this work. The basic configuration of an a4-k mesh is a sub-mesh composed by two adjacent faces sharing an edge. This sub-mesh can be produced by the removal of a vertex with degree (valency) equal to four. Here these two operations are represented in Figure 4.3.

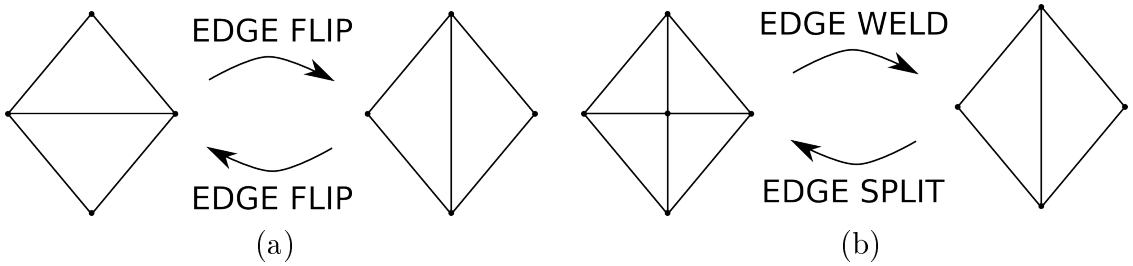

Figure 4.3: (a) Edge flip operation. (b) Weld operation. Figure recreated from [3].

In our case, the vertex removal is done by a restricted half-edge collapse, which points to a degree four vertex. One of the reasons for choosing this mesh structure is the fact that it uses simple local modifications, which forms a complete set of topology preserving mesh simplification and refinement operators.

The hierarchical structure used in this work is constructed through a mesh simplification algorithm.

4.4.1 Mesh Simplification

Our mesh simplification algorithm is similar to the four-face cluster technique presented in [3], but also extends it by using a feature-line sensitive approach. The idea is to apply only stellar weld operations to the mesh, creating local modifications, which alters its resolution in a minimum way without removing important characteristics (features).

This approach ranks vertices based on mesh quality criteria, which, in our specific case, is a combination of the removal error and the edge flip error. Both are measured

based on a quadric error metric and in our experiments the total error for a vertex removal uses the following weights: 0.75 for the removal error (re) and 0.25 for the swap error (se). This choice produced the best results in our experiments.

$$\text{total error} = 0.75 \times \text{re} + 0.25 \times \text{se}. \tag{4.1}$$

Feature lines are one of the most prominent characteristics of a surface, where sharp details usually appear. These are extremely important to this work, since it is possible to use such measures to preserve the most interesting features of a mesh through the simplification process. We will also use features to guide the addition of procedural details onto the mesh.

4.4.1.1 Feature analysis on meshes

In a tensor-based feature analysis, given a 2D manifold $M(V, E, F)$, where V is a vertex set, E an edge set and F a face set, feature analysis is done on local structure tensors. These are usually used to detect local features of a mesh based on the information they contain [77]. In our case, an extraction method based on eigen analysis for normal voting tensors is used to effectively extract feature details from mesh models. A normal voting tensor $T(v_i)$ of a vertex v_i can be computed as the sum of the weighted covariance matrices,

$$T(v_i) = \sum_{t_j \in N_t(v_i)} \mu_j n_{t_j} n_{t_j}^T, \tag{4.2}$$

where t_j is triangle, $N_t(v_i)$ is a set of triangles neighboring v_i, the normal of the triangle t_j is given by n_{t_j}, and μ_j is the weight coefficient. In order to deal with meshes with long and narrow triangles, we modify the weight μ_j according to [78]:

$$\mu_j = \frac{area(t_j)}{area_{max}} exp\left(-\frac{\|c_j - v_i\|}{\|c_j - v_i\|_{max}}\right), \tag{4.3}$$

where the $area(t_j)$ is the area of triangle t_j, $area_{max}$ is the maximum area among the triangles neighboring v_i, c_j is the barycenter of the triangle t_j, and $\|c_j - v_i\|_{max}$ is the maximum value among the neighboring triangles of v_i. It is easy to see that the weight μ_j depends on the distance between c_j and v_i.

By making use of the eigen-analysis [79] of the normal voting tensor in Equation 4.2 and also considering the neighbor relationship previously presented, it is possible to ex-

tract and analyze features of a mesh based on the classification proposed by [80], which extends the multi-type feature classification proposed in [78].

Considering the importance of the relative difference between eigenvalues λ_1, λ_2 and λ_3, these are normalized to guarantee the consistency when dealing with different data. This is achieved by $\frac{\lambda_i}{\sqrt{\lambda_1^2+\lambda_2^2+\lambda_3^2}}$, for $i = 1, 2, 3$. From now on, every eigenvalue is considered to be normalized.

Vertex type classification is done through the following algorithm:

```
for All vertices v_i do
    if λ3 > 0.1 then
        Mark v_i as corner vertex;
    end
    if λ2 < 0.02 then
        Mark v_i as face vertex;
    end
    if λ2 > 0.1 && λ3 < 0.02 then
        Mark v_i as strong-edge vertex;
    end
    if (λ2 ≥ 0.02 && λ2 ≤ 0.1) && λ3 < 0.02 && NVC then
        Mark v_i as weak-feature vertex;
    end
end
```

Algorithm 1: Vertex type classification

The *neighboring vertex coincidence*(NVC) criterion, introduced by Wang in [78], separates weak-edge vertices from noise vertices as seen in Algorithm 1. This concept takes into account the neighboring vertices of a noise vertex, that usually have different principal diffusion directions, which is defined by the eigenvector associated by the smallest eigenvalue [80]. Thus, given a vertex v_i (that is not a face vertex), we try to find, along its principal diffusion direction, neighboring non-face vertices which have similar principal diffusion direction. This is achieved by verifying the intersecting angle of these two vectors. If the angle is less than 15 degrees, then the vertex is marked and the process moves to a new one. If the number of found *coincidences* is larger than 2, we can affirm that the vertex v_i satisfies the NVC criterion. The values used in this classification are the same presented in [78] and produced good results. Two examples can be observed in Figure 4.4.

In our approach, we follow the simple idea of not removing a vertex if we want it in the base domain. Thus, we mark any feature we want preserved as unremovable. By doing this, we guarantee that a specific feature will be preserved through the simplification procedure.

After this process, an independent set of clusters that covers most of the mesh is se-

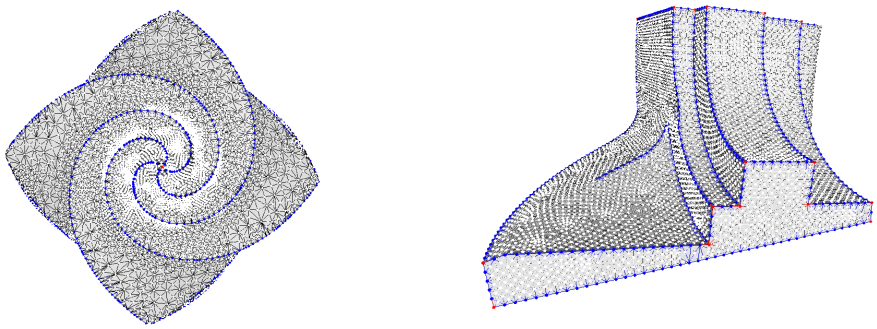

(a) (b)

Figure 4.4: Feature lines detected using our implementation where blue lines represent strong edge features and the red points are corner vertices. (a) Octaflower feature detection. (b) And fandisk.

lected. During this step, every vertex that is related to an important feature of the surface is marked as unremovable and is not included in the cluster list, thus maintaining feature lines and corners untouched. The cluster simplification creates a geometric modification in the 1-ring neighborhood of the faces of the vertex being removed, meaning that both boundary vertices and edges remain unchanged.

The feature preservation scheme creates a less uniform distribution of valences across the mesh. This is one of the reasons for using an a4-k mesh, since the maintenance of a a4-8 structure under this circumstance would be a hard task. The charts presented in Figure 4.5, shows the vertices valence distribution in the torus, fandisk and dragon models before and after the decimation process. In this specific case, the torus had, initially, approximately 18k vertices and was decimated to roughly 350. One might consider converting the base mesh back to its a4-8 form, but the cost of reparameterizing the entire mesh structure is really high and usually not an option.

Similarly to [3], a combination of edge flips and welds are used to perform the simplification process. Applying these operators can drastically change the surface and analyzing the error incurred by applying them is necessary. The edge flip operator is used to better approximate the original surface, in the case of choosing an interior edge to apply an edge weld; or to match the vertex degree requirement for the simplification, setting the vertex degree to 4 (four) in order to apply a weld operation. Regardless of the operation being processed, the error associated with these operations is estimated using quadric and dihedral error metrics.

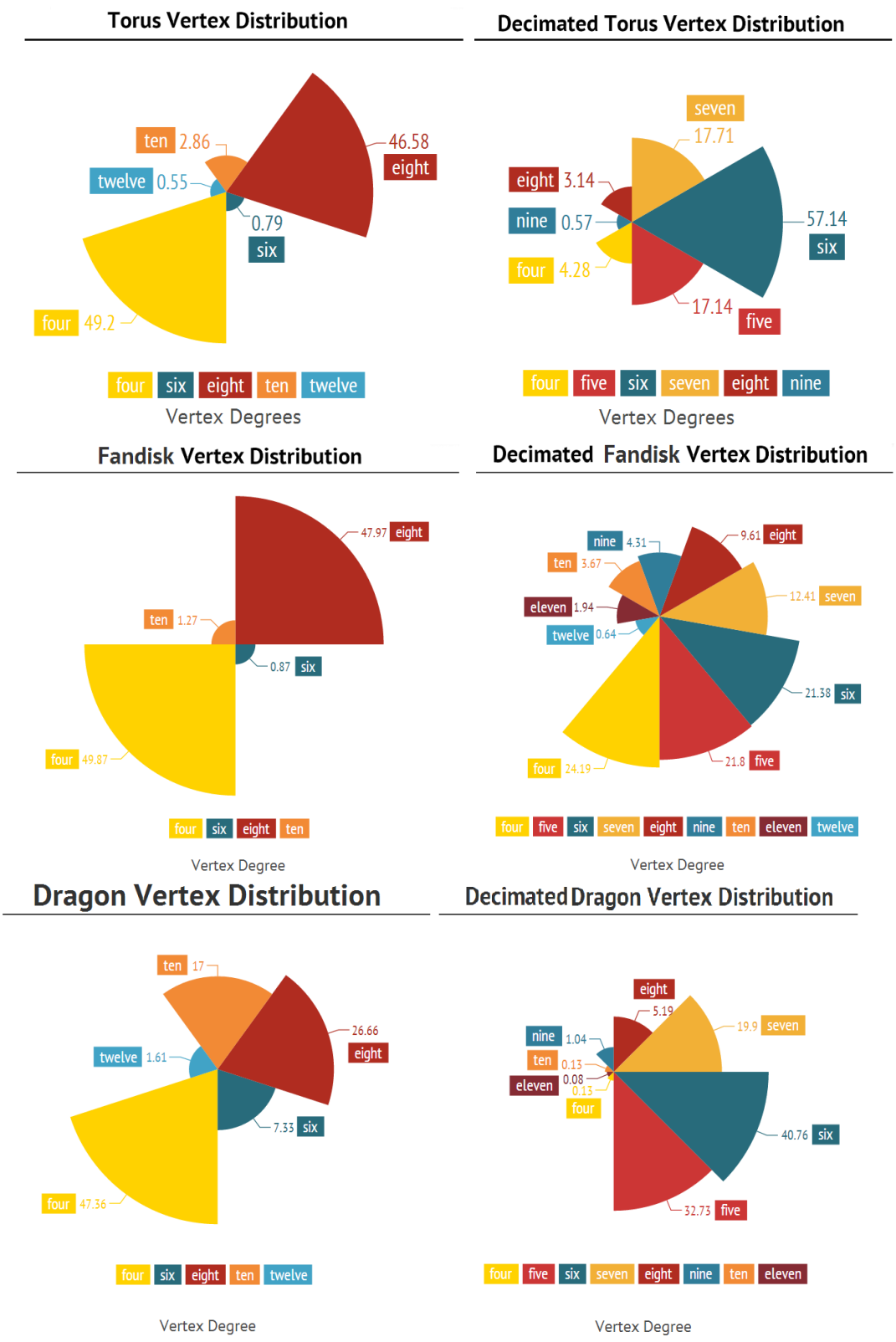

Figure 4.5: (left Column) A typical 4-8 vertex distribution for the input mesh, where the majority of the vertices have degree 4 or 8. (right Column) After the decimation process, the 4-8 structure is lost and the vertex valencies are spread across different values.

4.4.1.2 Mesh parameterization guided by simplification

Each simplification step, moving from the actual mesh level K^L to K^{L-1}, consists of removing a maximally independent set of vertices with degree four, where every removed vertex is parameterized on a simplified face in the level K^{L-1}. This creates a hierarchical parametrization of the surface that is propagated through each simplification step. This is done through the re-mapping of previously mapped vertices using barycentric coordinates. Here we include the explanation from [4] to make the text more comprehensive.

"Consider K^L an original mesh and K^0 a base mesh obtained through this simplification process. Also, considering $\varphi(K^L)$ and $\varphi(K^0)$ as the geometric realizations of K^L and K^0. A parametrization Ψ can be obtained from the bijection $\Pi : \varphi(K^L) \rightarrow \varphi(K^0)$, such that $\Pi(p) = \alpha p_i + \beta p_j + \gamma p_k$ for all $p \in K^L$, where p_i, p_j, p_k are vertices i, j, k coordinates of a triangle in K^0 and α, β and γ are the barycentric coordinates, in the triangle $\{i, j, k\}$. Finally, $\Psi = \Pi^{-1}\varphi(K^0)$.

This parametrization can be constructed concomitantly with the hierarchy, through simplification, by building successive bijections $\Pi : \varphi(K^L) \rightarrow \varphi(K^l)$, being the first bijection of the process $\Pi^L = I$ (identity) and the last $\Pi^0 = \Pi$. Assume a given bijection Π^l, it is possible to obtain Π^{l-1} for each vertex $\{i\} \in K^L$considering the following three categories:

- $\{i\} \in K^{l-1}$: the vertex $\{i\}$ was not removed. In this case, $\Pi^l(p_i) = \Pi^{l-1}(p_i) = p_i$
- $\{i\} \in K^l \setminus K^{l-1}$: the vertex $\{i\}$ was removed from level l to $l-1$; Determine the conformal mapping $\mu_i(p_i)$ at $\{i\}$ and, after the vertex removal followed by a mesh reconfiguration (in our case a stellar movement), the 1-ring flattening origin will be mapped to a triangle $t = \{j, k, m\} \in K^{l-1}$ with barycentric coordinates α, β, γ. In this case, $\Pi^{l-1}(p_i) = \alpha p_j + \beta p_k + \gamma p_m$
- $\{i\} \in K^L \setminus K^l$: $\{i\}$ was removed in a previous stage. Thus, $\Pi^l(p_i) = \alpha' p_{j'} + \beta' p_{k'} + \gamma' p_{m'}$ will be mapped to a triangle $t' = \{j' + k' + m'\} \in K^l$. If $t' \in K^{l-1}$, then nothing needs to be done, otherwise it is necessary to reparameterize $\{i\}$. Considering that this hierarchical construction is done through the removal of an independent set of vertices at each level l, then it can be stated that only one of the vertices of the triangle was removed, i.e. $\{j'\}$. Let $\mu_{j'}$ be the mapping related to the $\{j'\}$ removal. Then, after the mesh reconfiguration, $\mu_{j'}(p_i)$ will be mapped to a triangle $t = \{j, k, m\} \in K^{l-1}$ with barycentric coordinates α, β, γ leading to a parametrization $\Pi^{l-1}(p_i) = \alpha p_j + \beta p_k + \gamma p_m$."

This is presented by Lee et al. in [4] on page 5.

After the simplification process, the resulting structure is a base domain containing a locally parametrized dense mesh as shown in Figure 4.6.

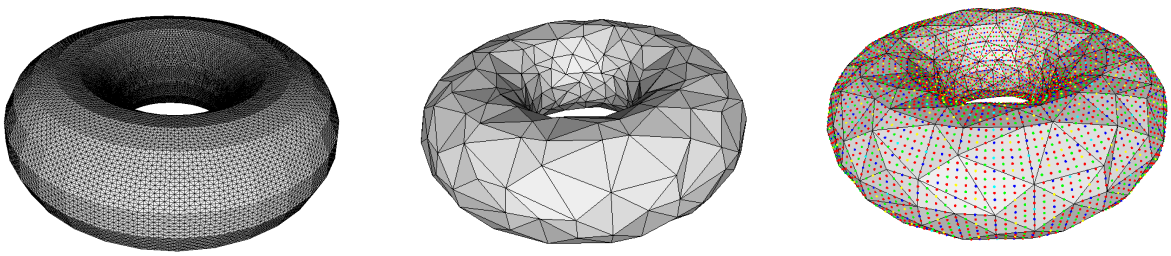

(a) (b) (c)

Figure 4.6: (a) Original dense mesh. (b) Torus base domain $\varphi(K^0)$. (c) Smooth parametrization over the base domain, where each point from the original mesh is shown with a dot.

4.5 Detail Generation

Given a base domain, we can start manipulating its geometry through detail generation using a general procedural function or a specific local deformation. A typical approach is to align the noise scale with the level of detail of the mesh geometry; this can be done in many different ways.

We must make it clear that in our problem definition, the deformation is only applied to the vertices of the mesh. Nevertheless, by using noise functions we can create details inside the meshes' faces using a approach based on different mapping strategies such as, i.e., normal mapping or relief textures. This approach is used by [6], but they do not deal with the aspects concerning the level of detail of the geometry as we do.

The deformation operator can be defined by the following function:

$$D(VS \subset V, l, f(p_0, p_1, ..., p_n)) \tag{4.4}$$

where, VS is a set containing one or more vertices of the mesh, l is the level of detail of the vertex in the variable resolution representation, and f is an arbitrary function defined on a list of parameters $p_0, ..., p_n$. This parameter list can also include a vertex v and/or a level l. One might notice that VS defines the area where the detail will be inserted. Observe that noise functions are particular cases of the function f. Here we investigate

the use of two powerful noise functions: the Perlin and Gabor noise functions.

A simple example can be obtained by regulating the noise intensity based on the mesh resolution level. Deformation results can be easily achieved by moving a vertex towards the normal direction $\vec{n}(p)$ according to the noise level (nl), i.e. given a point p, with coordinates (x, y, z) at a level l, a deformation can be computed using:

$$p \leftarrow p + (nl/l)\vec{n}(p) \tag{4.5}$$

Here, the base domain will be less modified and the original mesh will suffer the most significant changes. We also mark a vertex as *noised* to avoid accumulating these modifications, but its also possible to combine noise values generated in different levels to achieve a particular result.

Using noise functions has many advantages, most of them related to its procedural nature. Lagae [6] points the three principal ones related to our work: compactness, described by few parameters and can be quickly evaluated at any point in space. Since noise is mainly used to add details to surfaces it was a natural choice to our approach. Also, the parameter manipulation can be a powerful tool when combined with our variable resolution approach.

The generation of visually rich and appealing content from noise is not a simple task. The random nature of the noise is a difficult problem to work with, also preventing the prediction of the function results [62]. Since controlling the appearance of the noise is of great importance to our manipulation scheme, defining a framework for controlling it is a primary goal. Interestingly enough, the power spectrum of the noise provides part of such control. For instance, Perlin achieves spectral control using a weighted sum of band-pass octaves of noise [5].

4.5.1 Parameterization update after deformation

After applying any deformation to the mesh, we must update the parametrization and stored coordinate values, since applying changes to the vertices coordinates results in changes in the barycentric coordinates previously defined. This can be done performing a simple check, verifying whether a vertex in the current triangle is noised or not. In case of affirmative, we must update all triangles that share that vertex. This update is performed once, immediately after the completion of the noise process.

This correction is important, mainly because, after a mesh deformation process is

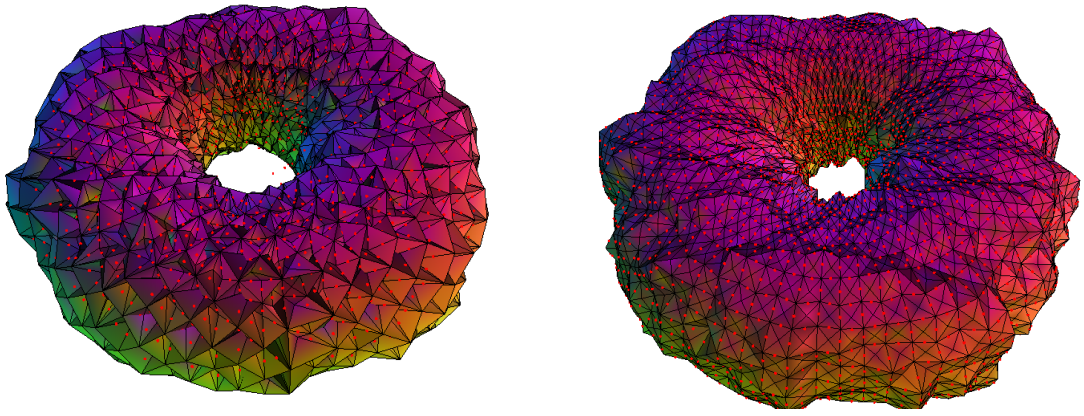

(a) (b)

Figure 4.7: (a) Refinement step without the coordinate update after a noise process. (b) Noised mesh after a refinement step with correct parametrization over the surface.

applied, any original coordinate stored in the structure during the parametrization step loses its meaning. This has a direct impact on the refinement process, where the vertex positioning depends on the stored values in order to re-insert a vertex. As mentioned previously, this is done by retrieving the vertex coordinates using the barycentric information stored. After a deformation this information changes and must be updated in order to present correct results. An example of this issue can be seen in Figures 4.7 and 4.8.

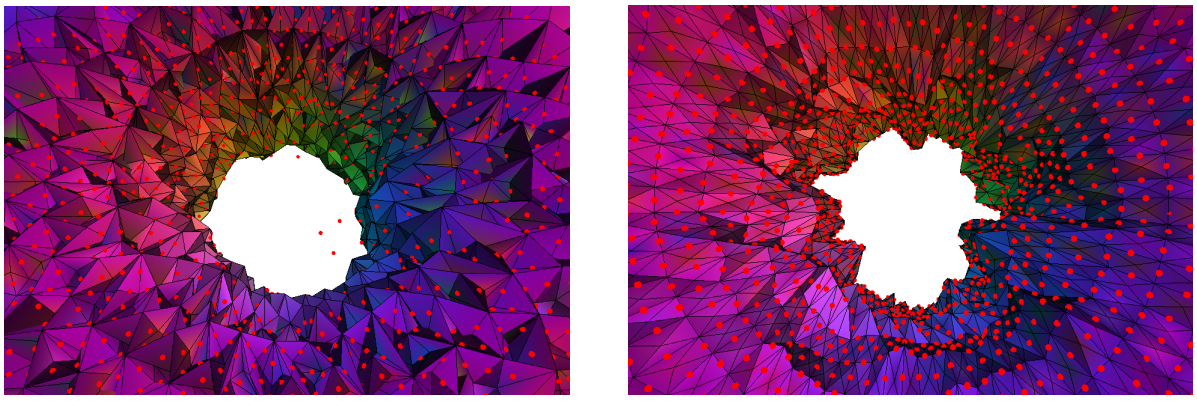

(a) (b)

Figure 4.8: (a) Parametrization problems at the torus center, when refining without coordinate correction. (b) Close-up view of the torus center after a noise process and with correct parametrization over the surface.

4.6 Adaptive Refinement

In order to reconstruct the original or modified mesh we follow a simple approach. At a certain level K^l, to reconstruct a level K^{l+1} we walk across the current level triangles checking which vertices in the parametrized structure needs to be re-inserted in the current mesh level. Each triangle posses a multimap data structure containing its parameterized vertices, where the access key is the vertex original level l. Notice that a multimap can handle duplicated keys, which fits perfectly in our vertex storage scheme. Thus, to obtain the vertices that must be re-inserted at each level l, we only need to recover the entries with that key value. These vertices are then stored in a temporary queue ordered by their removal order. This guarantees that the insertion will happen according to the simplification process, avoiding geometric errors that could happen in a random insertion approach.

```
Data: Vertex v_i from the queue
Result: Edge to be split
getBarycentricCoordinate(v_i);
for All edges of the current triangle do
    Find the euclidian distance of the barycentric coordinate of v_i to the
    currentEdge middle point;
    if diantance < lowerDistance then
        closerEdge = currentEdge
    end
end
return closerEdge;
```

Algorithm 2: Selection of the edge to be split

As mentioned before, the simplification process is associated with a stellar weld process, more specifically with an edge weld operation, where a vertex is decimated. Intuitively, in order to re-insert a vertex, an edge split operation is an obvious choice. Also, each vertex being inserted has its parametrization based on barycentric coordinates with relation to the vertices of a triangle at the current level (Figure 4.9), meaning that it is trivial to decide which edge must be split. This can be achieved by an Euclidean distance check from the parameterized point to the triangle edges and choosing the closer one as shown in Algorithm 2.

A clear advantage in using stellar subdivision is that the adaptive mechanism can be completely general. Here we have two options for an adaptation function, a simplification step based on vertex decimation through edge weld and a refinement one associated with edge split. As mentioned before, this function can evaluate and rank a region according to

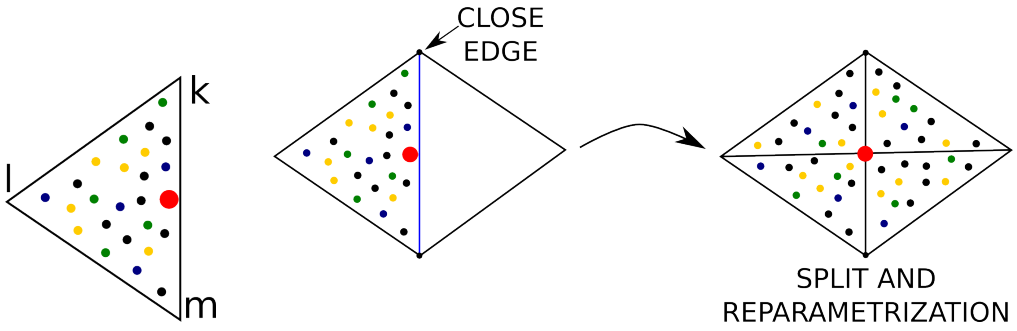

Figure 4.9: (a) Local view of the parametrization on a triangle, where the colors represent the level of each vertex. (b) Refinement step with the current level vertex insertion and reparameterizing all remaining vertices.

a predefined criteria (i.e a vertex removal error or an edge flip restriction). Also, differently from other similar works, our approach does not store any operation performed in any previous step; the entire refinement process is done on-the-fly using the described method.

Considering the parameterization, there is a special issue regarding the vertices of some triangles of the input mesh that are mapped (parameterized) during the simplification process to different triangles in the base domain. These singular cases generate overlapping edges during the refinement process and must be dealt with in order to properly rebuild the original geometry. A common approach is subdividing such triangles, mapped onto the base mesh, until all vertices that belong to the same triangle are reparameterized to the same triangle in the base domain [1].

Another approach, used in this work, is checking, during the insertion step, whether the distance from the current vertex p_v position to the center of the edge e to be split is greater than the length of any of the edges $(e_{t_1}, e_{t_2}, e_{t_3})$ of the new triangle t. Just in case this occurs, we must search for the right insertion edge $e_n t$, which, usually, is in one of the neighboring triangles nt. Figure 4.10(a) presents this idea, where the red edge is the edge to be split and the red dot is the vertex to be inserted. In (b) the blue lines identify the lengths we must verify in order to check the insertion. This algorithm does not fix overlaps in the parameterization, but during the insertion operation.

There are many challenges regarding the process of reconstructing the original surface. A particularly tough one is how to represent the original mesh state, when operations of vertex valence correction were needed. Intuitively, while refining, we want the vertex degree to be the same as before it was when removed. To achieve that, a vertex degree check must be performed, verifying if the inserted vertex has its original degree and performing the necessary neighborhood adjustment to achieve that. Notice that, when

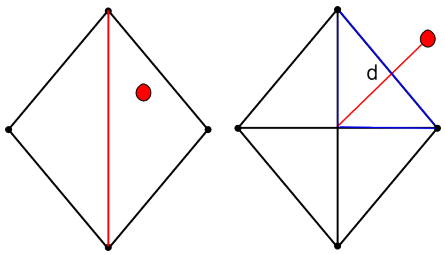

(a) (b)

Figure 4.10: (a) In red, the edge that is going to be split. (b) In blue, all edges that must be tested before inserting the vertex.

correcting a vertex degree while refining, we approximate that region geometry to the original input mesh.

The Figure 4.11, an example of the importance of the degree fix approach is presented. At the right side, we can see a comparison of both final meshes, without degree fix and with it respectively. From these results, we can see that approximating the original geometry during the refinement process is essential for the correctness of the method when dealing with a4-k meshes.

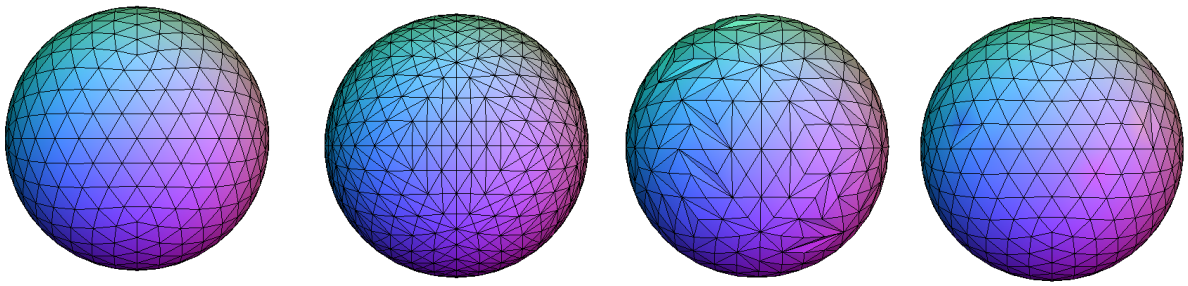

(a) (b)

Figure 4.11: (a) Input triangle mesh (left) and 4-k Mesh representation (right). (b) Refinement without flip verification (left). Vertex degree correction(right).

Obviously, we must not generalize such solution, since it does not need to be applied in every situation. For instance, when dealing with a 4-8 mesh, where the simplification scheme will remove vertices usually without the need of flipping, this verification is not necessary. Basically, we need this check when our input structure is a 4-k mesh. Figure 4.12(a) show the normal degree fix for the simplification process and, in Figure 4.12(b), how it is possible to obtain the same configuration while reconstructing each level.

A more complex example can be seen in Figure 4.13, where at the top left, we have an input mesh, in this case a tri-torus(zoomed in to facilitate the visualization of the mesh).

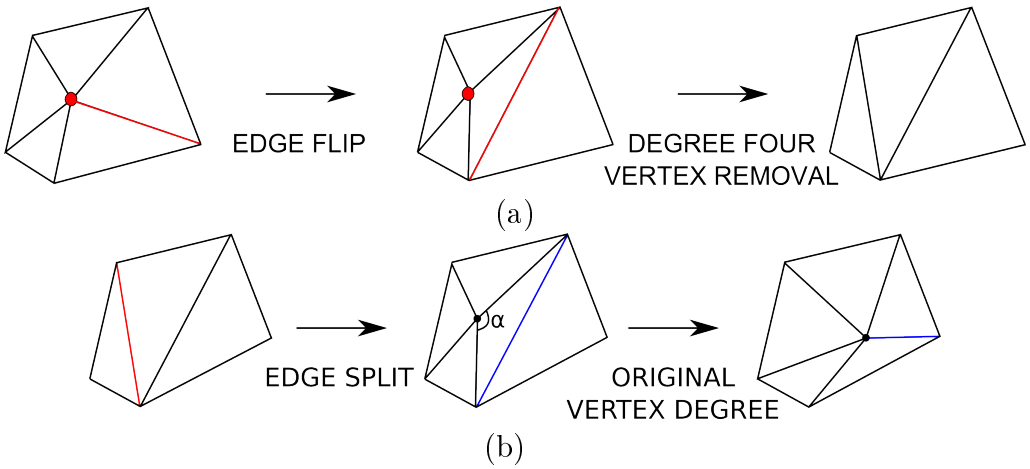

Figure 4.12: (a) Vertex removal process. (b) Refinement step with degree check and fix.

At the top right, we can see how the refinement process can change the original geometry. At the bottom left, the result of the degree fix which is performed at each refinement step.

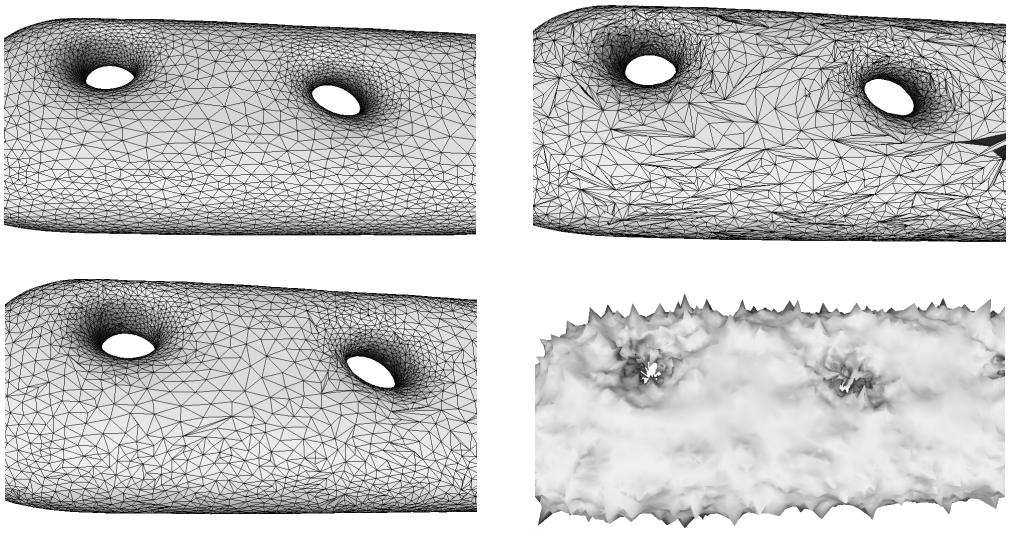

Figure 4.13: Vertex degree fix. At the top left an input mesh. At the top right, changed geometry through refinement. At the bottom left, the resulting mesh after degree fix. The final mesh after a noise process at the bottom right.

The algorithm behind this check is presented in the Algorithm 3. The *threshold* is a variable used to find which edges should be flipped in order to increase the vertex degree. After the edge split operation, the newly created vertex always has degree four. We verify if that vertex has the correct valence for the current resolution and proceed accordingly. We also show in Figure 4.13(bottom right), the resulting deformation using a turbulence function with the following parameters: 4 octaves, 0.5 gain and 2.0 lacunarity.

For example, given a new inserted vertex, whose original degree for the current level is five, we must find a link edge to flip in order to increase its degree. In this particular

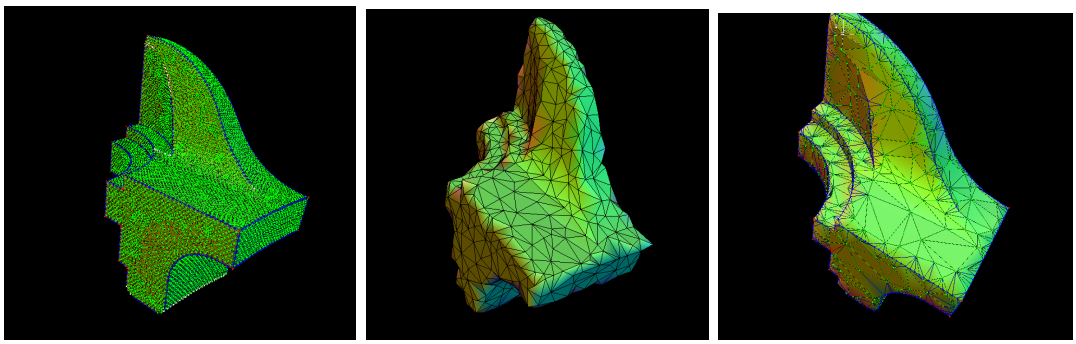

(a) (b) (c)

Figure 4.14: (a) Fandisk feature detection, where blue represents strong-edge vertices, red are corner vertices white are weak-edge vertices and green represents face vertices. (b) A mesh simplification process where the mesh prominent characteristics are not preserved. (c) Simplification result when preserving features.

example, the *threshold* can be set to find an edge that is opposite to an angle higher than 90 degrees, because vertices with valency equal to four (4) will have approximately 90 degrees between each edge in its star. So after inserting a vertex, if we find such angle after positioning it, we also find a suitable edge to be flipped in order to increase the vertex degree (see Figure 4.12(b)).

```
Data: Input vertex v to have its degree fixed
Result: Vertex with correct degree for the current mesh level
for All edges in the star of v do
    Find the angle α between the edges that share that vertex;
    if α > threshold then
        Put the link edge, the one at the opposite side in relation to the angle α, in
        an ordered temporary array
    end
end
while Vertex degree is lower than the correct degree do
    Extract an edge from the temporary array;
    Flip that edge in order to increase the vertex degree;
    if array == empty then
        break;
    end
end
```

Algorithm 3: Vertex degree fix

Another important result is related to the feature guided simplification. In Figure 4.14, an example of the simplification process, guided by the mesh features, is presented. As mentioned previously, to maintain the most prominent characteristics of the input mesh, we just mark strong-edge and corner vertices as non-removable.

Naturally, a feature based decimation can produce thin triangles (with bad aspect ratio) for the parametrization process. This is due the rules presented earlier that prevents important vertices and edges to be removed during the decimation step. We do not solve this issue in this work, but we believe that a possible approach to minimize this problem is to perform a subdivision scheme (i.e. $\sqrt{2}$) in the neighborhood of the feature, creating smooth transitions and less clustered triangles with a better aspect ratio.

4.7 Operators

This section presents the main operators created and used in this thesis in order to produce our results. These are further divided into categories according to its characteristics and applications, and each one has common and specific parameters. The main ones are: subdivision and smoothing operator; geometric operator; procedural detail operators and Feature-based Operator.

4.7.1 Subdivision and Smoothing Operator

The intent of the subdivision and smoothing operators is to provide mesh manipulation options that can assist all other operators. Thus, the main advantage of them is their ability to be combined with any other deformation operator. The following sections describe its definitions and applications.

4.7.1.1 Subdivision Operator

The main objective of the subdivision operator is to create an area with higher local resolution, in which other operators will be applied. The motivation behind this is the possible need to insert rich details at lower resolution levels, which is a difficult task when dealing with an extremely simple mesh that has only a few number of vertices.

The subdivision is based on a locally 4-8 mesh structure, where the process follows a concentric pattern based on a valence four vertex and proceeds refining from its link edges moving inward. One might notice in Figure 4.15 that this approach only modifies the 1-ring of the selected vertex. In this case, VS (shown in Equation 4.4) is an independent vertex set.

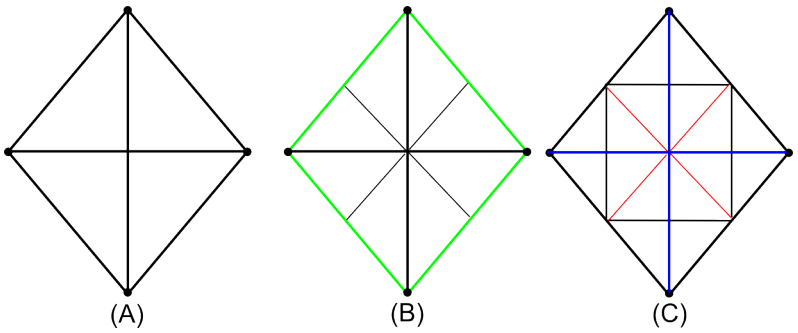

Figure 4.15: (a) Input example of a degree four neighborhood. (b) One step of subdivision, where all link edges (green) are split. (c) Second step, where all even edges (red) are split. Every step following this one, switches between even (red) and odd edges (blue) for splitting.

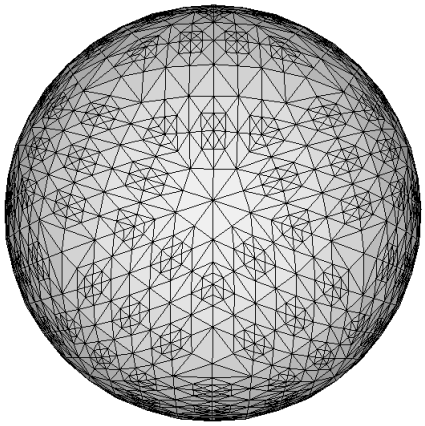

Figure 4.16: An overview of the sphere with many subdivided areas.

4.7.1.2 Smoothing Operator

In order to create specific and smooth deformations at global or local ranges, we make use of the masks proposed by Loop in [7]. These are described in Figure 4.17 and create a gaussian look when applied to an area.

In general for local modifications, to create a desirable appearance, this operator is used together with the subdivision operator. This is due the number of vertices needed to apply Loops's mask, the more vertices available at a neighborhood the better is the result.

4.7.2 Geometric Operators

The geometric operators defined here focus on modifying an area, creating wide details. Thus, VS, in this case, will be a set of connected vertices that forms a ROI. The pa-

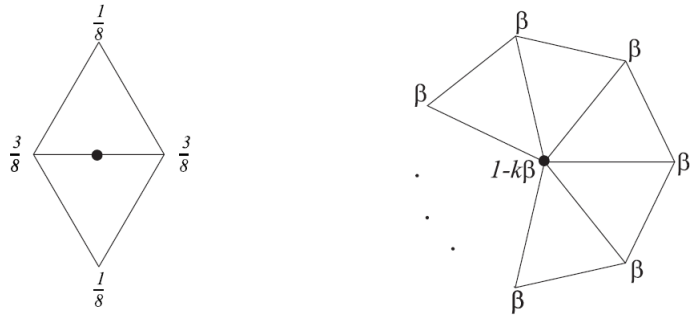

Figure 4.17: Loop's proposed masks for vertex positioning.

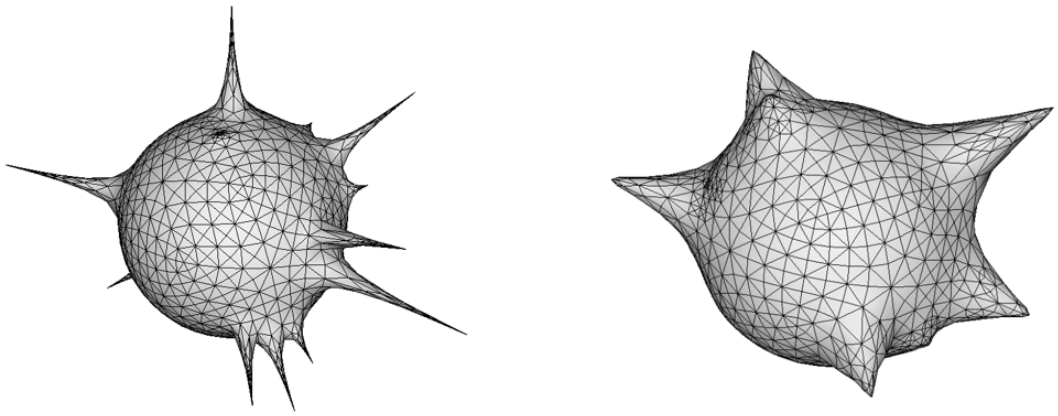

Figure 4.18: High frequency peaks being smoothed locally, using subdivision to obtain better results.

rameters for this operator will be a *scale* that controls the intensity of the deformation and a level l that defines the resolution level, in which these modification will be applied. Here, we present the tapering and twisting operations as special cases of the function f defined at the deformation operator in Equation 4.4. The main objective of this operator is to create wide deformations across considerable areas of the mesh, although it could be applied to a more restricted area.

Below, we show two examples of operators that are integrated with the adaptive multiresolution properties of the data structure we use in this work.

4.7.2.1 Tapering

The tapering operation is relatively similar to scaling, but differentially from it, changes the length of two components without changing the length of the third. Equation 4.6 shows a deformation operation that creates modifications along the axis X and Y according to

a function based on z coordinates [81].

$$\begin{aligned} r &= g(z), \\ X &= rx, \\ Y &= ry, \\ Z &= z. \end{aligned} \tag{4.6}$$

In the specific case of Figure 4.19, r is defined according to Equation 4.7:

$$g(z) = (1 + z)/scale, \tag{4.7}$$

where the *scale* dictates how strong the deformation will be. Also, depending on how the coordinate system is defined, changes must be made to create a better result. For example, if z is defined between -1 and 1, the Equation 4.7 will produce a coherent appearance, but if z has a different range it might be necessary to normalize it. It is desirable to use this tapering operator to deform coarse meshes, since it creates a wide deformation moving many points at once, usually, without high frequencies.

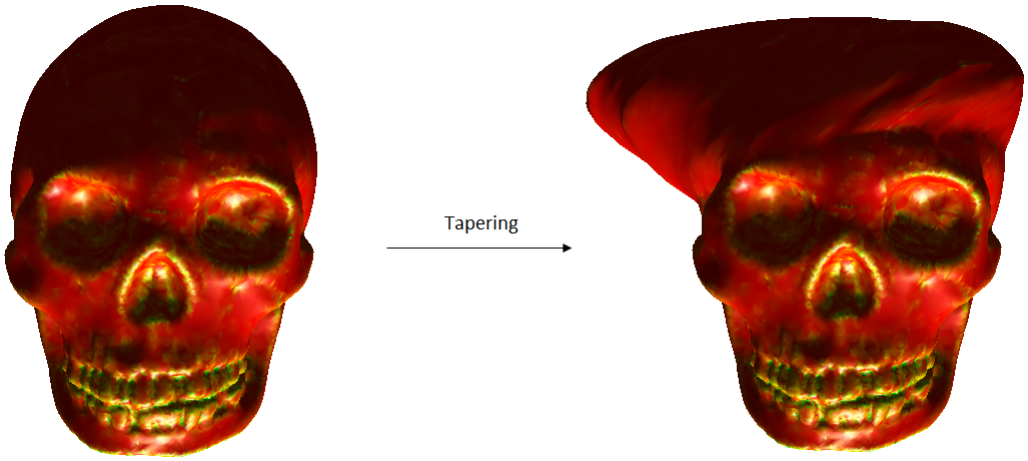

Figure 4.19: Example of a local tapering deformation simulating hair appearance.

One can notice that the deformation in Figure 4.19 only affects part of the model, that can be achieved through a coordinate restriction, where the operator is only applied at certain regions of the model.

4.7.2.2 Twisting

For some deformations, it is useful to simulate the twisting of an object. A twist can be approximated as a differential rotation, similarly as tapering is a differential scaling [81]. We also choose two deformation directions and maintain the third unchanged, just like mentioned before.

A global twisting around the z axis can be produced by the following equations:

$$\begin{aligned} \theta &= g(z), \\ C_\theta &= \cos(\theta), \\ S_\theta &= \sin(\theta) \end{aligned} \tag{4.8}$$

$$\begin{aligned} X &= xC_\theta - yS_\theta, \\ Y &= xS_\theta + yC_\theta, \\ Z &= z. \end{aligned} \tag{4.9}$$

In this work, $g(z)$ is given by $g(z) = (z * scale)\pi/180$, where the *scale* dictates how far the twist will bend towards the z axis. An example of this approach can be seen in Figure 4.20, where we use the exact same functions presented in Equations 4.8 and 4.9. This is also a wide deformation and can be used in conjunction with the tapering operator. In Figure 4.19, the curl details that can be seen on the *hair* of the skull were created using this twisting operator and also follow the coordinate restrictions mentioned earlier.

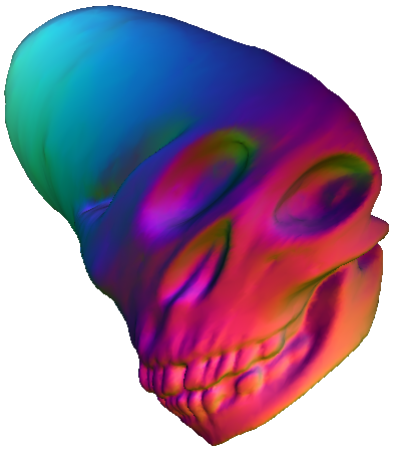

Figure 4.20: Example of a global twisting operator, giving a ghostly appearance to the skull.

These operators can be used together with all other deformation schemes presented so far, which makes them useful tools in order to create powerful manipulations across our meshes.

4.7.3 Procedural Detail Operators

Procedural detail operators follow the same idea presented in Equation 4.5, where we manipulate each function according to the mesh resolution level and attributes, such as curvatures and features. Each procedural noise function presented here can be used in the deformation operator, but each has specific results according to the restrictions and parameters defined according to Equation 4.4.

4.7.3.1 Perlin Noise Operator

Following this idea, a deformation effect can be obtained by modifying the noise parameters according to the resolution level. In the noise function proposed by Perlin, presented in Equation 3.15, we can manipulate the noise amplitude a, frequency f, gain and lacunarity parameters in accordance to the resolution level. Usually, the modulation of the amplitude and the frequency is defined as the *Persistence* of the noise.

Considering the weighted sum of band-pass noises, the lacunarity and gain are the rate at which the frequency and amplitude changes per octave. The lacunarity must be between 1.0 and 3.0 for the noise to be considered fractal. Values outside this range can lead to a result that becomes similar to a white noise (static). The gain value is normally set as the inverse of the lacunarity. For example, defining the lacunarity value as 2.0 would imply in a gain value of 0.5. Keeping this ratio is not mandatory, but the noise might otherwise lose its fractal properties.

A good result can be obtained using the turbulence function (see Equation 4.10), also presented by Perlin, through the modulation of the amplitude according to the multiresolution scale. Since we are dealing with the fractal sum of the absolute value of the noise, we can change the gain amount to dictate how the amplitude will impact the resulting noise value. We can also manipulate the lacunarity, which expresses how tightly the wavenumbers are packed together along the progression. The most common value used

for the lacunarity is 2.0 and is also used by Perlin in his work [5].

$$N(p) = \sum_i \left| \frac{f(2^i p_x, 2^i p_y, 2^i p_z)}{2^i} \right| \tag{4.10}$$

Using this number specifically causes wavenumbers to be successive octaves along the spacial frequency spectrum. However, keeping this value leads to an artificial alignment of surface features across scales, Hence, the manipulation of the lacunarity is critical when the aim is to apply different deformations to a surface without such artifacts. Results of such scheme, with usual parameter values as mentioned earlier, can be seen in Figure 4.21.

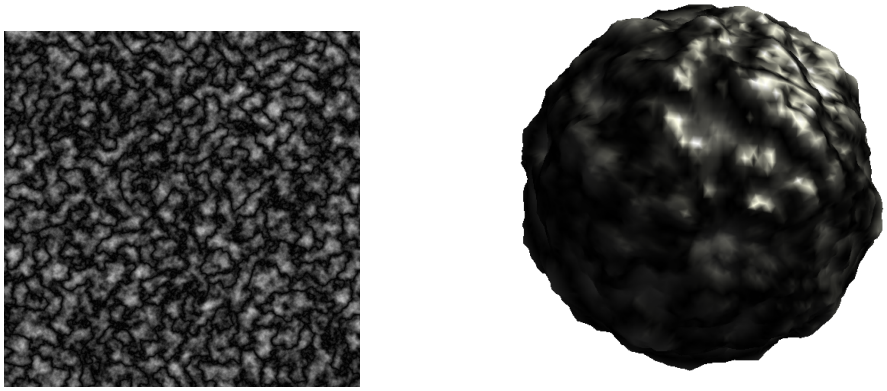

(a) (b)

Figure 4.21: (a) Turbulence texture with a 0.5 gain and 2.0 lacunarity. (b) Noise mapping and deformation over a sphere model with approximately 20k vertices.

The lacunarity change must be soft since it can really change the surface appearance. In our experiments, given a mesh level l, setting this value to $1.1 + (l + 1/10)$ presented a nice mountainous result combined with a $0.8/(l+1)$ gain value when applying a turbulence modifier. As we can see in Figure 4.22, when applying these modifiers to the function we obtain a more diversified result (Figure 4.22(b)).

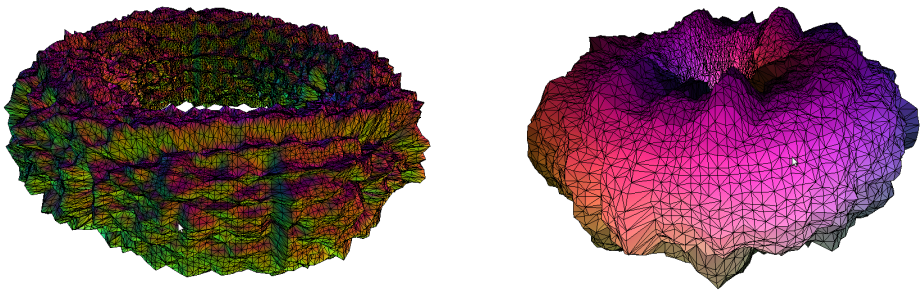

(a) (b)

Figure 4.22: (a) Noised surface with a fixed 0.6 gain and 2.0 lacunarity. (b) Varying gain and lacunarity as mentioned in section 4.5.

A different result can be obtained through the manipulation of the turbulence function with a sinusoidal component, as presented in Equation 4.11 and in Figure 4.23. This pattern resembles marble stripes and can be used used to achieve deformations with wide amplitude and low frequencies. These are useful for manipulating meshes with a low amount of vertices.

$$N(p) = (\sin(p_x + 4 + \left(\sum_i \left|\frac{f(2^i(p_x/2), 2^i(p_y/2), 2^i(p_z/2))}{2^i}\right|\right) * 4.0) + 1) * 0.5; \quad (4.11)$$

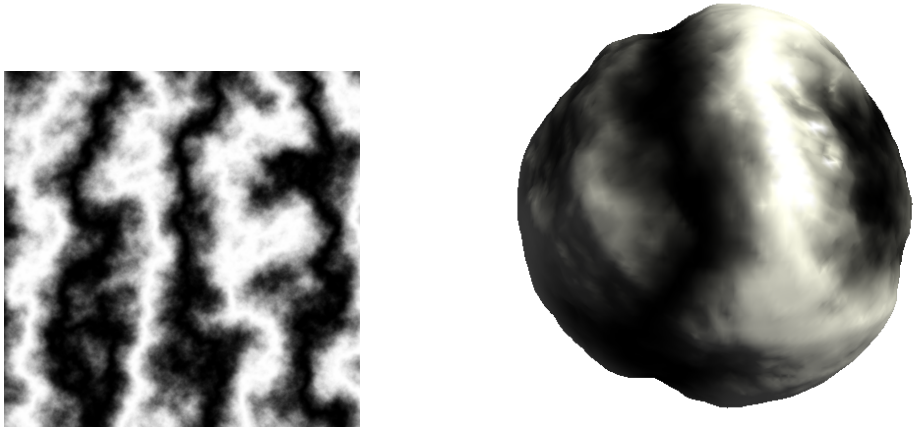

(a) (b)

Figure 4.23: (a) Marble texture using the turbulence function with 0.5 gain and 2.0 lacunarity as parameters and a sinusoidal component, where each coordinate is weighted by the value 0.5. (b) Mapping and deformation of over a sphere. This kind of deformation is interesting for coarser resolution levels, since it has a higher amplitude and low frequencies.

Of course, it is possible to think in different forms to manipulate the geometry. An example is a multifractal approach that creates nice mountains across the entire surface. The Equation 4.12 represents such modification:

$$N(p) = \sum_i \left[\left|d - f(2^i p_x, 2^i p_y, 2^i p_z)\right|\right]^2 a^i N(prev), \quad (4.12)$$

where d is an offset, a is the amplitude and $N(prev)$ is the value of the previous iteration. Figure 4.24 shows how this function can be used to create interesting shapes for mountain and valleys.

A really interesting pattern, resembling wood, can be achieved using a similar function represented in Equation 4.13, where the noise is obtained by the difference of the function

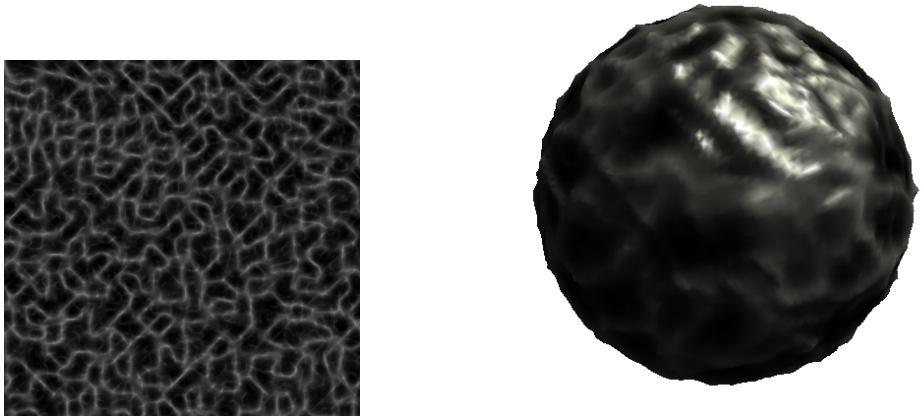

(a) (b)

Figure 4.24: (a) Multifractal texture with a 0.5 gain, 2.0 lacunarity and offset 1.0. (b) Resulting appearance after deforming the sphere.

$N(p)$ with its integer part and then scaled by a factor of ten.

$$N(p) = \left|f(2^i p_x, 2^i p_y, 2^i p_z)\right| * 10 - int\left(\left|f(2^i p_x, 2^i p_y, 2^i p_z)\right| * 10\right). \tag{4.13}$$

The resulting model, presented in Figure 4.25, has a really unique look that can be classified as different objects, like a wood sphere or an organic organism. It is possible to see that such extensive modification is a challenge to the simplification and the parametrization algorithms due to its high complexity.

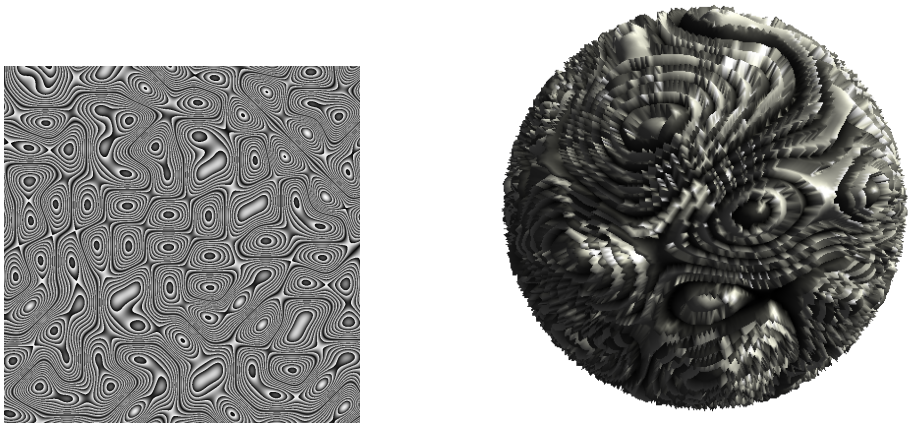

(a) (b)

Figure 4.25: (a) Wood/Organic texture defined by a basic noise function. (b) The pattern created in this mesh is similar to a wood object, an organic organism or even an alien planet.

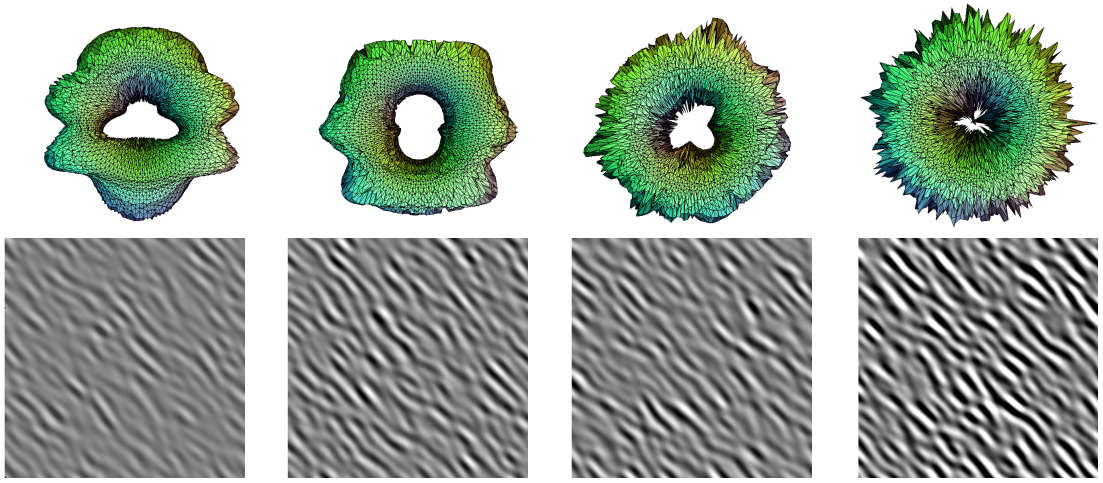

(a - 32 impulses/kernel) (b - 64 impulses/kernel) (c - 256 impulses/kernel) (d - 1024 impulses/kernel)

Figure 4.26: We can observe the variation created by each impulse density in a 2D texture representation and the same function applied to deform a 3D mesh.

4.7.3.2 Gabor Noise Operator

According to the Gabor noise description presented in Chapter 3, we can either modify the noise function directly or change the phase-augmented Gabor kernel. Perturbing the Gabor kernel can be done by regulating the K, a, ω variables, all at once or individually, according to the resolution level, which is similar to what is proposed for the turbulence and other functions. We also can modify the number of impulses per kernel according to this method, moving this value always as a power of two.

The idea is to find a nice relation between the many levels of resolution. Intuitively, for a better distribution, a higher number of impulses is preferred while manipulating the coarser levels, since the higher frequencies will be a dominant force. Also, this is a valuable tool for controlling which frequencies we want at each scale. The main objective here is to show the frequency variation according to the parameter settings, this is presented in Figure 4.26.

Another important characteristic of the Gabor noise is its manipulable directionality. This is a really important tool while dealing with features, mainly because we might want to guide the noise across the main characteristics of the model. These directions are obtained manipulating the kernel cosine orientation, using the ω_0 variable.

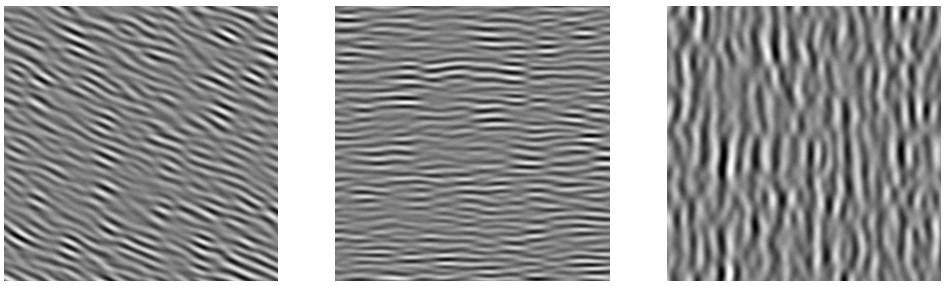

(a) (b) (c)

Figure 4.27: (a) Kernel with orientation ω_i as $\pi/4.0$. (b) Orientation ω_i as $\pi/8.0$ (c) Orientation ω_i as $\pi/5.0$

4.7.4 Feature-based Operator

This operator explores the meshes' feature information to create details. There are two main ways to use this: the first one focus on modifications specifically over the features, meaning that the surrounding areas will not suffer any deformation; the second is the opposite, only areas that are not considered as features will be modified. One can see that the classification of a vertex or edge as a feature becomes an input parameter to Equation 4.4.

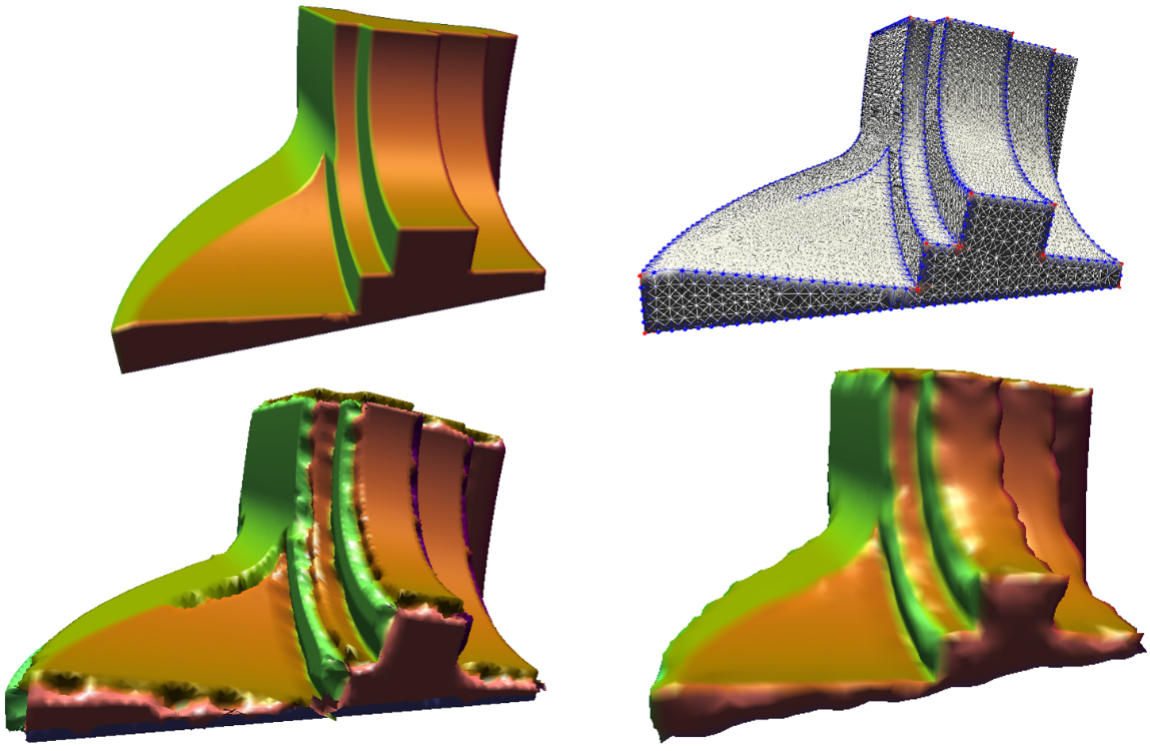

Figure 4.28: Example of deformation restricted to the feature line area. Bottom left we see a erosion on the fandisk across feature lines and, at the bottom right, a deformation to create a kneaded effect.

This operator inserts, in Equation 4.4 parameters, restrictions that are tied to the feature detection. For instance, a simple example of this can be achieved by filtering vertices that will be added to the set of vertices VS, defined in general deformation equation, in order to perform the deformation. In Figure 4.28, VS is composed by vertices that are considered as features, more specifically, strong-edge vertices.

This operator can also be combined with all the previous presented operators and also has the propagation capabilities, but with improved control. Instead of just propagating the deformation, through modulation of the function used through distance or neighborhood, we can, with this operator, propagate the feature information, creating entire areas that can be seen as modifiable or non-modifiable. This propagation is defined in Algorithm 4.

```
Data: Input vertex v to be verified
Result: True if can insert into the priority queue or false otherwise
bool insert = true;
for All mesh vertices do
    if v is not in an important feature then
        int counter;
        for All vertices in the star of v do
            if Any of these is in an important feature then
                insert = false;
                ++counter;
            end
        end
        if counter ≥ 2 then
            v becomes an important feature
        end
    else
        insert = false;
    end
end
if insert then
    v is inserted into the simplification queue
end
```

Algorithm 4: Feature verification for conditional removal.

4.7.5 Composite Operators

The intent of these operators is to produce visually complex results, through the combination of two or more of the previously presented operators.

Here, we show two of these, which were used to produce several results presented in

Chapter 5.

4.7.5.1 Organic Operator

The objective of this operator, as its name suggests, is to create organic looking structures. It relies on the subdivision and smoothing operators to create some of its forms, but, for more general purposes, can be used without them.

Usually, this operator has two steps, a global one and a local one, but, if needed, one of the steps can be suppressed. The global step generates a deformation that gives the mesh an specific appearance, i.e. the patterns obtained through the noise functions presented before (marble, wood and so on). The local step is a more specific manipulation and produce better results when a subdivision operator is applied, since the objective is to create a sharp detail (tree, rock, foliage etc). Of course, this also depends on the resolution level in which this operator is applied.

Algorithm 5 shows an implementation example of the organic operator, which is used to create some of our results in Chapter 5.

```
Data: Input vertex v to be noised
Result: Noised vertex with propagation and a k − ring refinement
for Each v to be noised do
    noise(v);
    propagateNoise(k − ring of v);
    apply n passes of: refineNeighborhood(v);
    find a new direction d in the 1 − ring of v;
    pointNoise(d);
end
```

Algorithm 5: Creating extensions with the organic operator.

This algorithm, apply a deformation at a vertex and propagate its effect to the 2-ring around the center of modification, Also, modifying the direction of the extension choosing a random point and pick its normal to guide this new direction.

4.7.5.2 Variation Operator

The main purpose of this operator is to create detail variation across the surface of the object and its many levels of resolution. This is achieved by modulating the frequency and the amplitude of the noise function, through each resolution level, in order to obtain the desirable level of detail.

This is the direct application of Equation 4.5, but we can also use, as shown in

Chapter 5, a slight variation of it, as presented in Equation 4.14.

$$p \leftarrow p + (nl/l)(-\vec{n}(p)) \tag{4.14}$$

This operator can explore the 4-k mesh structure by using a neighborhood relationship to propagate the noise and increase or decrease its influence according to a distance metric. This is achieved by modifying the previous equations as follows:

$$p \leftarrow p + (nl(1/d)/l)(-\vec{n}(p)), \tag{4.15}$$

where d is a distance value obtained by a function, an example of d is the Euclidean distance between the original vertex v and its neighbor. One might notice that the neighborhood can be defined by the user, i.e. 1-ring, 2-ring and so on.

Chapter 5

Results

In this Chapter we present our results, analysis and future works. Our testes were performed in a Asus GT50vt laptop with an Intel Core 2 Duo CPU with 4GB of RAM and a nVidia 9800M GTS GPU with 512MB. Many deformations were performed, using different models with varying resolutions, genuses and complexity.

5.1 Results

This section will be divided according to the detail created or/and the method used to produce each specific result.

5.1.1 Deformation Variation Across Surfaces

Figure 5.1 presents an example of our deformation scheme. We first show a deformation variation across the torus surface, using the *variation operator* (presented in Section 4.7.5), representing different kinds of manipulation over its body. Basically, in Figure 5.1(a) we show a default turbulence noise perturbation with lacunarity = 2.0 and gain = 0.6. And, in Figure 5.1(b), a demonstration of how our previously defined method can alter the configuration and distribution of the detail over the surface, which follows the definitions presented in Section 4.5. Since, at a coarser level, the noise attenuation is greater, it implies that the frequency is also decreased. There is a match between a mesh level l and the influence of the lacunarity, since this information represents how tightly the wavenumbers are packed together, a greater resolution is needed to better map high frequency levels. Thus, we attenuate its influence while moving to coarser levels. This concept is valid due to the low amount of vertices of the mesh at such resolution, resulting

in wide deformations with low frequencies such as the ones presented in Figure 5.1(b). After a few refinement steps, where the noise attenuation is lower, a new deformation is applied to regions that have not been modified in any previous step, creating high frequency peaks at the affected area. It is easy to observe the influence variation over the surface, when the noise is applied in different resolutions with specific local configurations.

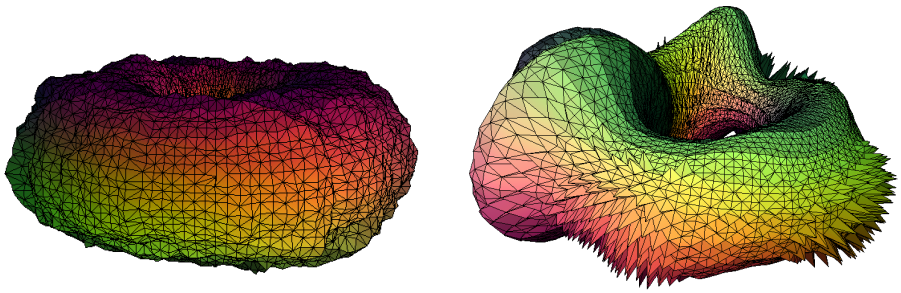

(a) (b)

Figure 5.1: (a) Lateral view of a torus perturbation with default turbulence noise configuration. (b) Overview of a multiscale noise modification.

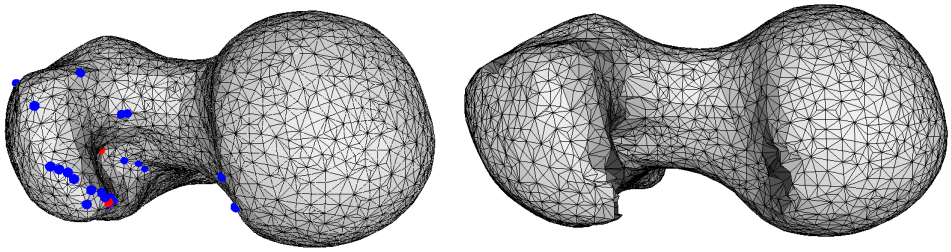

(a) (b)

Figure 5.2: (a) A femur bone model with feature vertices highlighted in blue and red colors, these are areas more sensible to wearing and friction damage. (b) Wearing simulation, using Perlin noise to represent fraying or local damage.

5.1.2 Feature Vertex Deformation

We also present a specific modification to a femur bone model, where we used *feature-based operator* (presented in Section 4.7.4) to perform our deformation. This is an interesting application of our method, that shows the wearing out process of the bone. It could also represent the smooth articular cartilage that lies at the end of the femur being damaged by repetitive micro-traumas or fraction (these traumas could be related to daily activities, sports, work or a genetic predisposition). Here we use Equation 4.14.

Figure 5.2(a) shows the mapping of these characteristics, which were used to perform the deformation in (b). In this specific example, we used that blue vertex as a deformation center and propagated the noise towards the 2-ring of it. In a certain way, this is a kind of region of interest(ROI) deformation in which the ROI is defined by a combination of metric and topological information (the use of the 2-ring of a feature vertex). According to the distance, an attenuation factor lowers the noise influence over the current vertex to avoid random spread across the original vertex neighborhood. In this specific example, we used the Gabor noise, all the chosen values and influence area can be observed in Table 5.1. Figure 5.3 show two examples of how the deformation can represent a more destructive problem on the femur head. To achieve this result we use the same arguments presented in Table 5.1, but also augmented the noise influence by a factor of two, based on the Equation 4.5. Figure 5.2(c) shows the final result of the entire mesh.

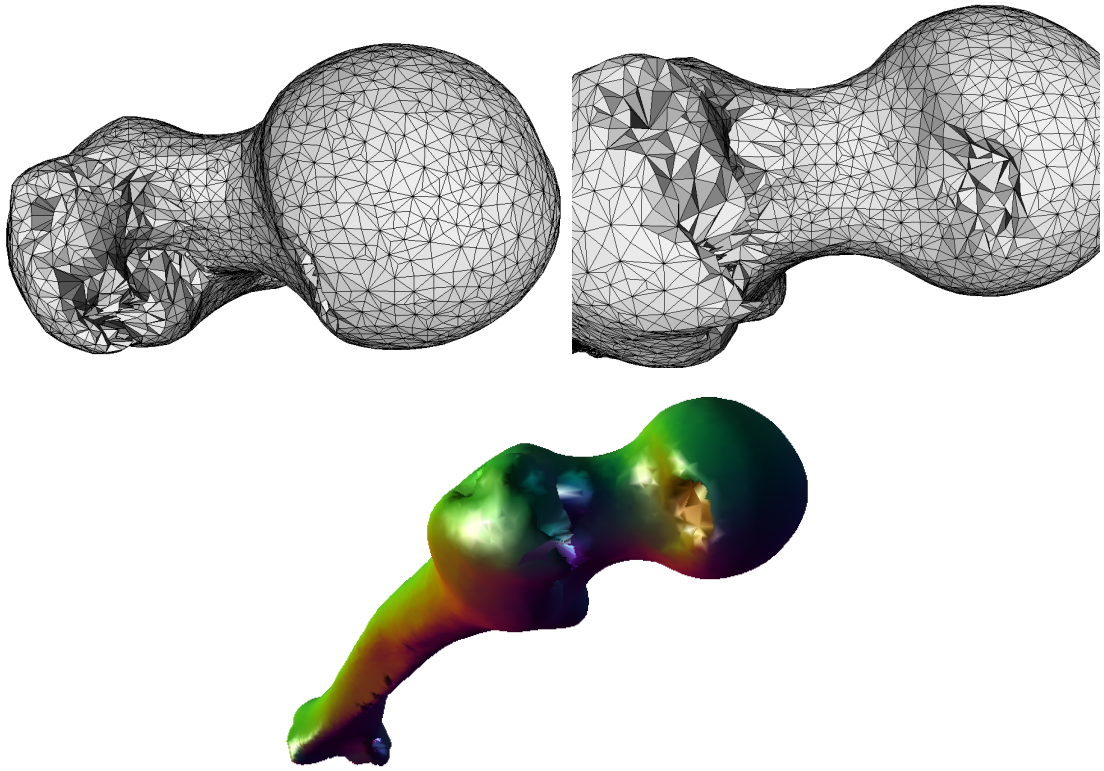

Figure 5.3: (a) Femur with a more intense erosion on the left side. (b) Focusing the erosion on the right side of the bone. (c) Overview of the entire mesh. Model obtained from [8].

Neighborhood	Noise Influence	K	a	w
1-ring	80%	1.0	0.05	0.0625
2-ring	50%	0.8	0.04	0.0625
3-ring	25%	0.6	0.03	0.0625
4-ring	10%	0.4	0.02	0.0625

Table 5.1: Deformation parameters for the noise propagation used in the femur example.

5.2 Subdivision and Smoothing Operator Usage

An interesting application of these operators is presented in Figure 5.4. In this example, we make use of the *procedural operator* (presented in Section 4.7.3) with the Gabor noise function, the feature detection as a constraint and the *smoothing operator* (see Section 4.7.1). Given an input mesh, in this case a dragon, we initiate with the detection of the feature lines, to obtain the most significant areas. With this calculation, we also obtain the diffusion flow which we will use in order to guide the direction of the noise. With this information we proceed extrapolating these ROI and after a significant amount of deformation is done we perform an smoothing step across the mesh. Note that the smoothing step does not recognize important features, thus making them more evident, provides enough strength for them to survive the smoothing process. This method provides a different approach regarding mesh deformation. The result in Figure 5.4(b) is really different when compared with the input mesh, but it can be a creative alternative to produce detail. Figure 5.4(c), shows how the dragon would look like without our localized enhancement. Notice that most of the details are lost and the dragon is pretty much a plain smooth surface. This can be understood as a process of abstraction, where we take a detailed model and preserve only those considered relevant with small modifications.

Another example combining the *subdivision and the organic operators* can be seen in Figure 5.5. The process, initially, subdivide the selected areas of the mesh, in this specific case, an independent set of vertices. These are the basic input of both *subdivision and procedural operators*. After this step, we use the *organic operator*, using the resolution level to modulate the amplitude and the frequency, following the idea of Equation 4.5. Usually, we start with a lacunarity of 2.0 and a gain of 0.5.

5.2.0.1 Deformation Based on the Data Structure Properties

We can also explore the data structure proposed here to reach our objectives. For instance, in Figure 5.6 we exploit the neighborhood relationship to position these different details

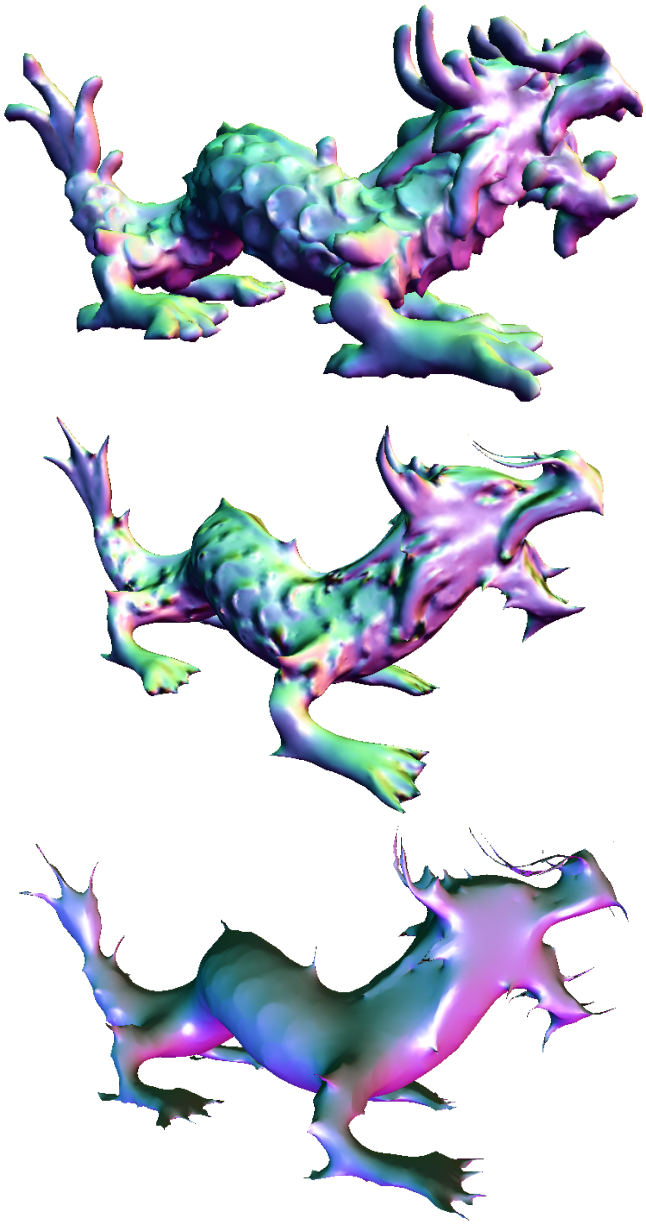

Figure 5.4: (Top) Input dragon with extrapolated areas. (Middle) Resulting appearance after the smoothing process, note that the horns, teeth and scales remain (smoothed) as details across the mesh. (Bottom) Resulting smoothing process without local feature enhancement. Model obtained from [8].

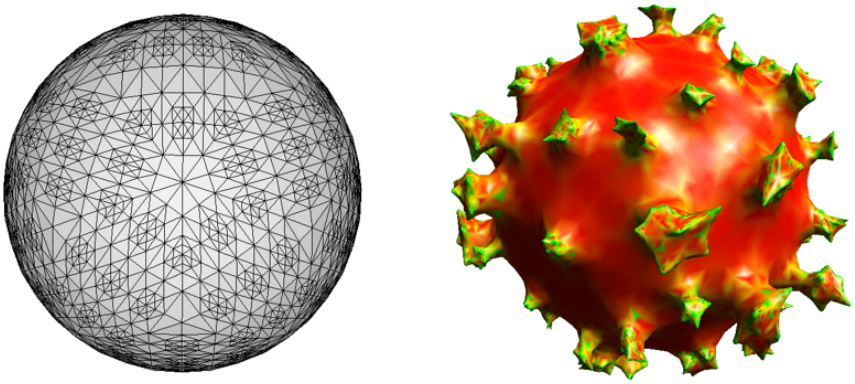

Figure 5.5: Applying the subdivision and procedural operators to create organic shapes.

using the organic operator. Specifically, we create a list containing all the vertices of the mesh and loop through this structure to obtain our deformation points. For each selected vertex, we search in the list for all vertices belonging to its 2-ring and remove them. This guarantees an even distribution across the mesh surface since we are selecting independent clusters.

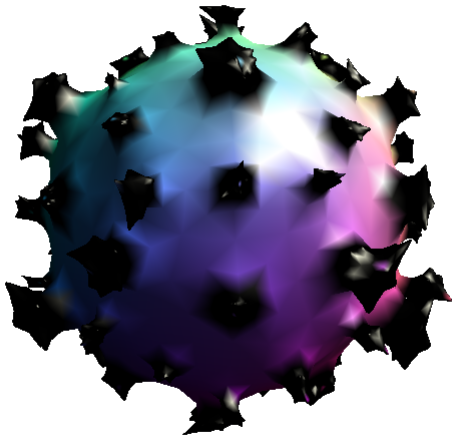

Figure 5.6: Virus looking surface with black coloring at the deformed areas to give a more threatening look. Deformation performed using the Equation 4.5.

A valid analysis is comparing some of our results with Velho et al. [75] work, which in its essence is similar to ours. In this first example, presented in Figure 5.7(a), Velho creates a mushroom planet inspired on the planet from *The Little Prince of Saint-Exupery*. In Figure 5.7(b) we can see a similar positioning for some details following the same idea of (a) and finally in (c) we can produce similar results using a noise function.

For this specific example, as it uses the organic operator, there are several steps to achieve this appearance. First, we must select the desired points and deform them and their 2-ring neighborhood area. Here, we apply a procedural operator, moving the vertex in the direction of its normal and then propagate this value to the neighboring area with the weights defined as noise value divided by 1.5 for the 1-ring and noise value divided by 2.0 for the 2-ring vertices. The objective of this displacement is used to create a hill with a smooth appearance. The next deformation is used to move the vertices to opposite directions creating a wide area at the top of the hill. Obviously, this area will vary from vertex to vertex due the pseudo-random nature of the noise, which is desirable to create an heterogeneous look among each detail. After this stage, a procedural operator where f is a turbulence function, with high frequency and low amplitude, is used to create the idea of trees and bumpy ground, for this function we chose as the values 6.0 for the lacunarity and 0.3 for the gain. The result can be seen in Figure 5.7(c).

Another comparison is done in Figure 5.8. In [75], to achieve the results seen in (Figure 5.8(a)) they realize a local feature placement at the same resolution level. In this example, we explore the mesh coordinates in order to position the detail, more specifically, we use the vertical component as a parameter constraint while constructing our VS in Equation 4.4. We explored a variation of frequencies across the head to make the resulting detail more appealing. In this case, we selected an independent set of vertices to be displaced, which is also a constraint to the VS, and defined a random *shift* at each influence area. One can notice that there are spots relatively flat in comparison to its neighborhood. To control the appearance, we changed the lacunarity and the amplitude using this *shift* value. Here, the initial values for them were 2.0 and 0.5 respectively, with a shift of 0.5 plus the noise contribution for the lacunarity and 0.1 plus the noise contribution for the amplitude (Figure 5.8(b)). In (c), we explored a more homogeneous approach to obtain a hair or hood aspect, for that we just removed the shift from formula and used a procedural operator with Gabor noise function, using the parameters defined in Equation 3.20, and the deformation approach described by Equation 4.5.

It is also possible to create a more organic looks using local modifications and refining the neighborhood around that region, this is done using an organic operator, which combine procedural and subdivision operators, as presented in Figure 5.9(Top Left). In this example, we also perform a selective decimation process, where only vertices that are not considered as details are candidates for removal. This guarantees that the created detail will be presented across the many resolution levels, if the user wishes so. Any extension or detail (blue and red) are kept unchanged. Note that only the yellow area

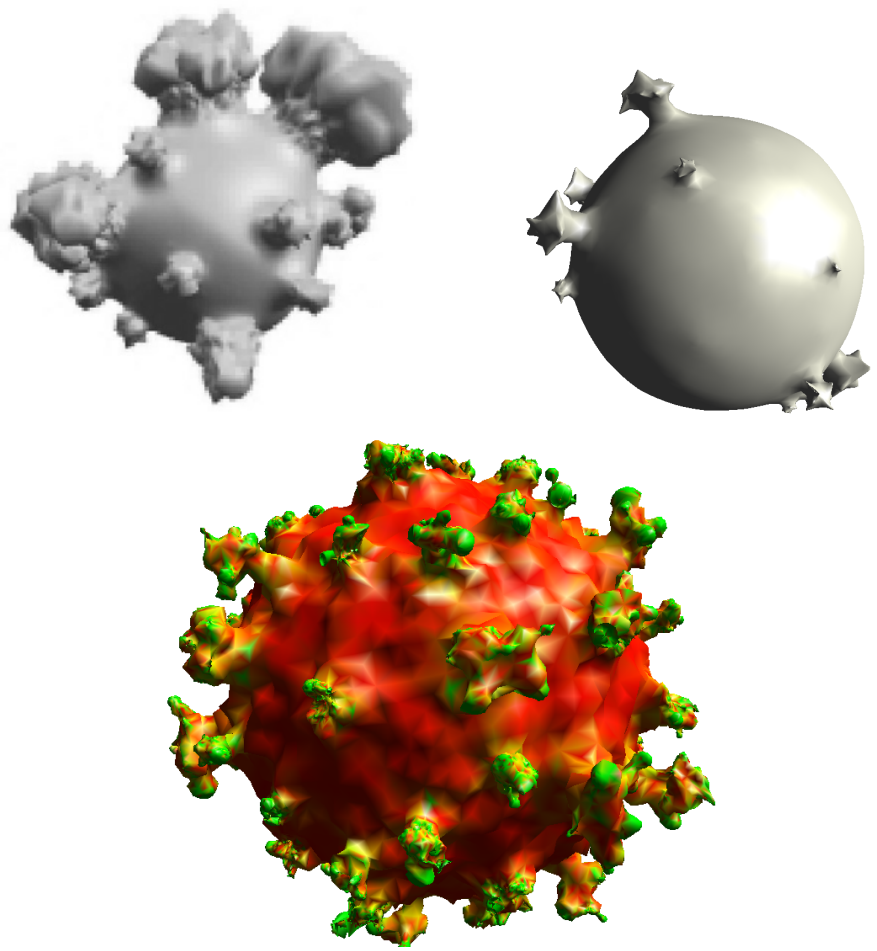

Figure 5.7: (Top Left) Mushroom planet using a mushroom cloud approach introduced by Velho et al. in [75]. (Top Right) Simple example o randomly placed small mushrooms using our approach. (Bottom) Complex example of a mushroom planet using guided positioning (similar to the description of Figure 5.6) and multiple displacement steps.

has parametrization vertices, creating variable resolution areas (Figure 5.9(Bottom). The pseudo-code that describes these extensions can be seen in Algorithm 5.

Here, we raise a valid discussion regarding the decimation and parametrization of the generated detail. Since forms and patterns are procedurally generated (i.e. it could be created using a geometry shader and not even be represented on the mesh), it might not make sense to decimate and parametrize such information. Also, considering that the detail can be created at any level, its maximum resolution will be the same as the current level, making it hard to create sharp details at certain mesh levels. A possible solution could be a subdivision scheme that, when applied to the deformed area, creates a more smooth appearance, but increases its geometric complexity.

Another example of using features, in order to guide the simplification process, can be observed in Figure 5.9(Top Right). Here, we noticed that some detail, added through a

(a) (b) (c)

Figure 5.8: (a) Original skull presented by Velho et al. in [75]. (b and c) Resulting mesh created using our approach, in this case the detail positioning was guided by the vertex position in space.

deformation process, might need to remain unchanged throughout the various resolutions. Upon finding a ROI and, detecting an important feature, if we want to maintain such structure and keep its neighborhood untouched, we must guarantee that none of those vertices will be removed. This is done by propagating the feature to its neighborhood, thus making it unremovable. To achieve this we follow the strategy defined in Algorithm 4.

5.2.1 Examples Illustrating the Entire Process

In Figure 5.15, the whole process can be observed, where an input dense dragon is simplified (middle right). In this example, we decided to maintain all vertices classified as corner vertices in order to apply a more sharp modification. At the top right, parameterized points are highlighted in order to show the surface mapping.

We show an example using the geometric operator combined with the variation operator and also explore the curvature detection for a more specific and localized result. Specifically, we use a geometric operator using the tapering operation, followed by a twisting and a final touch is done using a procedural modification through the turbulence noise function.

In Figure 5.10, we use as an input a skull with its mean curvature calculated, where the color variation indicates the curvature values. It is easy to spot the areas around the eyes, nose and teeth. In this particular example, we want to create a beard effect, without deforming the area of the teeth, and also to give a hair appearance to this bald model.

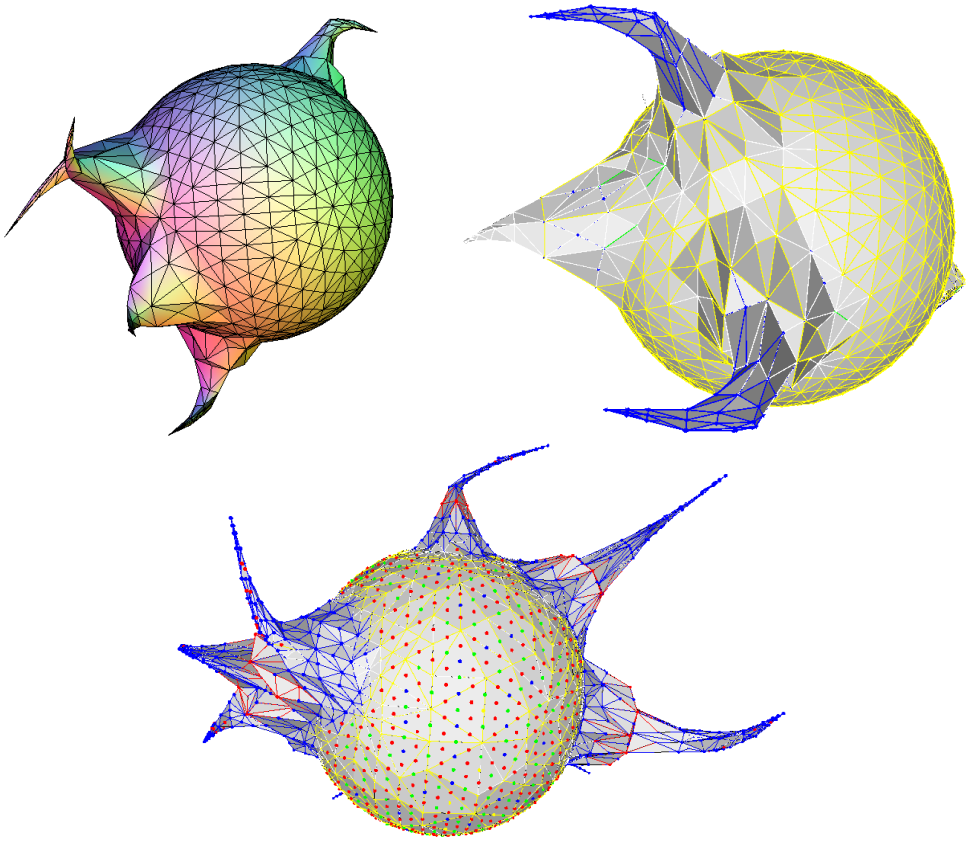

Figure 5.9: (Top left) An sphere with extensions creating a more organic look. (Top right) Feature detection used in a different fashion, with region propagation. The extensions (horns) are in blue. (Bottom) Example of a simplification process, where only the yellow area was allowed to be simplified. Any extension or detail (blue and red) are kept unchanged.

This variation operator does not use the propagation method mentioned in Chapter 4, since we need many high frequency points, we let each point be processed individually at a high resolution with almost no change at lower resolution levels. The geometric operator is applied, using a tapering operation at a lower resolution level modifying the x and y coordinates while maintaining z untouched. After enough refinement steps, the geometric operator performs a twisting operation in order to create a curl effect, to give the impression of a combed hair. The twisting follows the same rules set for the tapering operation.

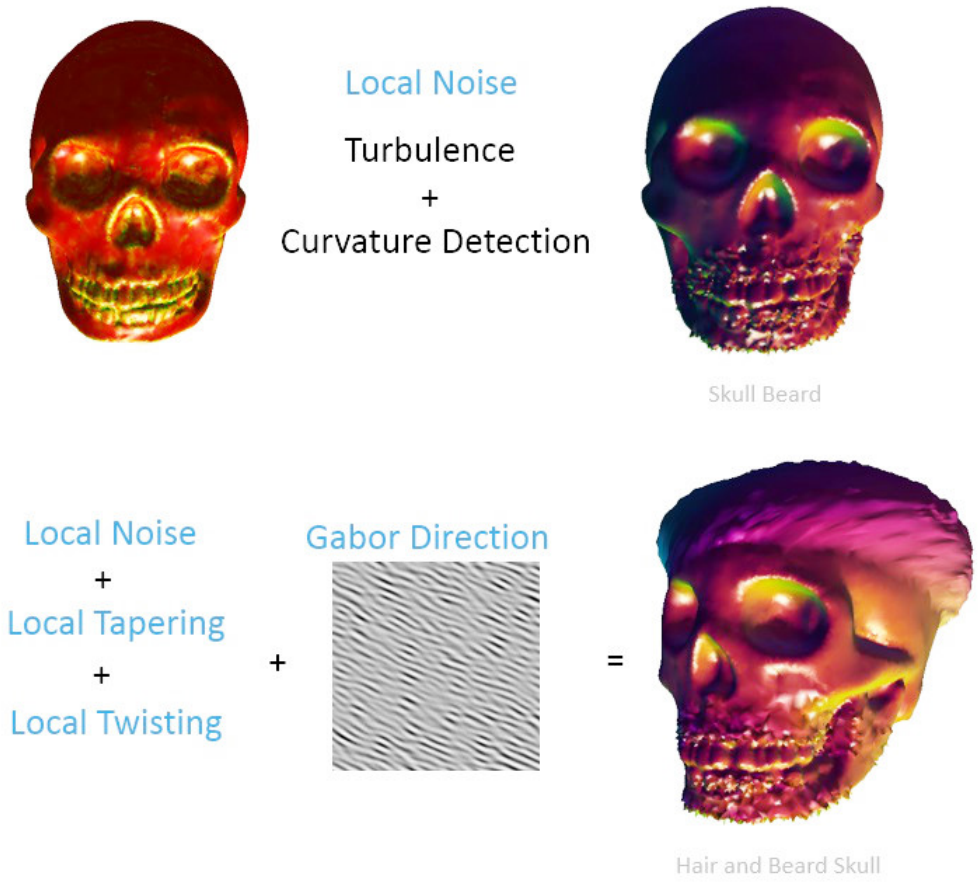

Figure 5.10: Complete example of the operators usage with a curvature detection as restriction to the noise deformation.

5.2.2 Diffusion Flow Images and Curvature Analysis

Feature detection provides yet another useful information in the mesh, in this case, the diffusion flow across the triangles as we can see in Figure 5.11. Using this metric alone is not ideal, since it does not provide all the information necessary to locally deform the mesh (although, one can still use it for other means). For a better result, combining the diffusion direction with the normal direction (cross product) usually provides a better angle between the surface and the displacement direction, this comparison can be seen in Figures 5.12 and 5.13. This together with feature lines can lead to a good visual, without creating the random look that is common to noise approaches.

Our work focus on exploring the many ways of analyzing the input mesh in order to deform it. An interesting result of our research is how the simplification process can

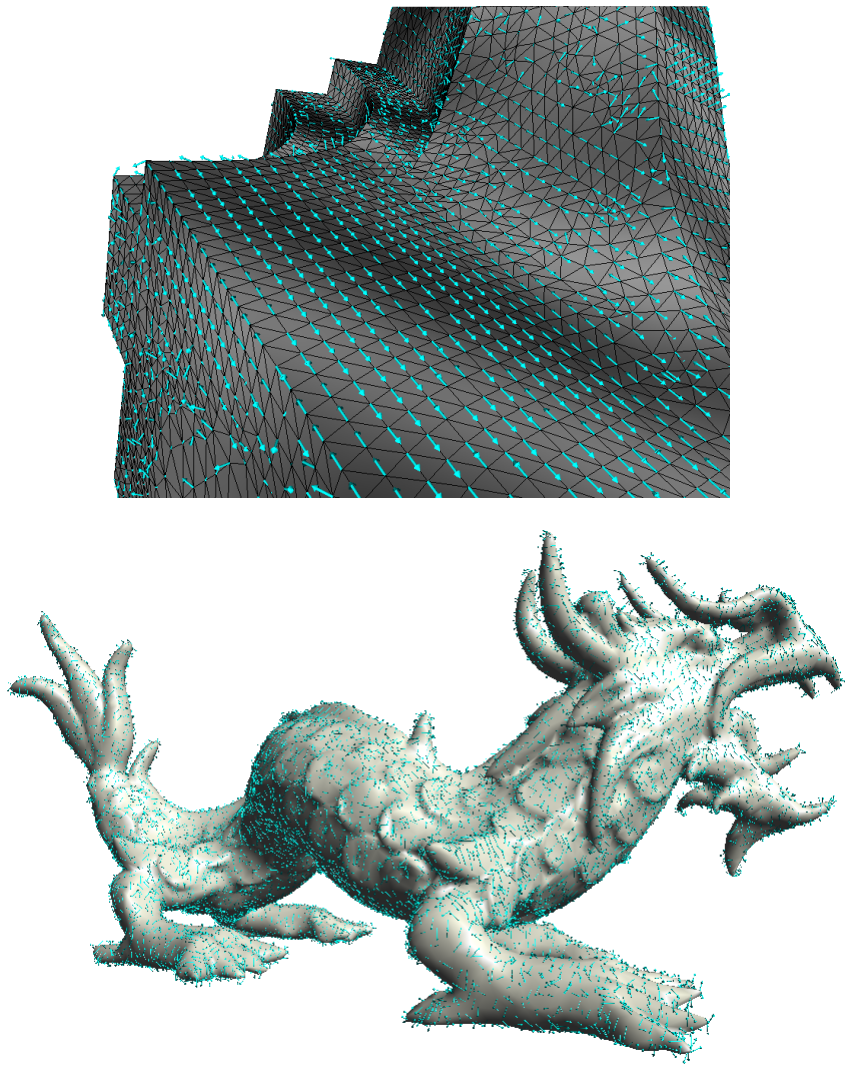

Figure 5.11: Here we can see how the flow is distributed along two different meshes, a fandisk model and an overview of these directions on the dragon. These are already used in the calculation of the feature lines in order to differentiate weak vertices from noise ones. We use this information to guide our detail generation and move it along features.

help us detect a region we want to manipulate. This is better explained with the help of Figure 5.14, where we see the comparison of the Gaussian curvature over the femur model. Reddish areas represent negative curvatures, and one can notice that at the head of the bone a few small regions are detected with such values (Figure 5.14(a)). This is due minimal differences in the height of the triangles, but after applying the simplification process that problem is drastically reduced or even eliminated (Figure 5.14(b, c and d)). One step of simplification is presented in (b), removing approximately 1/4 of the vertices, interest regions become more evident, but some unimportant areas are still visible. In (c), the only location left to be removed is the reddish area at the body of the bone (almost flat area). Finally, Base mesh, with approximately 1% of the original mesh shows a way

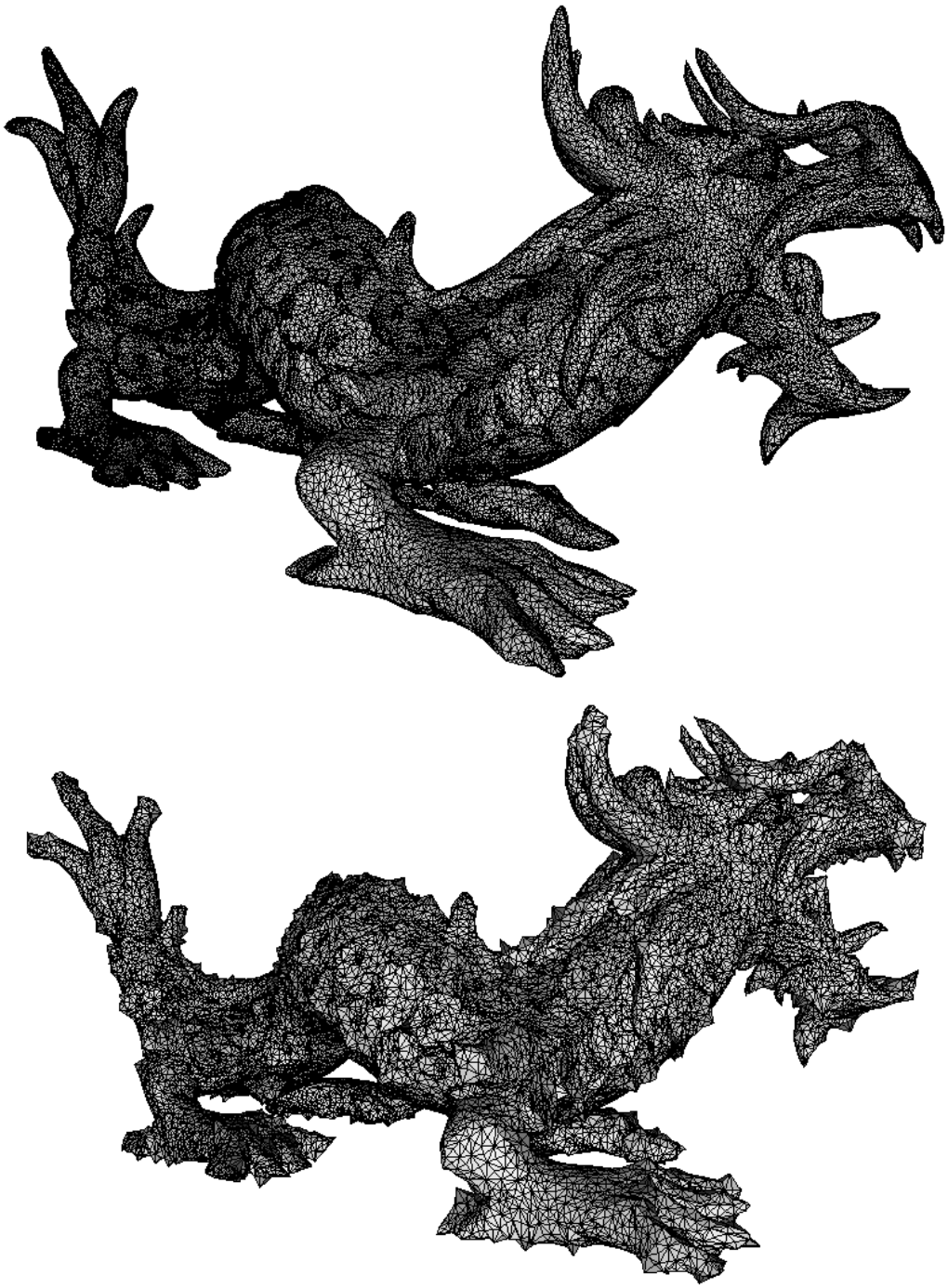

Figure 5.12: Comparison of the normal direction influence. (top) Original input dragon mesh. (bottom) Procedural operator using only the diffusion direction.

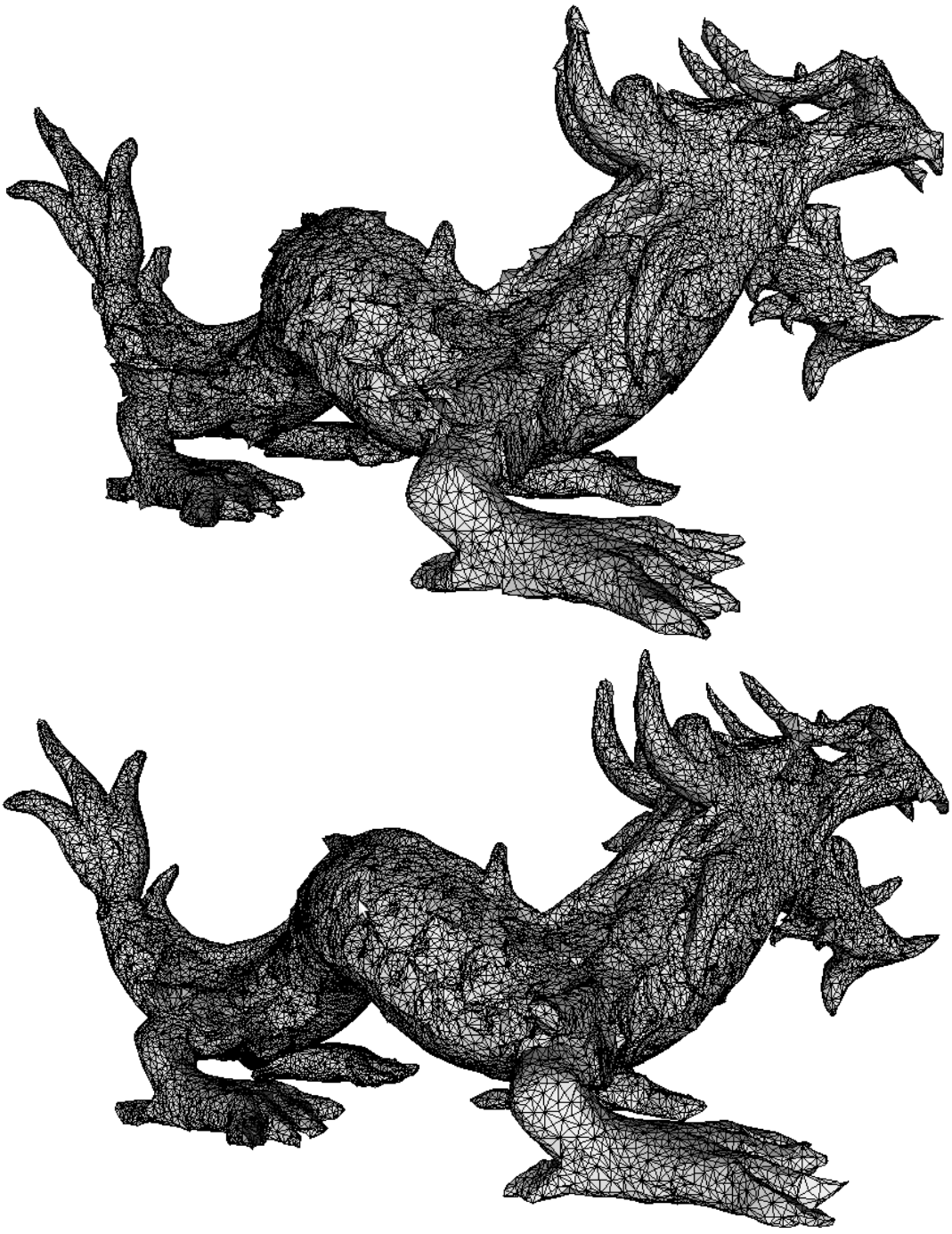

Figure 5.13: Comparison of the diffusion direction influence. (top) Procedural operator using only the diffusion direction. (bottom) Now, using the normal and diffusion direction combined to guide the deformation.

better selection of the area of interest. Figures 5.14(e and f), demonstrate the resulting deformation, creating a thin area where the Gaussian curvature has the defined threshold. This is of great interest to this work, since the area detection must be precise in order to apply a coherent local deformation. We must emphasize that we can use different curvatures, such as the mean, maximum and minimum curvatures.

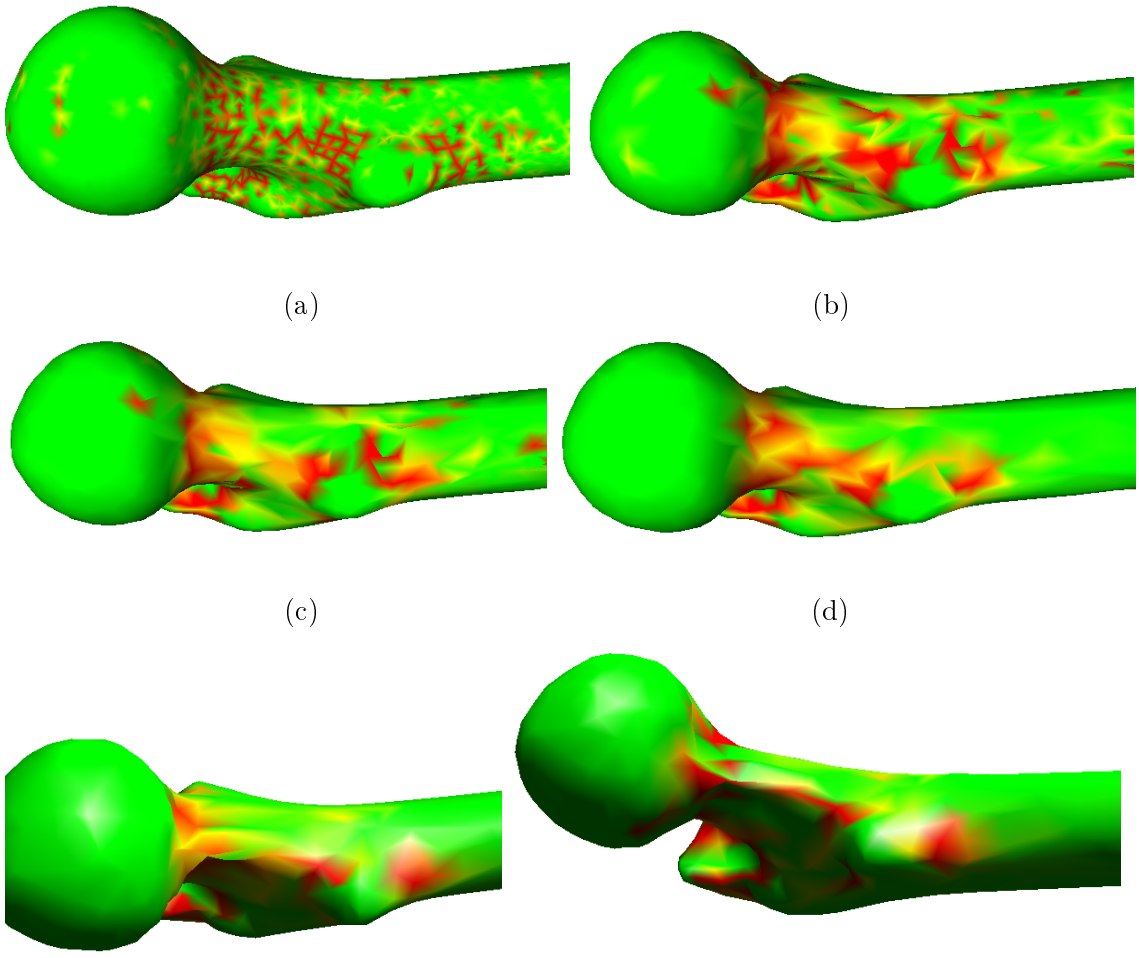

(a) (b) (c) (d) (e) (f)

Figure 5.14: (a) Full resolution bone, where detecting the specific area (below the bone head) is not fully possible. (b) Bone mesh after one simplification step. (c) The only location left to be removed in red. (d) Base mesh, with approximately 1% of the original mesh. (e) Resulting view of the local deformation. (f) Same resulting, new viewing from below. Model obtained from [8].

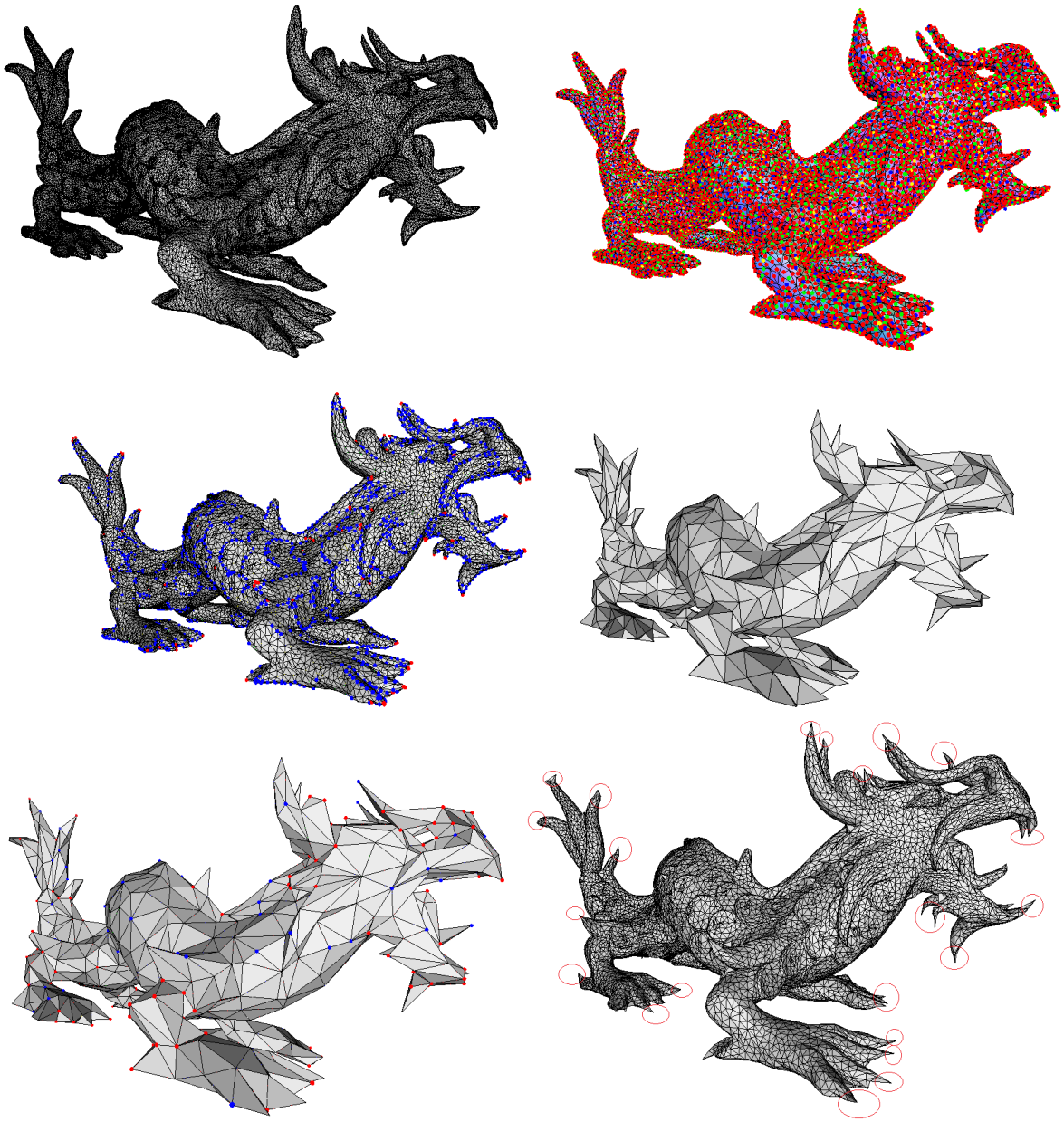

Figure 5.15: Input dense triangle mesh $\approx 70k$ triangles (top left). Parametrization map over the dragon mesh after the simplification steps (top right). Features marked as strong-edges and corner vertices (middle left). Dragon after simplification process ≈ 700 triangles (middle right). Features vertices at the base mesh (bottom left). Small detail modification, where we just sharpened the tail, claws, teeth and horns (bottom right). Model obtained from [8].

5.3 Final Comments

This chapter has shown several possibilities of using our method to deal with the problem of detail generation onto meshes of arbitrary genuses. By using an appropriate mesh representation, and choosing the appropriate primitive procedural and geometric operators, we could devise new different operators, integrated with our mesh representation, that supports better control in the deformation and detail insertion in the many levels of resolution and spatial locations of the mesh. We have also shown in the results the ways our operators can be combined to obtain many different effects granting a much better control to the modeler than with previous approaches. A final challenge remains regarding the problem of designing novel interactive ways to define and apply our detail and deformation generation pipeline.

Chapter 6

Conclusion and Future Works

In this thesis we presented a new method for adding details generated by noise functions to arbitrary genus surfaces using adaptive multiresolution mesh representations. We introduce forms of matching the noise parameters with the adaptive level of the mesh and also many deformation aspects using procedural approaches. The results obtained through this method are compatible to the proposed objectives and presents a new way of manipulating the different noise information through a variable resolution scheme.

We described a new method based on a combination of variable resolution mesh representations and procedural noise function for adding details to meshes with arbitrary genuses with control over the noise scales and mesh local resolution. Also, introduced a novel way to build 4-k meshes without relying on storing local combinatorial operations, by simply storing the original vertices in the base domain and refine it by inserting the vertices in the decimation order. This is achieved through a vertex degree fix algorithm, which approximates the original geometry. In order to obtain a better decimation process we introduced an improvement in the 4-k base domain generation by using a feature guided decimation. And, finally, for a more precise control over the detail generation process a new way to map these onto meshes, using features and geometric properties, is described.

We believe that our methods show promising results and presents many possibilities for future researches. One direction of our work is to study new ways of matching the noise parameters with the levels of detail. Also, find mechanisms for iterative deformation through the base mesh vertex manipulation using for example, bending, twist and tapper operations. Finally, use a manifold based representation in order to guarantee a smooth transition through different charts of with triangles in different levels of detail.

Also, an implementation that contemplates shaders for geometry and tessellation is something that we must pursue in further investigations. The latter can be done via software, but the tessellation implemented by hardware can generate an incredible amount of visual detail, including support for displacement mapping (which is important to this work), without adding the visual detail to the model sizes and hindering refresh rates. Following this idea, the usage of a relief mapping in order to map the noise inside the triangles could generate richer results for the representation of 3D surface detail, producing self-occlusion, self-shadowing, view-motion parallax, and silhouettes.

Another interesting idea is to explore spectral characteristics of the mesh, which can be combined with the spectral nature of the noise functions, which, in result, expand the number of operators that can be created.

6.0.1 Limitations

It is important to recognize the limitations of our approach. Initially, we can point that the mesh quality is an issue, since quality of the triangles can directly affect the parametrization. Thus, dealing with these meshes can be troublesome for our approach. Preprocessing the mesh might solve this problem, but it is an additional step in the process.

The detail generation always present a certain challenge level. Although an extensive description of ways to control the random nature of the noise was presented, this step requires a some training in order to achieve spectral control(as was described in many works in the literature, including [14, 6, 62]). We have also not dealt with the problem of detecting auto-intersection in the surface as a consequence of detail generation. This limitation must be overcome in further works.

References

[1] MAXIMO, A.; VELHO, L.; SIQUEIRA, M. Adaptive Multi-chart and Multiresolution Mesh Representation. *Computers and Graphics*, Elsevier Inc., v. 38, n. 0, p. 332–340, 2014. ISSN 0097-8493.

[2] ECK, M.; DEROSE, T.; DUCHAMP, T.; HOPPE, H.; LOUNSBERY, M.; STUETZLE, W. Multiresolution analysis of arbitrary meshes. In: *Proceedings of the 22Nd Annual Conference on Computer Graphics and Interactive Techniques*. New York, NY, USA: ACM, 1995. (SIGGRAPH '95), p. 173–182.

[3] VELHO, L. Mesh simplification using four-face clusters. In: *Shape Modeling International*. [S.l.]: IEEE Computer Society, 2001. p. 200–208. ISBN 0-7695-0853-7.

[4] LEE, A. W. F.; SWELDENS, W.; SCHRöDER, P.; COWSAR, L.; DOBKIN, D. Maps: Multiresolution adaptive parameterization of surfaces. In: *Proceedings of the 25th Annual Conference on Computer Graphics and Interactive Techniques*. New York, NY, USA: ACM, 1998. (SIGGRAPH '98), p. 95–104. ISBN 0-89791-999-8.

[5] PERLIN, K. An image synthesizer. In: *Proceedings of the 12th Annual Conference on Computer Graphics and Interactive Techniques*. New York, NY, USA: ACM, 1985. (SIGGRAPH '85), p. 287–296.

[6] LAGAE, A.; LEFEBVRE, S.; DRETTAKIS, G.; DUTRÉ, P. Procedural noise using sparse gabor convolution. In: *ACM SIGGRAPH 2009 Papers*. New York, NY, USA: ACM, 2009. (SIGGRAPH '09), p. 54:1–54:10. ISBN 978-1-60558-726-4.

[7] LOOP, C. *Smooth Subdivision Surfaces Based on Triangles*. [S.l.]: Department of Mathematics, University of Utah, 1987.

[8] VISIONAIR. *A World-class Infrastructure for Advanced 3D Visualization-based Research*. Jun 2014. Disponível em: <http://shapes.aimat-shape.net/ontologies/shapes/viewmodels.jsp>.

[9] HOPPE, H. Progressive meshes. In: *Proceedings of the 23rd Annual Conference on Computer Graphics and Interactive Techniques*. New York, NY, USA: ACM, 1996. (SIGGRAPH '96), p. 99–108. ISBN 0-89791-746-4.

[10] FLORIANI, L. D.; PUPPO, E. Hierarchical triangulation for multiresolution surface description. *ACM Transactions on Graphics*, v. 14, p. 363–411, 1995.

[11] PUPPO, E. Variable resolution triangulations. *Computational Geometry*, v. 11, n. 3-4, p. 219238, 1998. ISSN 0925-7721.

[12] FLORIANI, L. D.; MAGILLO, P.; PUPPO, E. Efficient implementation of multi-triangulations. In: *Proceedings of the Conference on Visualization '98*. Los Alamitos, CA, USA: IEEE Computer Society Press, 1998. (VIS '98), p. 43–50. ISBN 1-58113-106-2.

[13] VELHO, L.; GOMES, J. Variable resolution 4-k meshes: Concepts and applications. *Comput. Graph. Forum*, v. 19, n. 4, p. 195–212, 2000.

[14] EBERT, D. S.; MUSGRAVE, F. K.; PEACHEY, D.; PERLIN, K.; WORLEY, S. *Texturing and Modeling: A Procedural Approach*. 3rd. ed. San Francisco, CA, USA: Morgan Kaufmann Publishers Inc., 2002. ISBN 1558608486.

[15] KELLY, G.; MCCABE, H. *A Survey of Procedural Techniques for City Generation*. [S.l.], 2010.

[16] PERLIN, K. *Making Noise*. 1999. Http://www.noisemachine.com/talk1/index.html.

[17] PRUSINKIEWICZ, P.; LINDENMAYER, A. *The Algorithmic Beauty of Plants*. New York, NY, USA: Springer-Verlag New York, Inc., 1990. ISBN 0-387-97297-8.

[18] SPITZER, J.; GREEN, S. *Noise and Procedural Techniques*. 2003. In Proceedings of Game Developers Conference.

[19] MUSGRAVE, K. *Pandromeda*. 2006. Mojo World Applications. http://www.pandromeda.com/products/.

[20] INTERACTIVE Data Visualization Inc. SpeedTree RT. 2006. Http://www.speedtree.com.

[21] SIDE Effects Software. Manufacturer of Houdini. 2005. Http://www.sidefx.com.

[22] KELLY, G.; MCCABE, H. *ITB Journal A Survey of Procedural Techniques for City Generation*. 87 - 130 p.

[23] DEMBOGURSKI, B. J. *GeraÃ§Ã£o Procedural de Terrenos atravÃ©s de ExtraÃ§Ã£o de IsosuperfÃcies na GPU*. Thesis (Master) — Instituto de ComputaÃ§Ã£o, Universidade Federal Fluminense, MarÃ§o 2009.

[24] PERLIN, K.; HOFFERT, E. M. Hypertexture. In: *Proceedings of the 16th Annual Conference on Computer Graphics and Interactive Techniques*. New York, NY, USA: ACM, 1989. (SIGGRAPH '89), p. 253–262. ISBN 0-89791-312-4.

[25] PERLIN, K. Improving noise. In: *Proceedings of the 29th Annual Conference on Computer Graphics and Interactive Techniques*. New York, NY, USA: ACM, 2002. (SIGGRAPH '02), p. 681–682. ISBN 1-58113-521-1.

[26] LAGAE, A.; DRETTAKIS, G. Filtering solid gabor noise. In: *ACM SIGGRAPH 2011 Papers*. New York, NY, USA: ACM, 2011. (SIGGRAPH '11), p. 1–6. ISBN 978-1-4503-0943-1.

[27] GALERNE, B.; LAGAE, A.; LEFEBVRE, S.; DRETTAKIS, G. Gabor noise by example. *ACM Trans. Graph.*, v. 31, n. 4, p. 73, 2012.

[28] BOTSCH, M.; PAULY, M.; ROSSL, C.; BISCHOFF, S.; KOBBELT, L. Geometric modeling based on triangle meshes. In: *ACM SIGGRAPH 2006 Courses*. New York, NY, USA: ACM, 2006. (SIGGRAPH '06). ISBN 1-59593-364-6.

[29] SORKINE, O.; BOTSCH, M. Tutorial: Interactive shape modeling and deformation. In: *EUROGRAPHICS*. [S.l.: s.n.], 2009.

[30] BENDELS, G. H.; KLEIN, R.; SCHILLING, A. Image and 3d-object editing with precisely specified editing regions. In: ERTL, T.; GIROD, B.; GREINER, G.; NIEMANN, H.; SEIDEL, H.-P.; STEINBACH, E.; WESTERMANN, R. (Ed.). *Vision, Modeling and Visualisation 2003*. [S.l.]: Akademische Verlagsgesellschaft Aka GmbH, Berlin, 2003. p. 451–460. ISBN 3-89838-048-3.

[31] PAULY, M.; KEISER, R.; KOBBELT, L. P.; GROSS, M. Shape modeling with point-sampled geometry. In: *ACM SIGGRAPH 2003 Papers*. New York, NY, USA: ACM, 2003. (SIGGRAPH '03), p. 641–650. ISBN 1-58113-709-5.

[32] ZAYER, R.; RÃ¶SSL, C.; KARNI, Z.; SEIDEL, H.-P. Harmonic guidance for surface deformation. *Comput. Graph. Forum*, v. 24, n. 3, p. 601–609, 2005.

[33] BOTSCH, M.; KOBBELT, L. An intuitive framework for real-time freeform modeling. In: *ACM SIGGRAPH 2004 Papers*. New York, NY, USA: ACM, 2004. (SIGGRAPH '04), p. 630–634.

[34] VELHO, L.; PERLIN, K.; BIERMANN, H.; YING, L. Algorithmic shape modeling with subdivision surfaces. *Computers and Graphics*, v. 26, n. 6, p. 865–875, 2002.

[35] CATMULL, E.; CLARK, J. Seminal graphics. In: . New York, NY, USA: ACM, 1998. chap. Recursively Generated B-spline Surfaces on Arbitrary Topological Meshes, p. 183–188. ISBN 1-58113-052-X.

[36] BIERMANN, H.; MARTIN, I. M.; ZORIN, D.; BERNARDINI, F. Sharp features on multiresolution subdivision surfaces. *Graphical Models*, v. 64, n. 2, p. 61–77, 2002.

[37] SCHMIDT, R. *Part-Based Representation and Editing of 3D Surface Models*. Thesis (PhD) — University of Toronto, Canada, 2010.

[38] VELHO, L.; GOMES, J. Fundamentos da computaÃ§Ã£o grÃ¡fica. In: _____. [S.l.]: IMPA, 2008. (SÃ©rie ComputaÃ§Ã£o e MatemÃ¡tica).

[39] BOTSCH, M.; KOBBELT, L.; PAULY, M.; ALLIEZ, P.; LEVY, B. *Polygon Mesh Processing*. Taylor & Francis, 2010. (Ak Peters Series). ISBN 9781568814261. Disponível em: <http://books.google.com.br/books?id=8zX-2VRqBAkC>.

[40] TAUBIN, G. A signal processing approach to fair surface design. In: *Proceedings of the 22Nd Annual Conference on Computer Graphics and Interactive Techniques*. New York, NY, USA: ACM, 1995. (SIGGRAPH '95), p. 351–358. ISBN 0-89791-701-4.

[41] HILDEBRANDT, K.; POLTHIER, K.; WARDETZKY, M. On the convergence of metric and geometric properties of polyhedral surfaces. *GEOMETRIAE DEDICATA*, v. 123, p. 89–112, 2005.

[42] GRINSPUN, E.; DESBRUN, M. (Ed.). *Discrete differential geometry: an applied introduction*, (ACM SIGGRAPH Courses Notes). [S.l.]: ACM Press New York, NY, USA, 2006.

[43] WARDETZKY, M. *Convergence of the Cotangent Formula: An Overview*. 2008.

[44] WARDETZKY, M.; MATHUR, S.; KALBERER, F.; GRINSPUN, E. Discrete laplace operators: No free lunch. In: *Proceedings of the Fifth Eurographics Symposium on Geometry Processing*. Aire-la-Ville, Switzerland, Switzerland: Eurographics Association, 2007. (SGP 07), p. 33–37. ISBN 978-3-905673-46-3.

[45] ALEXA, M.; WARDETZKY, M. Discrete laplacians on general polygonal meshes. In: *ACM SIGGRAPH 2011 Papers*. New York, NY, USA: ACM, 2011. (SIGGRAPH 11), p. 102:1–102:10. ISBN 978-1-4503-0943-1.

[46] ZORIN, D.; SCHRöDER, P. *Subdivision for Modeling and Animation*. [S.l.], 2000. Course Notes.

[47] STAM, J. Exact evaluation of catmull-clark subdivision surfaces at arbitrary parameter values. In: *Proceedings of the 25th Annual Conference on Computer Graphics and Interactive Techniques*. New York, NY, USA: ACM, 1998. (SIGGRAPH '98), p. 395–404. ISBN 0-89791-999-8.

[48] VELHO, L.; ZORIN, D. 4–8 subdivision. *Computer Aided Geometric Design*, Elsevier, v. 18, n. 5, p. 397–427, 2001.

[49] STAM, J.; LOOP, C. Quad/triangle subdivision. *Computer Graphics Forum*, Blackwell Publishing, Inc, v. 22, n. 1, p. 79–85, 2003. ISSN 1467-8659.

[50] BAUMGART, B. G. *Winged Edge Polyhedron Representation.* Stanford, CA, USA, 1972.

[51] MäNTYLä, M. *An Introduction to Solid Modeling*. New York, NY, USA: Computer Science Press, Inc., 1987. ISBN 0-88175-108-1.

[52] ROSSIGNAC, J.; SAFONOVA, A.; SZYMCZAK, A. *Edgebreaker on a Corner Table: A simple technique for representing and compressing triangulated surfaces*. 2002.

[53] LAGE, M.; LEWINER, T.; LOPES, H.; VELHO, L. *CHE: A scalable topological data structure for triangular meshes*. [S.l.], May 2005.

[54] GURUNG, T.; LANEY, D. E.; LINDSTROM, P.; ROSSIGNAC, J. Squad: Compact representation for triangle meshes. *Comput. Graph. Forum*, v. 30, n. 2, p. 355–364, 2011.

[55] EDELSBRUNNER, H. *Algorithms in Combinatorial Geometry*. Springer, 1987. (European Association for Theoretical Computer Science: EATCS monographs on theoretical computer science). ISBN 9783540137221. Disponível em: <http://books.google.com.br/books?id=mxugg47mzK4C>.

[56] VELHO, L. Semi-regular 4-8 refinement and box spline surfaces. In: *SIBGRAPI*. [S.l.]: IEEE Computer Society, 2000. p. 131–138. ISBN 0-7695-0878-2.

[57] GOTSMAN, C.; GUMHOLD, S.; KOBBELT, L. Simplification and compression of 3d meshes. In: *In Proceedings of the European Summer School on Principles of Multiresolution in Geometric Modelling (PRIMUS*. [S.l.]: Springer, 1998. p. 319–361.

[58] HECKBERT, P. S.; GARLAND, M. *Survey of Polygonal Surface Simplification Algorithms*. 1997.

[59] FLOATER, M. S. Parametrization and smooth approximation of surface triangulations. *Comput. Aided Geom. Des.*, Elsevier Science Publishers B. V., Amsterdam, The Netherlands, The Netherlands, v. 14, n. 3, p. 231–250, apr. 1997. ISSN 0167-8396.

[60] DUCHAMP, T.; CERTAIN, A.; DEROSE, A.; STUETZLE, W. *Hierarchical Computation Of Pl Harmonic Embeddings*. [S.l.], 1997.

[61] TUTTE, W. *Convex Representation of Graphs*. [S.l.], 1960. 304–20 p.

[62] LAGAE, A.; LEFEBVRE, S.; COOK, R.; DEROSE, T.; DRETTAKIS, G.; EBERT, D. S.; LEWIS, J. P.; PERLIN, K.; ZWICKER, M. A survey of procedural noise functions. *Comput. Graph. Forum*, v. 29, n. 8, p. 2579–2600, 2010.

[63] PAPOULIS, A. *Probability, Random Variables, and Stochastic Processes*. [S.l.]: McGraw Hill, 2002.

[64] BRACEWELL, R. *The Fourier Transform and Its Applications*. McGraw-Hill Higher Education, 2000. (Electrical engineering series). ISBN 9780073039381. Disponível em: <http://books.google.com.br/books?id=ZNQQAQAAIAAJ>.

[65] ELIAS, H. *Perlin Noise*. Jun 2014. Disponível em: <http://freespace.virgin.net/hugo.elias/models/m_perlin.htm>.

[66] WYVILL, G.; NOVINS, K. Filtered noise and the fourth dimension. In: *ACM SIGGRAPH 99 Conference Abstracts and Applications*. New York, NY, USA: ACM, 1999. (SIGGRAPH '99), p. 242–. ISBN 1-58113-103-8.

[67] OLANO, M.; HART, J. C.; HEIDRICH, W.; MARK, B.; PERLIN, K. Real-time shading languages. In: *ACM SIGGRAPH 2002 Courses*. New York, NY, USA: ACM, 2002. (SIGGRAPH '02).

[68] PERLIN, K.; NEYRET, F. Flow noise. In: *Siggraph Technical Sketches and Applications*. [S.l.: s.n.], 2001. p. 187.

[69] BRIDSON, R.; HOURIHAM, J.; NORDENSTAM, M. Curl-noise for procedural fluid flow. In: *ACM SIGGRAPH 2007 Papers*. New York, NY, USA: ACM, 2007. (SIGGRAPH '07).

[70] KENSLER, A.; KNOLL, A.; SHIRLEY, P. *Better Gradient Noise*. [S.l.], 2008.

[71] LEWIS, J. P. Algorithms for solid noise synthesis. In: *Proceedings of the 16th Annual Conference on Computer Graphics and Interactive Techniques*. New York, NY, USA: ACM, 1989. (SIGGRAPH '89), p. 263–270. ISBN 0-89791-312-4.

[72] GAMITO, M. *Techniques for Stochastic Implicit Surface Modelling and Rendering*. [S.l.]: University of Sheffield, Department of Computer Science, 2009.

[73] WIJK, J. J. van. Spot noise texture synthesis for data visualization. *SIGGRAPH Comput. Graph.*, ACM, New York, NY, USA, v. 25, n. 4, p. 309–318, jul. 1991. ISSN 0097-8930. Disponível em: <http://doi.acm.org/10.1145/127719.122751>.

[74] STOLLNITZ, E. J.; DEROSE, T. D.; SALESIN, D. H. *Wavelets for Computer Graphics: Theory and Applications*. San Francisco, CA, USA: Morgan Kaufmann Publishers Inc., 1996. ISBN 1-55860-375-1.

[75] VELHO, L.; PERLIN, K.; BIERMANN, H.; YING, L. Algorithmic shape modeling with subdivision surfaces. *Computers and Graphics*, v. 26, n. 6, p. 865–875, 2002.

[76] DOBKIN, D. P.; KIRKPATRICK, D. G. A linear algorithm for determining the separation of convex polyhedra. *Journal of Algorithms*, v. 6, n. 3, p. 381 – 392, 1985. ISSN 0196-6774. Disponível em: <http://www.sciencedirect.com/science/article/pii/0196677485900070>.

[77] MEDIONI, G.; TANG, C.-K.; LEE, M.-S. Tensor Voting: Theory and Applications. In: *Proceedings of RFIA*. [S.l.: s.n.], 2000.

[78] WANG, S.; HOU, T.; SU, Z.; QIN, H. Diffusion Tensor Weighted Harmonic Fields for Feature Classification. In: . [S.l.: s.n.], 2011. p. 93–98.

[79] KIM, H. S.; CHOI, H. K.; LEE, K. H. Feature detection of triangular meshes based on tensor voting theory. *Comput. Aided Des.*, Butterworth-Heinemann, Newton, MA, USA, v. 41, n. 1, p. 47–58, jan. 2009. ISSN 0010-4485.

[80] WANG, S.; HOU, T.; LI, S.; SU, Z.; QIN, H. Hierarchical feature subspace for structure-preserving deformation. *Computer-Aided Design*, v. 45, n. 2, p. 545–550, 2013.

[81] BARR, A. H. Global and local deformations of solid primitives. In: *Proceedings of the 11th Annual Conference on Computer Graphics and Interactive Techniques*. New York, NY, USA: ACM, 1984. (SIGGRAPH '84), p. 21–30. ISBN 0-89791-138-5. Disponível em: <http://doi.acm.org/10.1145/800031.808573>.